I. PROTON MAGNETIC RESONANCE OF POLYNUCLEOTIDES AND TRANSFER RNA

II. ELECTRON SPIN RELAXATION STUDIES OF MANGANESE (II) COMPLEXES IN ACETONITRILE

Thesis by

Jane Ellen Crawford

In Partial Fulfillment of the Requirements
For the Degree of
Doctor of Philosophy

California Institute of Technology
Pasadena, California

1971

(Submitted November 24, 1970)

ACKNOWLEDGMENTS

謝謝陳長謙教授

During my years spent at Caltech, Professor Sunney I. Chan has been my teacher and my "boss". It is a pleasure to acknowledge his guidance and support.

I also acknowledge the support of past and present members of the Chan research group. A special "thank you" is given to Dr. Lahmer Lynds for his collaboration and guidance during my first years here.

In addition, I wish to express appreciation of the collaboration of Dr. Martin P. Schweizer of the International Chemical and Nuclear Corporation at Irvine, California.

I am indebted to Mrs. Karen Gleason for her accuracy and speed as a typist and for her good humor as I kept giving her section after section to type.

The financial assistance of a National Defense and Education Act Fellowship, of a California State Graduate Fellowship and of the California Institute of Technology is gratefully acknowledged.

ABSTRACT

Part I. Proton Magnetic Resonance of Polynucleotides and Transfer RNA.

Proton magnetic resonance was used to follow the temperature dependent intramolecular stacking of the bases in the polynucleotides of adenine and cytosine. Analysis of the results on the basis of a two state stacked-unstacked model yielded values of - 4.5 kcal/mole and - 9.5 kcal/mole for the enthalpies of stacking in polyadenylic and polycytidylic acid, respectively.

The interaction of purine with these molecules was also studied by pmr. Analysis of these results and the comparison of the thermal unstacking of polynucleotides and short chain nucleotides indicates that the bases contained in stacks within the long chain polynucleotides are, on the average, closer together than the bases contained in stacks in the short chain nucleotides.

Temperature and purine studies were also carried out with an aqueous solution of formylmethionine transfer ribonucleic acid. Comparison of these results with the results of similar experiments with the homopolynucleotides of adenine, cytosine and uracil indicate that the purine is probably intercalating into loop regions of the molecule.

The solvent denaturation of phenylalanine transfer ribonucleic acid was followed by pmr. In a solvent mixture containing 83 volume per cent dimethylsulfoxide and 17 per cent deuterium oxide, the tRNA molecule is rendered quite flexible. It is possible to resolve resonances of protons on the common bases and on certain modified bases.

Part II. Electron Spin Relaxation Studies of Manganese (II) Complexes in Acetonitrile.

The electron paramagnetic resonance spectra of three Mn^{+2} complexes, $[Mn(CH_3CN)_6]^{+2}$, $[MnCl_4]^{-2}$, and $[MnBr_4]^{-2}$, in acetonitrile were studied in detail. The objective of this study was to relate changes in the effective spin Hamiltonian parameters and the resonance line widths to the structure of these molecular complexes as well as to dynamical processes in solution.

Of the three systems studied, the results obtained from the $[Mn(CH_3CN)_6]^{+2}$ system were the most straight-forward to interpret. Resonance broadening attributable to manganese spin-spin dipolar interactions was observed as the manganese concentration was increased.

In the $[MnCl_4]^{-2}$ system, solvent fluctuations and dynamical ion-pairing appear to be significant in determining electron spin relaxation.

In the $[MnBr_4]^{-2}$ system, solvent fluctuations, ion-pairing, and Br^- ligand exchange provide the principal means of electron spin relaxation. It was also found that the spin relaxation in this system is dependent upon the field strength and is directly related to the manganese concentration. A relaxation theory based on a two state collisional model was developed to account for the observed behavior.

TABLE OF CONTENTS

Part	Title	Page
I	PROTON MAGNETIC RESONANCE OF POLYNUCLEOTIDES AND TRANSFER RNA	1
	1. General Introduction	2
	2. Proton Magnetic Resonance of Polyadenylic and Polycytidylic Acids	18
	2.1. Introduction	18
	2.2. Experimental	19
	2.3. Results and Discussion	20
	2.3.1. Proton Magnetic Resonance Spectrum of Polyadenylic Acid	20
	2.3.2. Temperature Variation of the Base Proton Chemical Shifts	26
	2.3.3. Temperature Variation of the $H_{1'}$ Resonances	59
	2.3.4. Purine Interaction	70
	2.4. Conclusions	92
II	ELECTRON SPIN RELAXATION STUDIES OF MANGANESE (II) COMPLEXES IN ACETONITRILE	145
	1. Introduction	147
	1.1. Spectral Analysis	148
	2. Experimental	149

3. Results and Discussion 152

 3.1. $[Mn(CH_3CN)_6]^{+2}$ 152

 3.2. $[MnCl_4]^{-2}$ 159

 3.3. $[MnBr_4]^{-2}$ 172

 3.4. Frequency Dependence of Resonance Widths 182

 3.5. Temperature Dependence of Resonance Widths 199

 3.6. Calculation of Resonance Widths 205

 3.7. Applications of Calculations to the $[MnBr_4]^{-2}$ System 212

4. Conclusions 217

PART I

PROTON MAGNETIC RESONANCE OF POLYNUCLEOTIDES AND TRANSFER RNA

1. GENERAL INTRODUCTION

The fundamental processes of the storage, expression, and transmission of genetic information and the capacity for genetic change are controlled by the chemical and physical characteristics of a class of compounds known as the nucleic acids. The mechanisms by which the nucleic acids fulfill their various roles is a very active area of research.

The nucleic acids are divided into two groups: deoxyribonucleic acids (DNA) and ribonucleic acids (RNA). The units (Figure 1) which make up a nucleic acid are the pyrimidine and purine bases, a sugar component and phosphoric acid. The common pyrimidine bases are cytosine which is found in both DNA and RNA, uracil which is found in RNA, and thymine which is found in DNA. The common purine bases are adenine and guanine which occur in both DNA and RNA. There are also small amounts of various modified bases which are derivatives of the common bases. The principal sugar in RNA is D-ribose with small amounts of 2′-O-methylribose. The sugar in DNA is D-2-deoxyribose.

A nucleoside is a purine or pyrimidine base and a ribose or deoxyribose. These components are connected by a glycosidic bond between the N-1 of a pyrimidine or the N-9 of a purine and the C-1 of the sugar moiety. The names given to the common nucleosides are cytidine, uridine, thymidine, adenosine, and guanosine.

A nucleotide is the phosphoric ester of a nucleoside. In the ribose nucleosides, there are three hydroxyl groups on the sugar

FIGURE 1

The primary structure of a nucleotide chain, the bases and the sugar moieties.

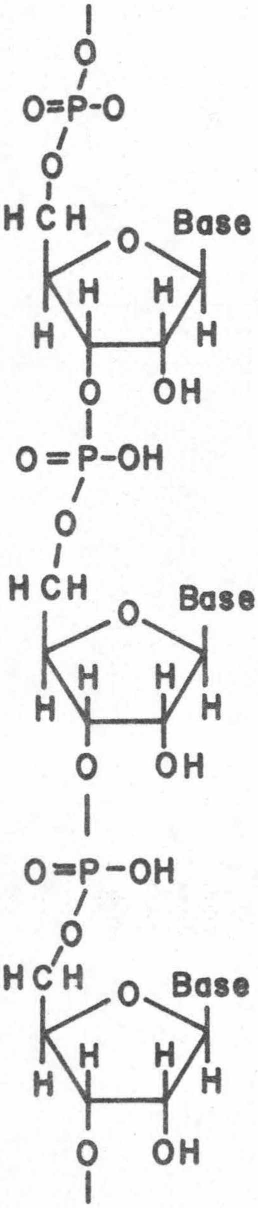
O=P-O
HCH
Base
O=P-OH
HCH
Base
O=P-OH
HCH
Base
OH

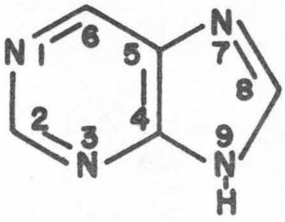

purine

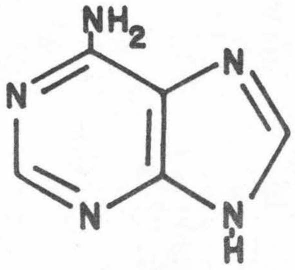

adenine

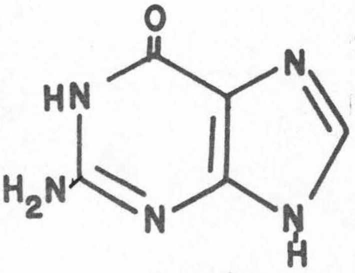

guanine

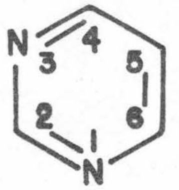

pyrimidine

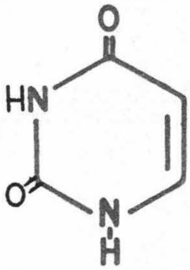

uracil

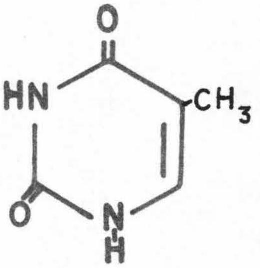

thymine

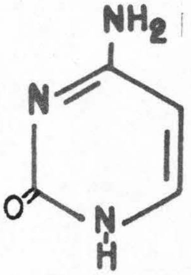

cytosine

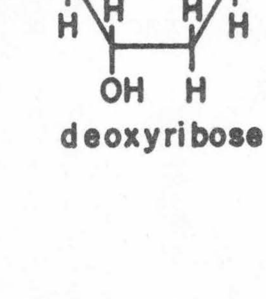

deoxyribose

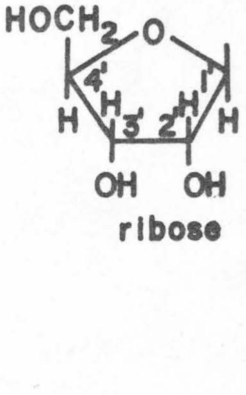
5'
HOCH2
4'
3'
2'
1'

ribose

and, consequently, there are three possible positions for phosphorylation. In the naturally occurring polynucleotides, each phosphate group is esterified to the 3′hydroxyl group of the preceding sugar and to the 5′hydroxyl group of the following sugar.

The two classes of nucleic acids have very specific biological roles. DNA is generally responsible for the hereditary transmission of genetic information. RNA is responsible for transcribing this genetic information and for translating it into the synthesis of proteins. Recently, two studies(1, 2) have indicated that there are instances when the normal process can be inverted and RNA can act as a template for the synthesis of DNA. The implications of these findings are intriguing.

RNA can be subdivided into three main types. Approximately 80 per cent of the RNA is ribosomal RNA (rRNA). The rRNA is of high molecular weight, and, together with protein, it forms the ribosome. The exact biological role of the rRNA is not known. About 15 per cent of the RNA is transfer RNA (tRNA). It is the smallest nucleic acid; each molecule has about 75 bases and is specific for a particular amino acid. The tRNA is recognized by a specific aminoacyl-tRNA synthetase and the appropriate amino acid is bonded to it. The tRNA then transports the amino acid to the ribosome. At approximately the middle of the tRNA chain there are three bases which are known as the anticodon. The anticodon links up with the corresponding codon of three bases on the messenger RNA (mRNA) which is at the ribosome. Subsequently, the amino acid carried by the tRNA is transferred to the growing polypeptide chain at the ribosome, and the uncharged tRNA is released. The mRNA composes approximately 5 per cent of the RNA. It acts as an intermediary between the cellular DNA and the ribosome. After being synthesized on a DNA template, the mRNA becomes attached to the ribosome which is thus activated and able to provide a template for the synthesis of a specific polypeptide chain. The roles of the various RNA molecules are depicted in Figure 2.

The structure of DNA proposed by J. D. Watson and F. H. C. Crick(3) in 1953 has been accepted. DNA is a double right-handed helix consisting of two polynucleotide chains winding around the same axis. The two strands are held together by hydrogen bonding between complementary bases. Adenine pairs with uracil, and guanine pairs with cytosine (Figure 3). The bases have a vertical spacing of 3.4 Å and a chain of ten nucleotides form one complete turn in the helix.

The structure of the RNA's has been more elusive. The most work has been done with tRNA because it is the smallest and the best defined of the RNA's. Considerable experimental evidence indicates that it does possess a stable three dimensional structure. A cloverleaf secondary structure has become accepted for tRNA (Figure 4). This structure maximizes the formation of complementary Watson-Crick type base pairing for the primary sequences of tRNA which are known. The structure features regions of base pairing and unpaired loops. The central loop of the three loop regions contains the anticodon. The tertiary structure obtained by the positioning of the loops and paired regions is not known at this time.

The significance of the double stranded structure of DNA has

FIGURE 2

The process of polypeptide formation takes place at the ribosome. As shown schematically in the drawing, the messenger RNA which carries the information stored in the DNA is attached to the ribosome. Transfer RNA, in this case alanine tRNA, becomes bound to the appropriate amino acid (at the top). The anticodon (IGC) of the tRNA then pairs with the appropriate codon (GCC) on the mRNA (center). Subsequently, the amino acid is transferred to the growing polypeptide chain and then the tRNA is released (at the bottom).

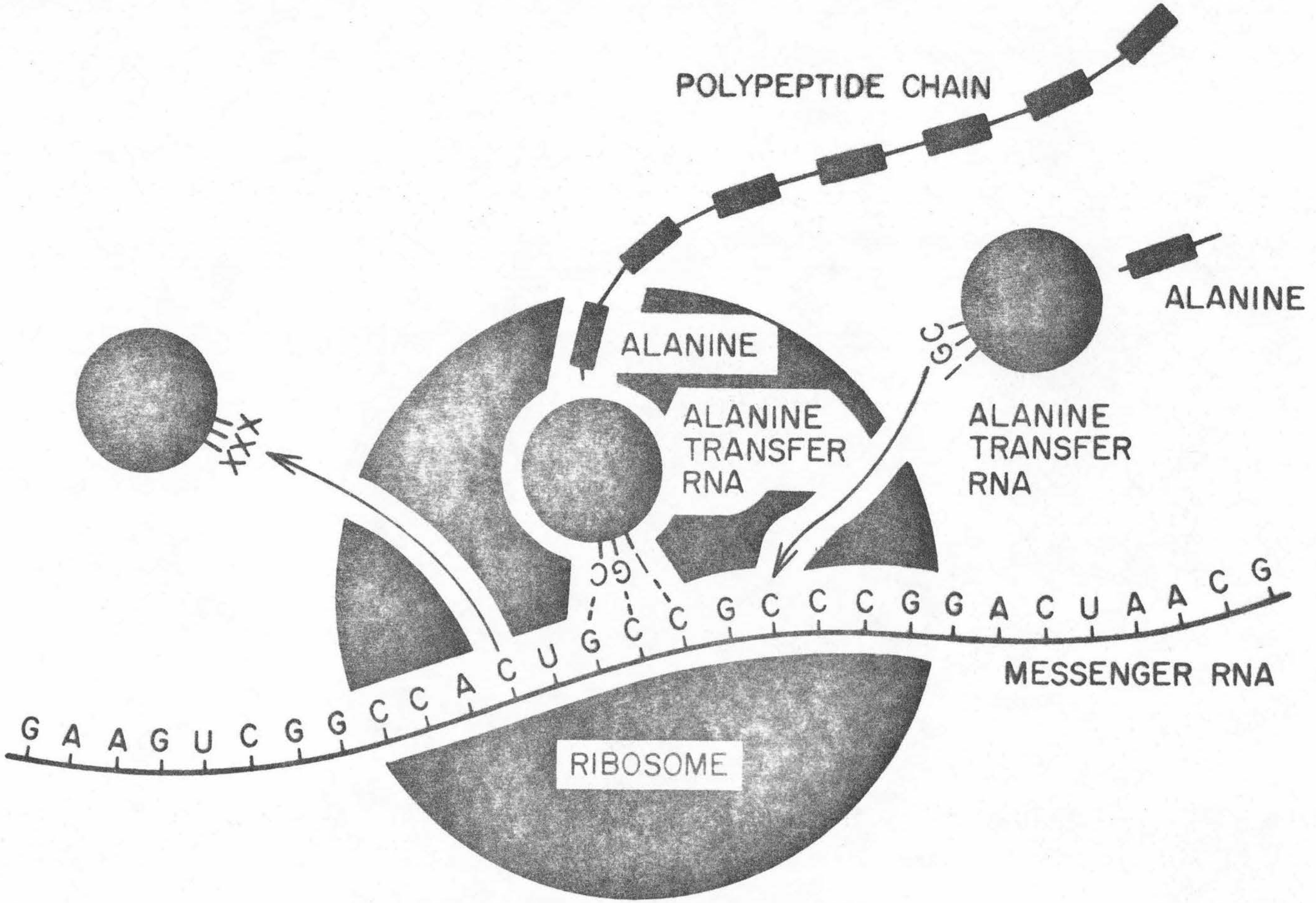
POLYPEPTIDE CHAIN
ALANINE
ALANINE
ALANINE TRANSFER RNA
ALANINE TRANSFER RNA
GC
GC
XXX
G A A G U C G G C C A C U G C C G C C C G G A C U A A C G
MESSENGER RNA
RIBOSOME

FIGURE 3

Watson-Crick base pairing of the common nucleic acid bases.

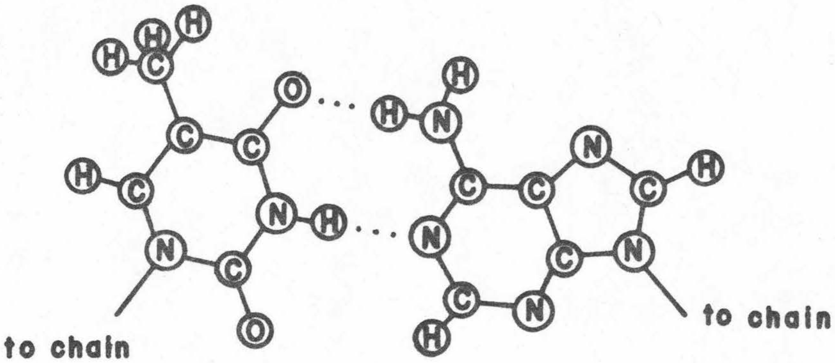
to chain
to chain

thymine adenine

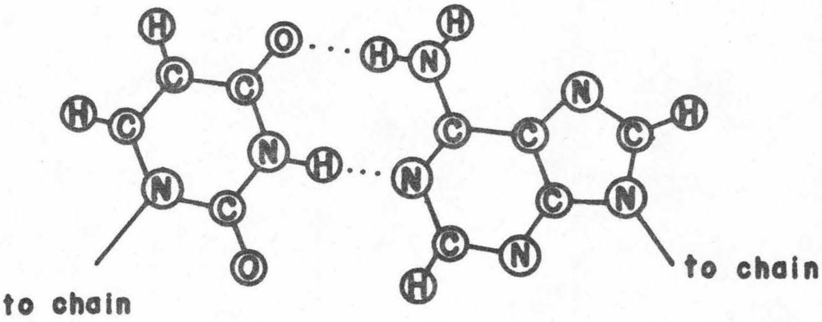
to chain
to chain

uracil adenine

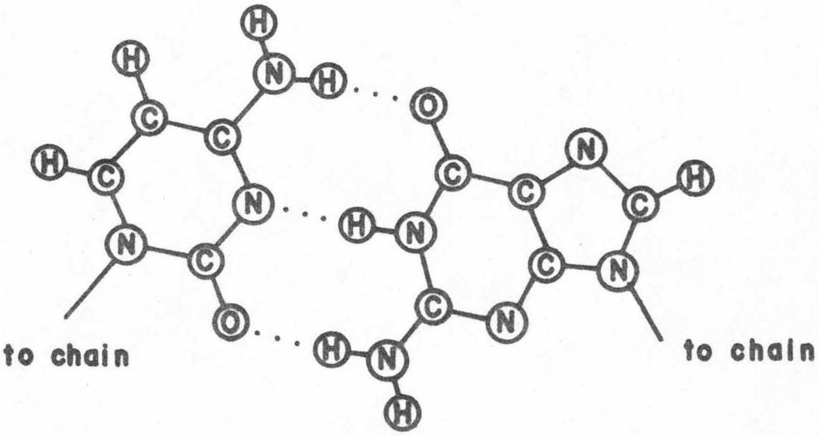
to chain
to chain

cytosine guanine

FIGURE 4

Generalized cloverleaf secondary structure of tRNA.

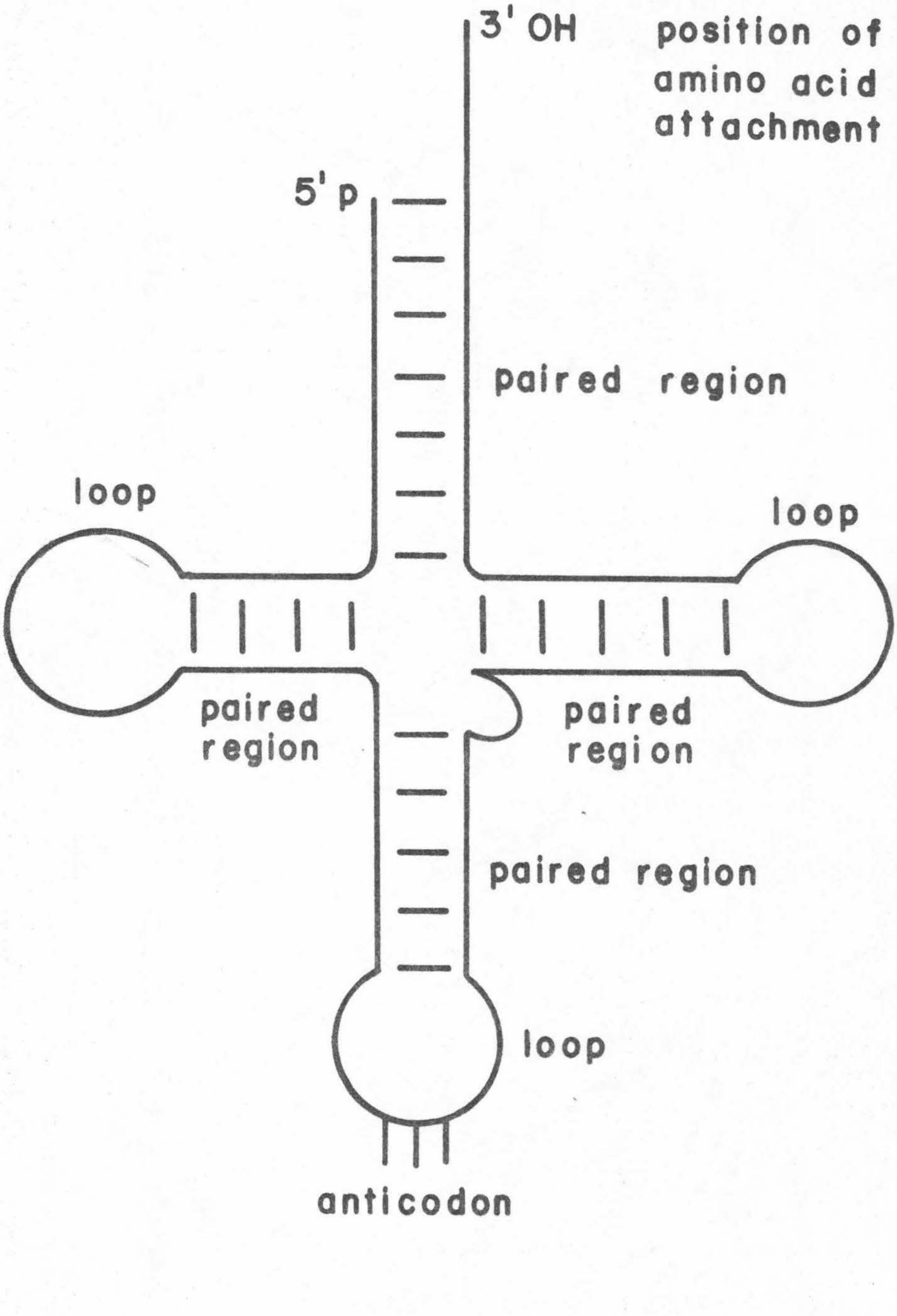
3' OH
position of amino acid attachment
5' p
paired region
loop
loop
paired region
paired region
paired region
loop
anticodon

been well established. The fact that the chains are complementary makes the process of duplication and hereditary transmission understandable.

The biological significance of the tertiary structure of tRNA is well recognized but poorly defined. At this point, it is not possible to separate entirely those characteristics of tRNA which are due to its tertiary structure and which are due to its base composition. The tRNA molecule must be recognized and bonded to a specific amino acid by a specific enzyme molecule. It must combine with the appropriate codon on the mRNA and position the amino acid so that it can be transferred to the growing polypeptide chain. Also, nucleases are able to split the tRNA molecules only at specific points. Any tertiary structure proposed for tRNA must be compatible with these, and other, observations.

In the period following the proposal of the double stranded helical structure of DNA,(3) it was believed that the base pairing hydrogen bonds provided the principal stabilizing force for the DNA helix in the solid state and in solution. Since then, however, it has become accepted that a very significant contribution to the conformation of the nucleic acids is provided by the vertical stacking of the adjacent bases along a nucleotide strand. The formation of a stack brings each planar base close to its neighbors and consequently maximizes van der Waals' and hydrophobic attractions. In addition to the overlapping of the bases, other degrees of freedom which play a role in dictating the overall conformation of a nucleic acid molecule include the orientation of a base with respect to its glycosidic bond and the conformation of the furanose ring of each sugar moiety. There is also a marked dependence of the conformation upon the concentration of divalent cation present.

The formation of stacks in solutions of mononucleosides and nucleotides is well established.(4-9) The work carried out on these systems indicates that purine-purine interactions are stronger than purine-pyrimidine interactions which, in turn, are stronger than pyrimidine-pyrimidine interactions.

Since it is reasonable to assume that the intramolecular base-stacking of the dinucleotides should be representative of the nearest-neighbor interactions in a polynucleotide, conformational studies were extended to the dinucleotide systems.(10-14) In these systems, as well, it was possible to make comparisons between the stacking tendencies of the various possible dinucleotide sequences. Consequently, the results are indicative of some of the sequence dependent properties which can be expected in the polynucleotide systems.

The next simplest system available for study is the trinucleotide chain. Here, the central base should be exposed to approximately the same forces as a nucleoside in a longer polynucleotide chain. Experimental results(15) show that the interactions of the central base in the trinucleotide can be predicted quite well by using the results of the studies on the dinucleotide system.

The homopolynucleotides have been used as model systems for RNA.(16-20) Studies on the homopolynucleotides have emphasized the point that the observed conformation which arises from the stacking of successive bases along the polymer chain is a dynamic arrangement in which ordered and unordered regions are constantly shifting. A detailed study of the polyribonucleotides of adenine and cytosine will be reported on in the following section.

The use of the homopolynucleotides as model systems is expedient because of their simplicity relative to tRNA itself. However, caution must be exercised in extending the results obtained for the homopolynucleotides to tRNA. In tRNA, there is a well defined sequence of nucleosides which make complementary hydrogen bonding of the various regions of the molecule possible. Studies of two specific tRNA molecules are also included in the following section.

Proton magnetic resonance (pmr) provides a sensitive method for studying the base-stacking tendencies of nucleotides in solution. When the π electrons of a ring molecule, such as a nucleic acid base, are sufficiently mobile, the application of an external magnetic field perpendicular to the plane of the ring produces a diamagnetic current in the plane of the ring. This ring current in turn produces a secondary magnetic field which opposes the primary field above and below the plane of the molecule and reinforces the primary field around the periphery of the ring.(21) Consequently, in a vertical base stack, protons on the bases above and below another base are shielded and thus are subjected to a field which is smaller than the applied field. The resonances of these protons consequently become shifted to higher fields. On the other hand, if the bases are in the same horizontal plane, each base will shift the resonances of the protons on the other base to lower fields since the protons will be in the deshielded region and thus subjected to a magnetic field which is larger than the applied field.

Proton magnetic resonance is also capable of monitoring the important horizontal interaction of hydrogen bonding. The formation of a hydrogen bond disturbs the electronic structure of the molecule and alters its magnetic susceptibility.(22) These changes can result in the shifting of the resonances of the molecule. At the hydrogen involved in the bonding, there is a reduction in the electron density due to the electrostatic character of the bond. Consequently, there is a reduction in the shielding at the hydrogen which is observed as a shifting of the resonance to lower field. The studies of the nucleotides are normally done on deuterium oxide solutions in order to minimize the interference of the resonance of the water protons with the resonances of the nucleotide. The protons which participate in hydrogen bonding also exchange rapidly with the water protons of the solvent. Thus, in deuterium oxide solution, the hydrogen bonded protons of the complementary bases cannot be observed by pmr.

The calculation of chemical shifts is quite complex and many factors must be taken into consideration.(23) In addition to the ring-current and hydrogen-bonding factors, other short range forces which are important include the anisotropy of neighboring atoms or molecules, van der Waals' or dispersion forces and permanent dipole or quadrupole interactions.

Proton magnetic resonance provides information concerning very specific regions of a molecule. Consequently, optical studies and magnetic resonance studies are often complementary since optical measurements are less localized and provide data involving the entire electronic system of a molecule. The pmr method clearly has its most important advantage in its extreme sensitivity to minute structural and conformational changes within molecules and to environmental effects. When the rotation of a molecule in solution is slow, the coupling of the various magnetic dipoles of the nuclei within the molecule are not averaged out and the linewidths of the resonances become large. Consequently, both the position and the width of a resonance provide information about the molecule or about a specific region of the molecule.

The conformations of the macromolecules in a biological system are of prime importance. In order to appreciate the functioning of the various units it is necessary to know in detail their three-dimensional form and their potentials for interaction. Progress has been made in the elucidation of the structures of the nucleic acids but there is still much which we do not know. Studies directed toward gaining a more detailed knowledge of the nucleic acids from the single base units to the complex double and single stranded forms is a necessary step toward understanding many biological processes.

The work described in the following section is an extension of earlier work(13, 14) on the pmr of dinucleotides. A study of the nearest neighbor interactions in a single stranded system capable of base stacking is conducted by using a trinucleotide and two homopolynucleotides. Comparisons are made between the short chain nucleotide and the long chain polynucleotide. Subsequently, two studies involving specific tRNA molecules are reported.

2. PROTON MAGNETIC RESONANCE OF POLY-ADENYLIC AND POLYCYTIDYLIC ACIDS

2.1. Introduction

The homopolynucleotides have frequently been used as models for the more complex RNA molecules. The use of the homopolynucleotides permits the investigation of the base stacking interaction which has been shown to make a significant contribution to the stability and conformation of the nucleic acids.(4-20) A knowledge of the intramolecular interactions in the simpler single stranded nucleic acids should provide a basis for understanding the mechanisms which control the physical characteristics of the biologically important RNA molecules.

Many studies have been carried out in an effort to understand the secondary structure of polyriboadenylic acid (poly A). In aqueous solution at neutral pH, poly A is usually described as forming a single stranded helix stabilized by stacking of the bases with their planes approximately perpendicular to the helical axis. Analysis of the thermal unstacking of poly A has been focused on the two state stacked-unstacked model. These analyses have been of limited success with ΔH° estimated as -6.5 to -13 kcal/residue mole and ΔS° estimated as -21.4 to -29.3 eu.(24-26) As an alternative to this two state model, the temperature dependence of the optical properties of the dinucleotide have been analyzed on the basis of a torsional oscillator model.(27) The torsional oscillator model is shown to work well for the optical rotatory dispersion of ApA but it does not explain the temperature dependence of the hypochromism. It is suggested that this failure may be due to neglecting oscillations involving the perpendicular separation of the two bases, R, since the hypochromism is proportional to $|R|^{-3}$ while the ORD is proportional to $|R|^{-2}$. It is not claimed that this particular model is more realistic than the two state model, but it is presented as an alternative approach to the problem.

The two state model has been used to predict the pmr results for the thermal unstacking of the tri-, tetra-, and polynucleotides of adenosine and of the polynucleotide of cytidine. The analysis contrasts the details of the stacking processes in the short and long chain nucleotides and suggests an explanation for the observed difference. The study indicates that considerable care must be taken in extrapolating the results of experiments on short chain nucleotides to long chain polynucleotides.

2.2. Experimental

Polyadenylic acid (poly A), K^+ salt, and polycytidylic acid (poly C), K^+ salt, were obtained from Sigma Chemical Company, St. Louis, Missouri, and were used without further purification. Purine was also obtained from Sigma Chemical Company and was sublimed *in vacuo* just prior to use. The ApApA was purchased from Miles Laboratories, Inc., Elkhart, Indiana, and had been converted from the acid form to the sodium salt by J. H. Nelson.(15)

All samples were lyophilized at least twice from either 99.5 atom % D D_2O obtained from Columbia Organic Chemicals, Columbia, South Carolina, or 100.0 atom % D D_2O obtained from Diaprep, Inc., Atlanta, Georgia. All samples except those used in purine concentration studies were prepared and sealed under vacuum in order to minimize the interference from the water resonance.

Tetramethylammonium chloride purchased from Matheson Coleman and Bell was used as an internal standard. It was dried *in vacuo* prior to use.

The proton magnetic resonance spectra were taken on a Varian HR-220 NMR spectrometer. The sample temperature was controlled to ± 1°C by a Varian V-4343 variable temperature unit. The temperature was measured by observing the spectrum of ethylene glycol and using a calibration curve supplied by Varian.

A Hewlett-Packard 200 ABR audio oscillator was used to produce frequency side bands for chemical shift measurements and for triggering a Varian C-1024 time-averaging computer when additional signal-to-noise was necessary. The frequency of these side bands was counted with a Hewlett-Packard 5221 B electronic counter.

Measurements of pH were made with a Leeds and Northrup 7401 pH meter equipped with a miniature electrode assembly. The system was standardized to read pH. The standard correction was applied to determine the pD:(28) pD = pH (meter reading) + 0.40.

2.3. Results and Discussion

2.3.1. Proton Magnetic Resonance Spectrum of Polyadenylic Acid.

The pmr spectrum of poly A has been observed previously.(29-31) The temperature dependence of the H_2 and H_8 proton resonances is shown in Figure 5. The H_8 resonance is broader than that of the H_2; the width difference becomes greater as the temperature is lowered, and below about 17°C the H_8 resonance is too broad to be observed while the H_2 resonance is about 20 Hz wide. In a study of the dinucleotide of adenine (ApA), Chan and Nelson(13) concluded that both of the bases in an ApA stack are oriented preferentially in the anti conformation relative to the ribose. The anti conformation has been shown to be favored in other ribonucleotide systems as well.(14, 32) In the anti conformation, the adenine base is oriented so that the H_8 is above the ribose ring.(33) Thus, in this conformation, the H_8 is close to the $H_{2'}$, $H_{3'}$, $H_{5'}$, $H_{5''}$ ribose protons and to the furanose ether oxygen. It is reasonable that the proximity of the H_8 to these atoms causes broadening of the resonance due to dipolar interactions. The broadening of this resonance as the temperature is lowered can be attributed to the bases becoming more nearly locked in the anti conformation as the molecule becomes more completely stacked.

The ribose region of the poly A spectrum is shown in Figure 6. The ribose region of the pmr spectra of adenine nucleotides has been studied previously.(34-36) The highest field resonance in the ribose region is assigned to the $H_{5'}$ ($H_{5''}$) protons. Using the same assignment for the poly A ribose region, it is observed that the $H_{5'}$ ($H_{5''}$) resonance becomes quite broad especially as the temperature is lowered. This broadening can be interpreted as evidence of restricted molecular motion and of dipolar interactions between the various ribose protons, the base H_8, the furanose ether oxygen, and the phosphate group.

FIGURE 5

220 MHz pmr spectra of the H_2 and H_8 of poly A at 17°C and 32°C.

H_8 and H_2 Proton Resonances of Polyadenylic Acid

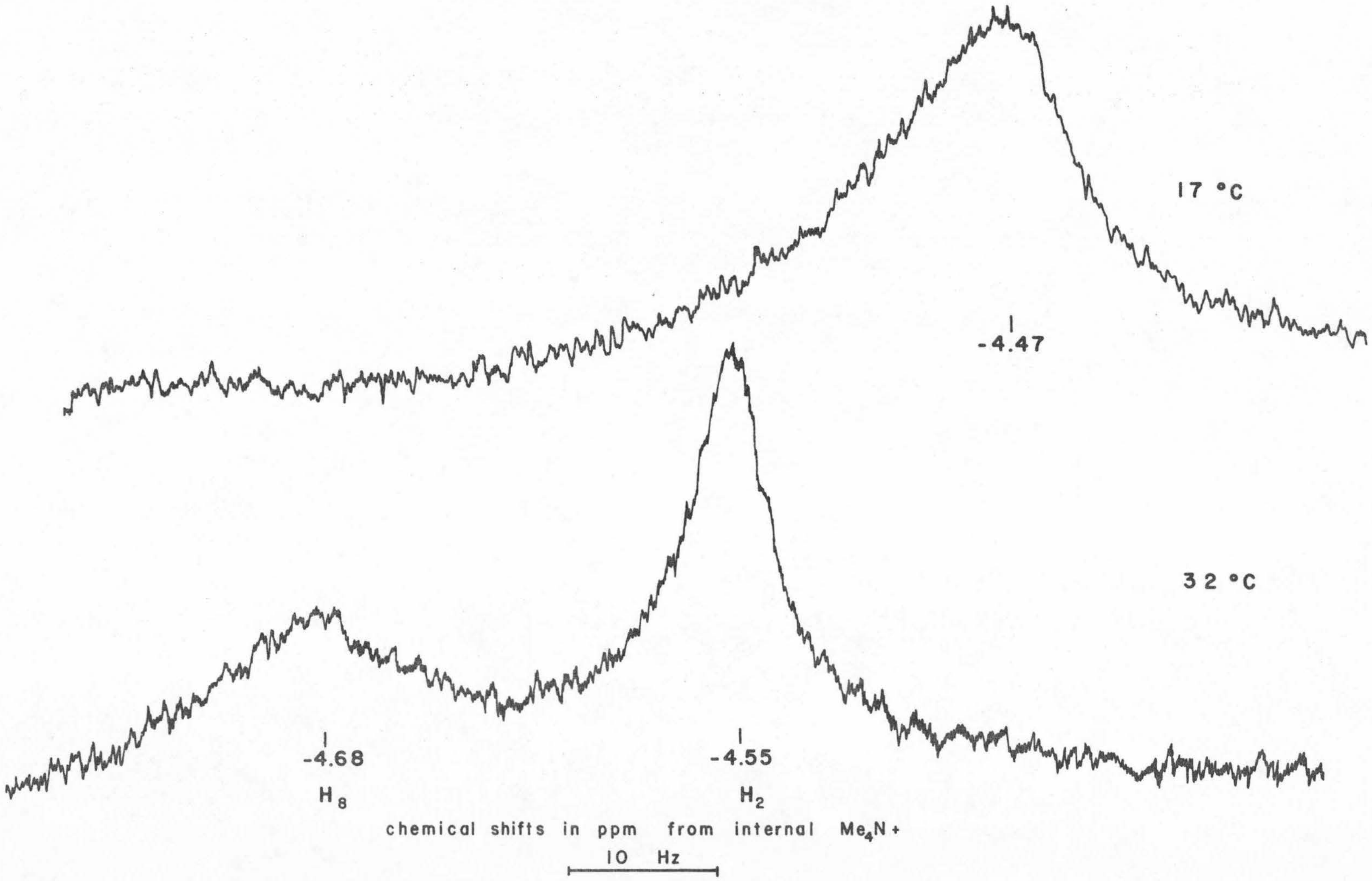

FIGURE 6

220 MHz pmr spectra of the ribose region of poly A at 17°C and 31°C.

Ribose Region of 220MHz pmr Spectra of Polyadenylic Acid

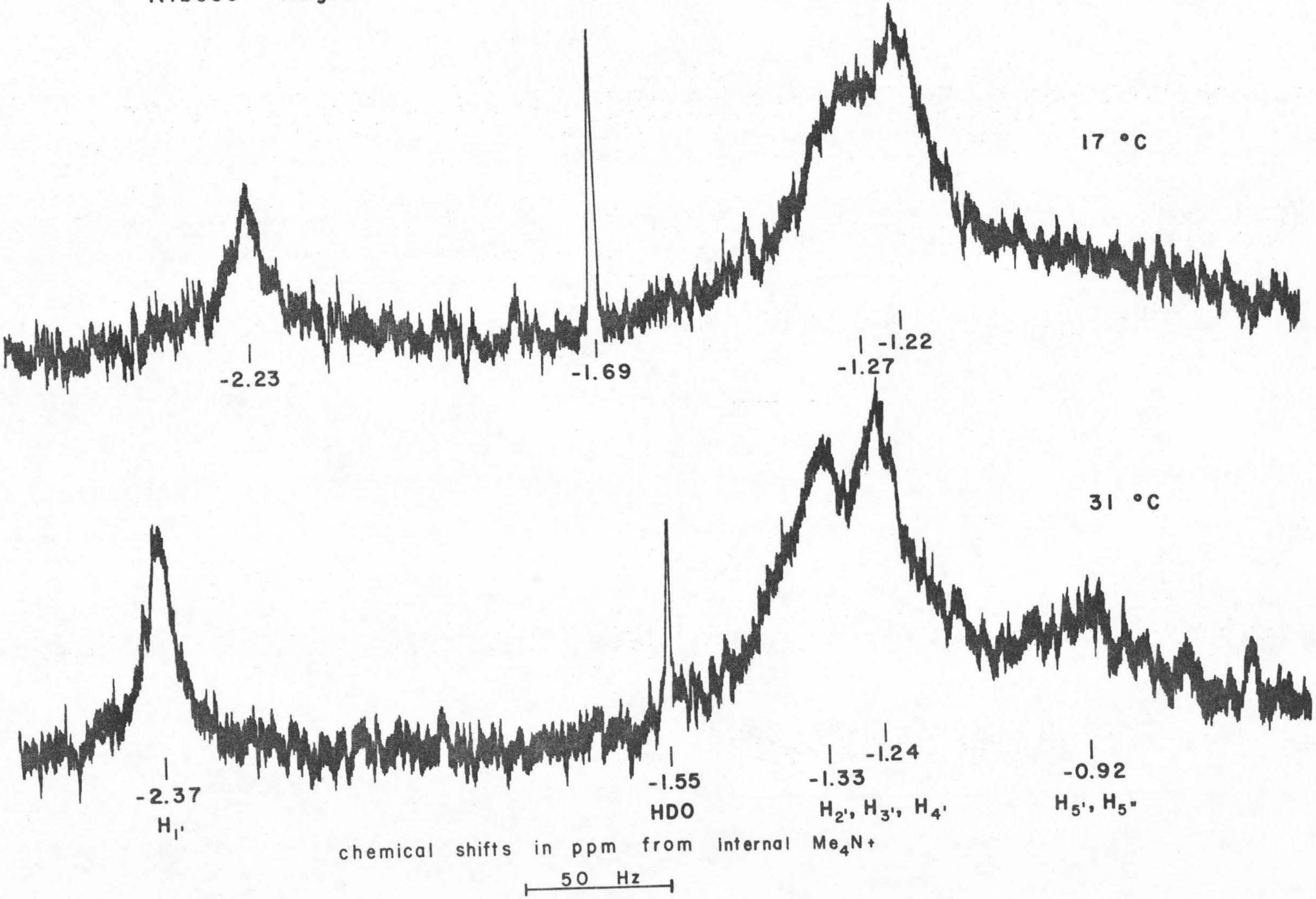

2.3.2. Temperature Variation of the Base Proton Chemical Shifts. In a base stack, the resonance position of the protons on one base are shifted by the diamagnetic ring currents of the neighboring bases. Consequently, the position of an observed resonance is indicative of the extent of stacking in the system. The shielding of the ring currents produced in a benzene molecule which is rotating rapidly about all axes in an external magnetic field has been calculated(37) by C. E. Johnson and F. A. Bovey. C. Giessner-Prettre and B. Pullman(38) have made calculations which compare the ring currents of the various purine and pyrimidine bases to the ring current of benzene. Some of their results are shown in Table I. Since the screening constant is directly proportional to the diamagnetic current(21) the Johnson-Bovey values for the shielding of benzene can be corrected to approximate the shielding expected for the various nucleic acid bases.

The distance of the base protons from the neighboring base centers can be approximated by using CPK space filling models. The overlap of the bases in the stacked anti conformation of an adenosine nucleotide chain is depicted in Figure 7.(13) From this drawing, one can approximate the distance from the H_2 and H_8 protons to the centers of the rings of the neighboring base. The horizontal distances of the protons from the centers of the neighboring base rings are the p values and are expressed in benzene ring radii (1.39 Å = 1 radius). The vertical distance, z, from the proton of interest to the neighboring ring plane is also expressed in ring radii. The vertical spacing of the adenine bases in a neutral polyadenylic acid helix was recently

TABLE I. Comparison of the ring currents of several nucleic acid bases with that of benzene.*

	Ring current
Benzene	1.00
Pyrimidine	0.905 - 1.067
Cytosine	0.169 - 0.308
Uracil	0.021 - 0.120
Purine:	
hexagonal ring	0.957 - 1.123
pentagonal ring	0.429 - 0.805
Adenine:	
hexagonal ring	0.767 - 0.978
pentagonal ring	0.427 - 0.792
Guanine:	
hexagonal ring	0.149 - 0.287
pentagonal ring	0.440 - 0.718

---

* C. Giessner-Prettre and B. Pullman, Compt. Rend., 261, 2521 (1965).

FIGURE 7

Overlap of the bases in a stacked adenosine nucleotide chain.

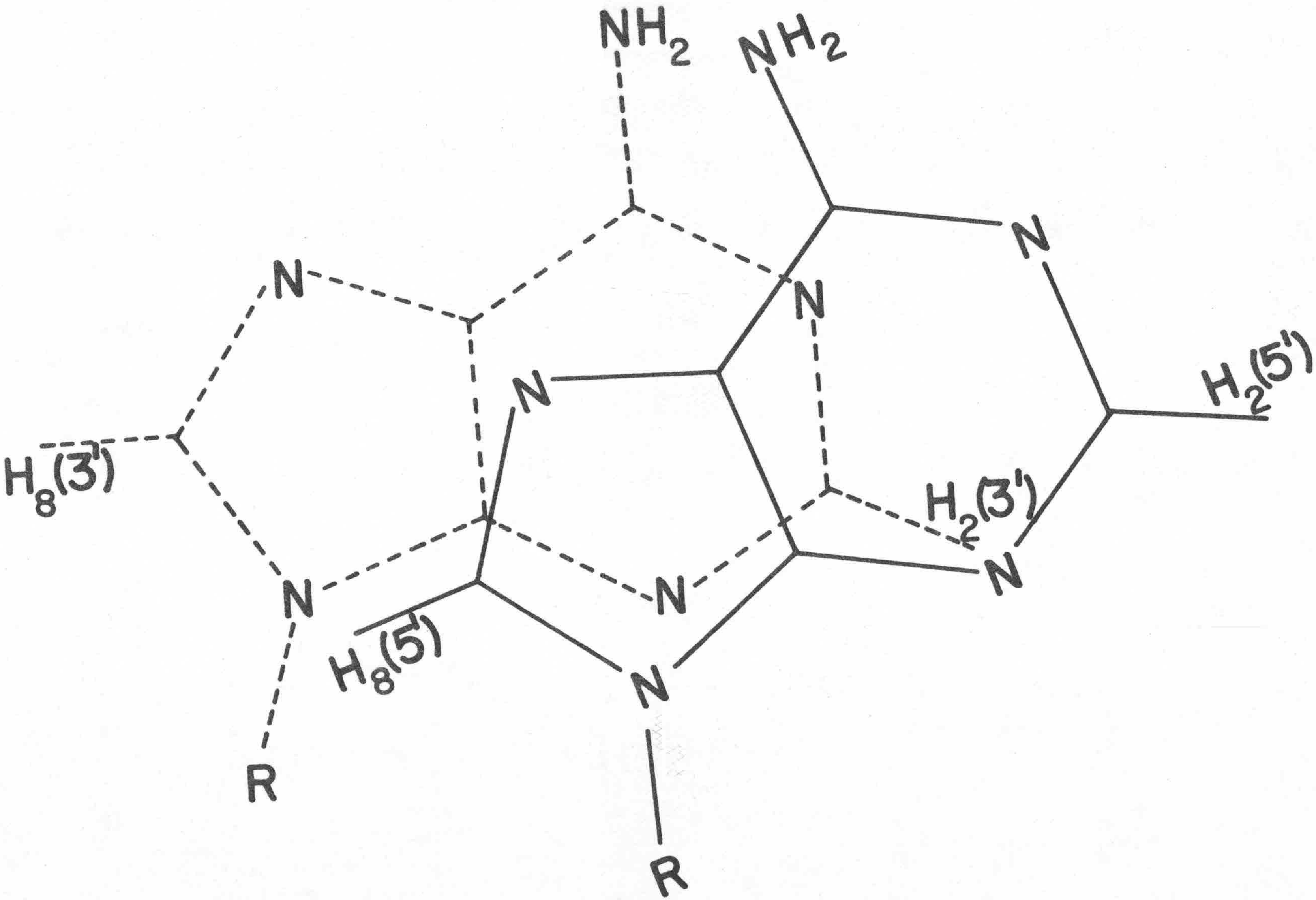
NH$_2$
NH$_2$
N
N
N
N
H$_2$(5')
H$_8$(3')
N
H$_2$(3')
N
N
N
H$_8$(5')
N
R
R

measured to be 3.62 Å.$^{(39)}$ Therefore, as an approximation, z can be set equal to 2.6 radii for the poly A base spacing in a neutral completely stacked poly A solution. The distances and the Johnson-Bovey screening constants estimated for the H_8 and H_2 protons of adenosine are shown in Table II. The screening constants obtained by using the Giessner-Prettre and Pullman ring current calculations are also shown in this table. From these approximations, one would expect the screening contribution of the neighboring base rings at the H_8 of the central base in a stack of A's to be between -0.6 and -0.9 ppm with respect to the H_8 of an unstacked adenosine. Similarly, the screening contribution at the H_2 of the central base should be between -0.8 and -1.1 ppm with respect to the H_2 of an unstacked adenosine. The negative values indicate a reduction of the apparent field which corresponds to a shifting of the resonances to higher field. These values are, of course, dependent upon the exact orientation of the bases in the stack and upon the vertical separation of the planes of the bases. When the same assumptions are made for a neutral poly C solution, the H_5 of a central base in a cytosine stack would be expected to be subject to a screening constant of -0.16 to -0.29 ppm and the H_6 to be subject to a screening of -0.14 to -0.26 ppm with respect to an unstacked cytosine. A cytosine stack is depicted in Figure 8 and the distances and screening constants are given in Table II. These rough estimates show that if all the assumptions are valid, the shifts of the base protons should be readily measurable and should provide a means of estimating the extent of base stacking in a nucleotide system. One approach to the problem is to use the

TABLE II. Screening contributions from ring currents.

Adenine Stack

	z (radii)	p (radii)	Johnson-Bovey* constant, ppm	corrected shielding constant, ppm minimum	corrected shielding constant, ppm maximum
H_8 (5′) to 3′ pentagonal ring	2.6	1.0	-.74177	-.317	-.587
H_8 (5′) to 3′ hexagonal ring	2.6	1.9	-.33734	-.259	-.330
H_8 (3′) to 5′ pentagonal ring	2.6	3.1	-.03839	-.016	-.030
H_8 (3′) to 5′ hexagonal ring	2.6	4.4	--	--	--
				-.614	-.947
H_2 (5′) to 3′ pentagonal ring	2.6	4.8	--	--	--
H_2 (5′) to 3′ hexagonal ring	2.6	3.2	-.02948	-.023	-.029
H_2 (3′) to 5′ pentagonal ring	2.6	1.8	-.33734	-.144	-.267
H_2 (3′) to 5′ hexagonal ring	2.6	.8	-.84636	-.649	-.828
				-.816	-1.124

Cytosine Stack

	z (radii)	p (radii)	Johnson-Bovey* constant, ppm	corrected shielding constant, ppm minimum	corrected shielding constant, ppm maximum
H_5 (5′) to 3′ ring	2.6	1.0	-.74177	-.125	-.228
H_5 (3′) to 5′ ring	2.6	2.2	-.19822	-.033	-.061
				-.158	-.289
H_6 (5′) to 3′ ring	2.6	1.0	-.74177	-.125	-.228
H_6 (3′) to 5′ ring	2.6	2.7	-.08868	-.015	-.027
				-.140	-.255

* J. W. Emsley, J. Feeney and L. H. Sutcliffe, High Resolution Nuclear Magnetic Resonance Spectroscopy, Pergamon Press, Oxford, 1965, Vol. 1, pp. 140, 595-604.

FIGURE 8

Overlap of the bases in a stacked cytidine nucleotide chain.

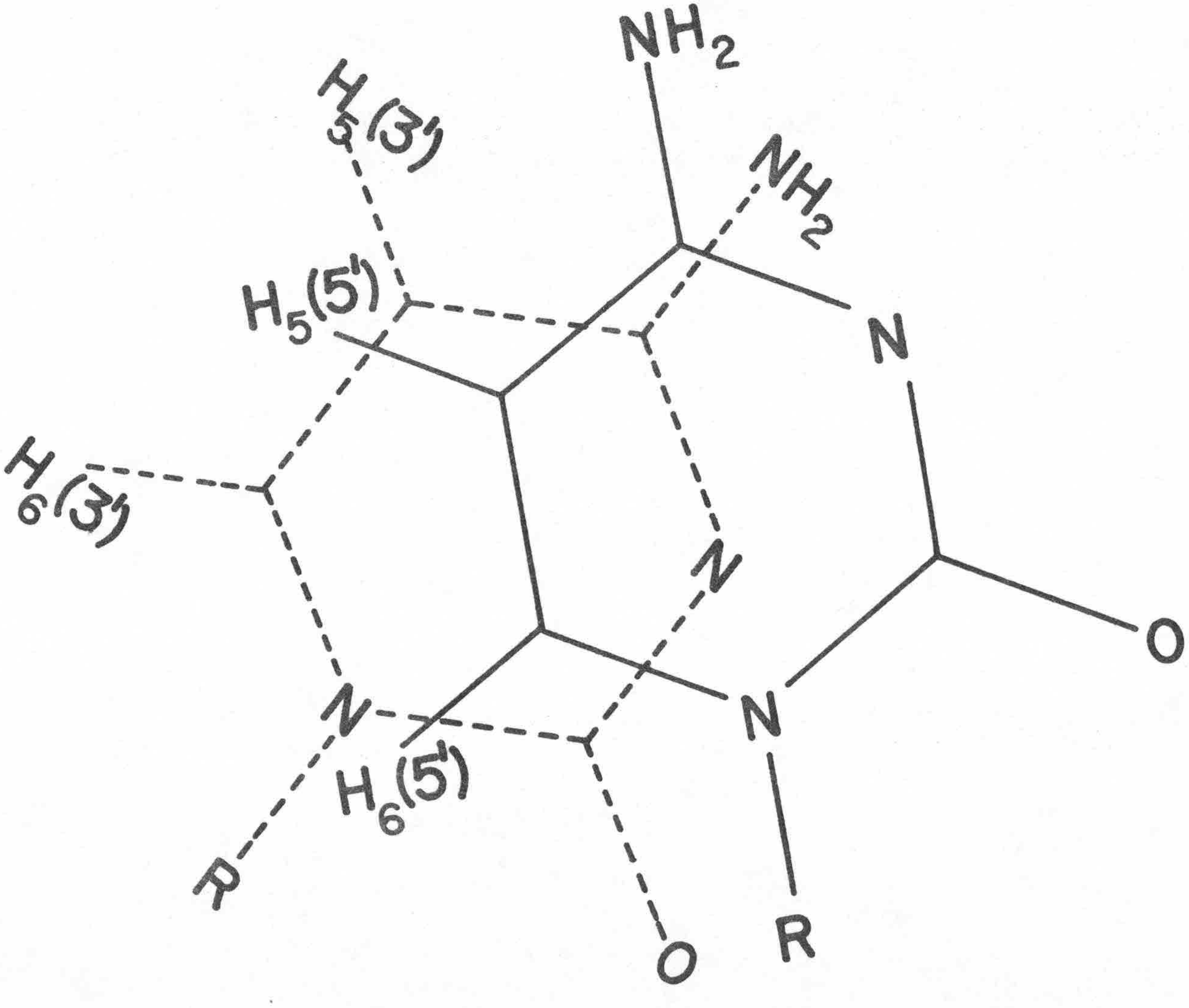
NH$_2$
$H_5(3')$
NH$_2$
$H_5(5')$
N
$H_6(3')$
N
O
N
N
$H_6(5')$
R
O
R

two state model developed for other systems.

The general problem of dealing with the theoretical principles for understanding and predicting the conformations of biological macromolecules was reviewed recently by H. DeVoe.(40) A number of attempts have been made to quantitatively correlate the optical properties of a nucleotide system to the extent of intramolecular base stacking in the system.(20, 24, 25, 41, 42) J. Applequist and V. Damle(24) have used a one dimensional Ising lattice as a model for the equilibrium between a random coil and a single stranded helix. They have derived exact equations for the sequence length distribution of stacked bases in chains of various lengths and have applied this analysis to the hypochromism of oligomers of adenylic acid. Poland, et al.(25) performed a similar analysis of the optical rotatory dispersion of the oligoadenylates.

The one dimensional model which is used in this analysis(24) assumes a single polynucleotide strand which is capable of forming a helix stabilized by the interaction of the bases in the linear array. The interactions of each base are limited to those with its two nearest neighbors. The interaction between two bases which results in a stacked configuration is referred to as an "s bond." Only completely formed or broken s bonds are considered. The accessible states of the molecule include all possible sequences of formed and broken s bonds along the nucleotide strand.

The expression derived by Applequist and Damle for the average number of helical sequences with k s bonds per molecular chain of N residues, $\langle v_k \rangle$, is $\langle v_k \rangle = \frac{\sigma s^k}{Z_N} \frac{\partial Z_N}{\partial v_k}$

where

Z_N = configurational partition function

$$Z_N = \frac{\lambda_0^N (1 - \lambda_1) - \lambda_1^N (1 - \lambda_0)}{\lambda_0 - \lambda_1}$$

$$\lambda_0 = \tfrac{1}{2}\left\{1 + s + [(1 - s)^2 + 4\sigma s]^{\frac{1}{2}}\right\}$$

$$\lambda_1 = \tfrac{1}{2}\left\{1 + s - [(1 - s)^2 + 4\sigma s]^{\frac{1}{2}}\right\}$$

$$s = \exp\left(\frac{\Delta S^\circ}{R} - \frac{\Delta H^\circ}{RT}\right)$$

σ = helix interruption constant

$$\frac{Z_N}{v_k} = (N - k)\left[\frac{(\lambda_0 - s)^2 \lambda_0^{N-k-1} + (\lambda_1 - s)^2 \lambda_1^{N-k-1}}{(\lambda_0 - \lambda_1)^2}\right]$$

$$+ 2\,\frac{(\lambda_0 - s)(s - \lambda_1)(\lambda_0^{N-k} - \lambda_1^{N-k})}{(\lambda_0 - \lambda_1)^3}$$

The quantity s is defined as the equilibrium constant for the addition of a residue to a previously existing stack of residues. The helix interruption constant, σ, can be defined as the equilibrium constant for the formation of an interruption in a stacked sequence by a process such that the number of stacked residues remains constant. (43) Alternatively, it can also be defined as a correction factor multiplying s to give the equilibrium constant for the stacking of the first pair of residues in a stacked sequence. (44) The quantity σ is thus a measure of the cooperativity of a transition. If the transition is completely noncooperative, then σ is equal to unity.

The two state, stacked-unstacked, model used in the analysis of Applequist and Damle can be applied to the pmr results for the thermal unstacking of the oligo- and polynucleotides. In the polynucleotide system, the resonance observed in the experiment is actually composed of a distribution of resonances from the various bases along the chain. The chemical shift calculation is made for a particular base located at a point away from the end of the chain. The shifts of the protons on this base are calculated using the assumption of fast exchange between the stacked and unstacked configurations. Consequently, for the polynucleotide the chemical shift is approximately given by

$$\delta_{\text{observed}} = \delta_c f + \delta (1 - f)$$

where δ_c is the chemical shift of a proton on a base centrally located in a stack; δ is the shift of a proton on a base which is not stacked and f is the probability that the base is stacked. If the chemical shifts are referenced to the monomer where intramolecular stacking is impossible, then the above relation is

$$\delta_{\text{observed}} = \delta_c f.$$

In the case of the trinucleotide, the resonances of the protons on each of the three bases are observed. The possible configurations are shown in Figure 9. The observed chemical shift for protons on the central base of the trinucleotide relative to the monomer should be

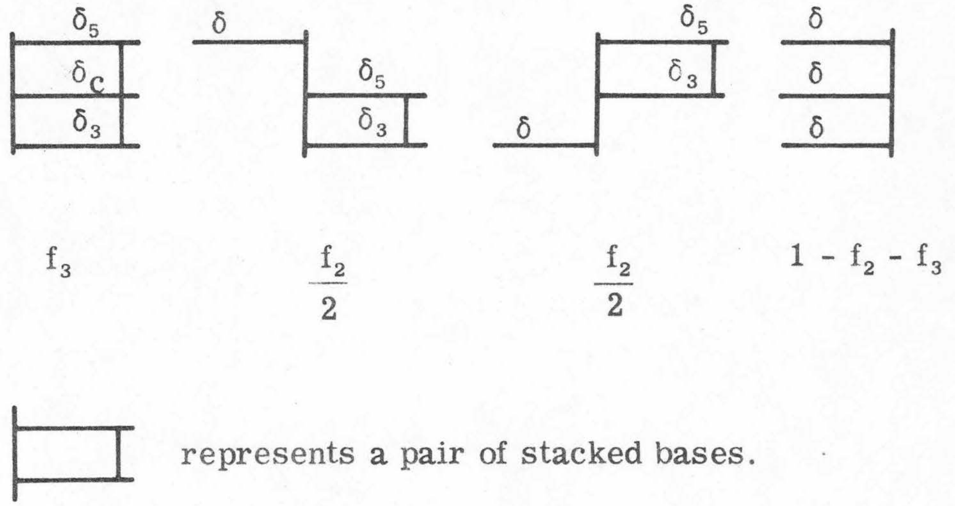
δ_5
δ_c
δ_3
δ
δ_5
δ_3
δ
δ_5
δ_3
δ
δ
δ
f_3
$\frac{f_2}{2}$
$\frac{f_2}{2}$
$1 - f_2 - f_3$
represents a pair of stacked bases.

FIGURE 9

The chemical shifts of the protons on the bases are designated as δ_3 for the protons on the 3′ base of a stack, δ_5 for the protons on the 5′ base of a stack, δ_c for the protons on the central base of a stack, and δ for the protons on a base which is not stacked. The probability of each configuration is given beneath the representation of that configuration.

$$\delta_{\text{observed}} = \delta_5 \frac{f_2}{2} + \delta_3 \frac{f_2}{3} + \delta_c f_3 .$$

For a tetranucleotide the possible configurations are shown in Figure 10. The chemical shifts of the protons on the two central bases relative to the monomer are

$$\delta_{\text{observed}} = \delta_3 \frac{f_2}{3} + \delta_5 \frac{f_2}{3} + \delta_5 \frac{f_3}{2} + \delta_c \frac{f_3}{2} + \delta_c f_4$$

and

$$\delta_{\text{observed}} = \delta_3 \frac{f_2}{3} + \delta_5 \frac{f_2}{3} + \delta_3 \frac{f_3}{2} + \delta_c \frac{f_3}{2} + \delta_c f_4$$

The pmr temperature data for the oligoadenylic acids, (15) for poly A, and for poly C can be fit reasonably well. Because of its position away from the phosphate ribose backbone, the temperature dependent shifts of the H_2 resonance of adenine and the H_5 resonance of cytosine should provide the clearest reflection of the fraction of these bases which are stacked. The influence of the phosphate group has been measured by comparing the nucleoside with the corresponding nucleotide in the monionic form. (9) This comparison shows that the H_8 of 5′AMP is shifted 0.137 ppm to lower field and the H_6 of 5′ CMP is shifted 0.132 ppm to lower field by the phosphate group. Consequently, when the pmr data for these protons were compared with the predictions, the experimental values were increased by 0.137 ppm for H_8 of adenosine and by 0.132 ppm for H_8 of cytidine.

The best fit of the pmr data on the H_2 of adenine is obtained for the enthalpy of stacking, ΔH°, equal to -4.5 kcal/residue mole. From the pmr temperature curves, the melting temperature, the temperature where the slope of the curve is greatest, is approximately

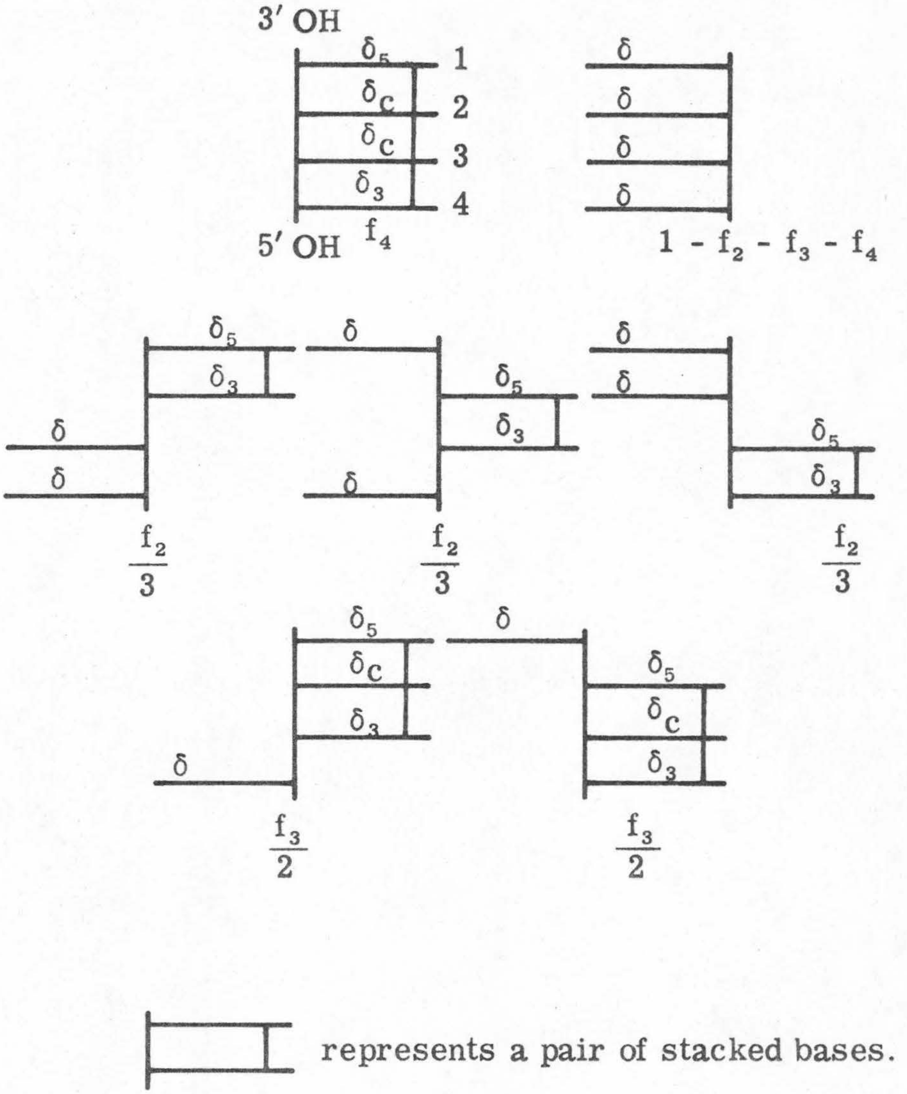
3′ OH
5′ OH
δ5
δc
δ3
δ
1
2
3
4
f4
1 - f2 - f3 - f4
f2/3
f2/3
f2/3
f3/2
f3/2

represents a pair of stacked bases.

FIGURE 10

The chemical shifts of the protons on the bases are designated as δ_3 for the protons on the 3′ base of a stack, δ_5 for the protons on the 5′ base of a stack, δ_c for the protons on the central base of a stack, and δ for the protons on a base which is not stacked. The probability of each configuration is given beneath the representation of that configuration.

50°C for poly A and approximately 35°C for the smaller oligoadenylates. The transition temperature is difficult to measure due to the broadness of the transition. This difficulty is not restricted to the pmr studies but is also apparent in optical studies on these systems. From optical work, A. M. Michelson(45) reports the transition temperature for ApA as 25°C, for poly A as 40°C and for $(Cp)_9C$ as 59°C. Poland, et al.(25) take 30°C as the transition temperature for the oligoadenylate series. Using the transition temperature of 50°C for poly A, the entropy of formation of the stacked state, ΔS°, is -13.9 e.u., and using the transition temperature of 35°C for the small chain molecule, ΔS° is -14.6 e.u.

The degree of cooperativeness as indicated by σ is approximately 0.6. Applequist and Damle(24) report a value of 0.6 and indicate that they can vary σ by as much as 50% before the agreement between experiment and theory becomes clearly poorer. Poland, et al.(25) obtain a value of 0.7. The pmr data was fit using 0.6 but the curves are not very sensitive to changes in this parameter.

Satisfactory agreement (see Figures 11-16) between the experimental data and the predictions was obtained when the above thermodynamic values were used and when the chemical shifts of the various protons for the molecules in the stacked configurations were those shown in Table III. The predicted fractions of s bonds occurring in the various length chains at different temperatures are shown in Table IV.

The necessity of using a larger chemical shift for poly A than for the smaller oligonucleotides indicates that the two state model is

FIGURE 11

Temperature dependence of the H_2 resonances of ApA and of the H_2 of the central base in ApApA.(15) The solid line indicates the predicted temperature dependence for the indicated values of the parameters.

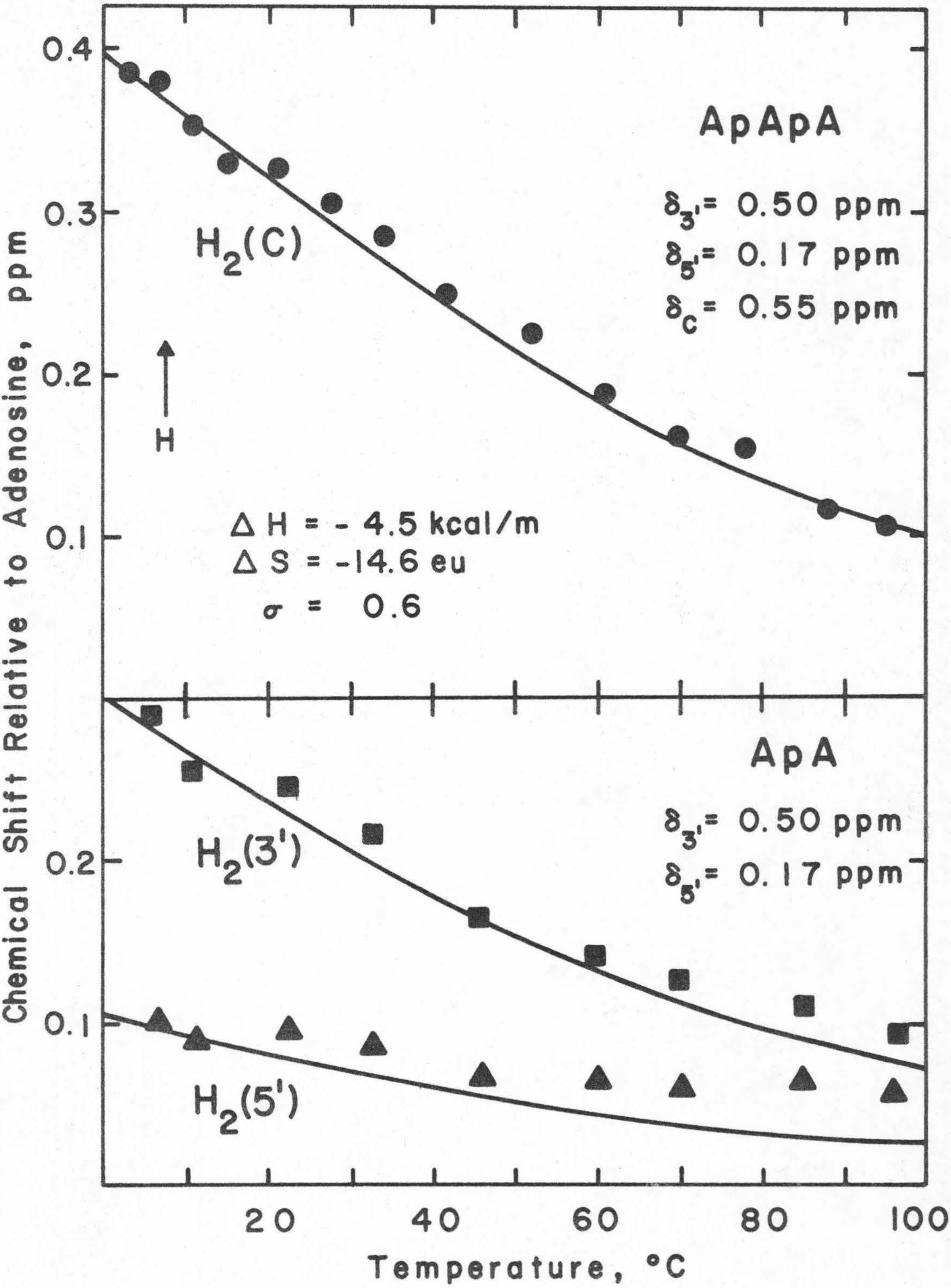
0.4
0.3
0.2
0.1
0.2
0.1
ApApA
$\delta_{3'}$ = 0.50 ppm
$\delta_{5'}$ = 0.17 ppm
δ_C = 0.55 ppm
$H_2(C)$
H
Δ H = - 4.5 kcal/m
Δ S = -14.6 eu
σ = 0.6
ApA
$\delta_{3'}$ = 0.50 ppm
$\delta_{5'}$ = 0.17 ppm
$H_2(3')$
$H_2(5')$
20
40
60
80
100
Temperature, °C
Chemical Shift Relative to Adenosine, ppm

FIGURE 12

Temperature dependence of the two H_8 resonances of the central bases in ApApApA.(15) The solid line indicates the predicted temperature dependence using the indicated values of the parameters.

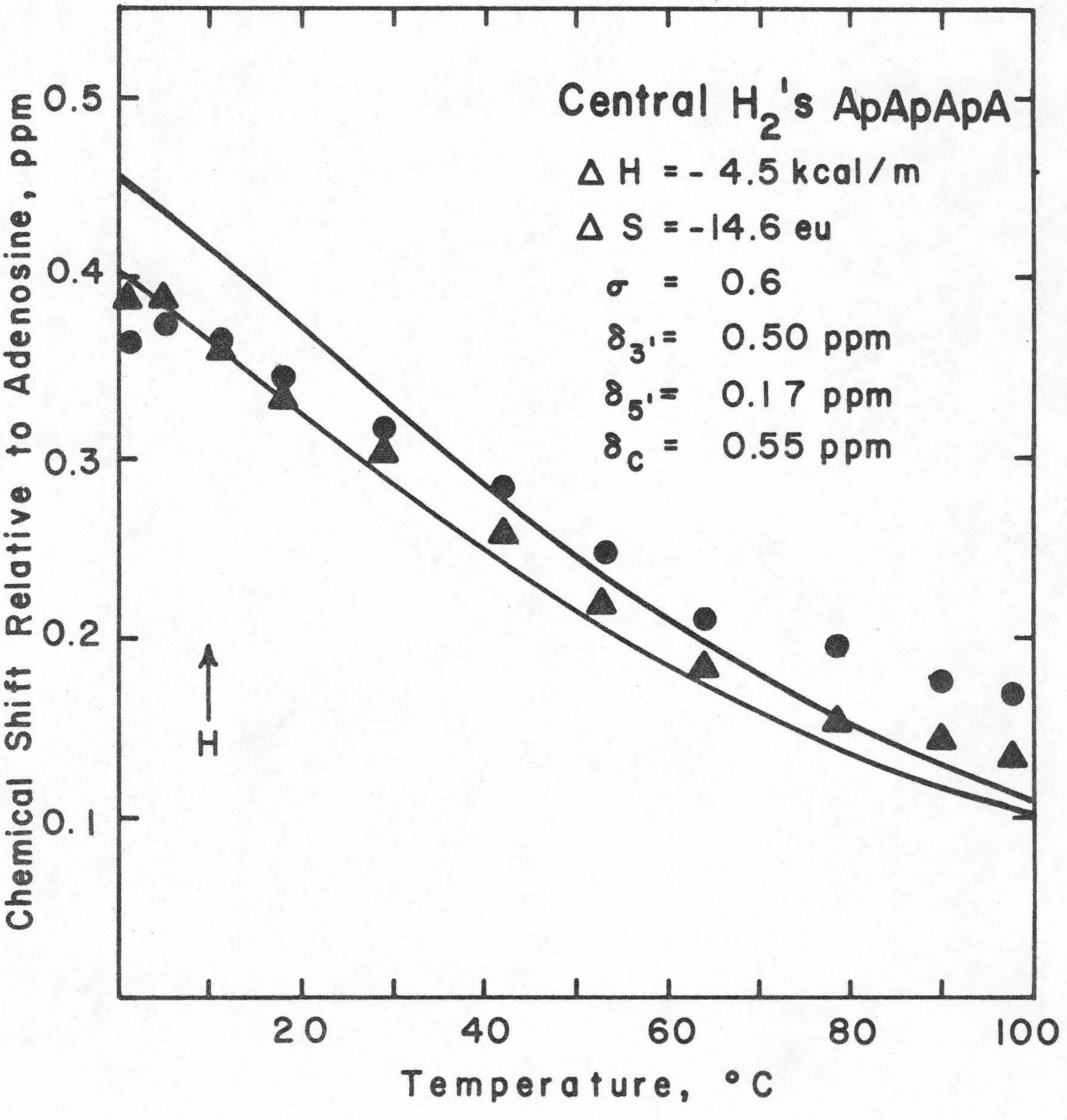
Central H_2's ApApApA
$\Delta H = -4.5$ kcal/m
$\Delta S = -14.6$ eu
$\sigma = 0.6$
$\delta_{3'} = 0.50$ ppm
$\delta_{5'} = 0.17$ ppm
$\delta_C = 0.55$ ppm
Chemical Shift Relative to Adenosine, ppm
0.5
0.4
0.3
0.2
0.1
H
20
40
60
80
100
Temperature, °C

FIGURE 13

Temperature dependence of the H_2 resonance of poly A. The solid line indicates the predicted temperature dependence for the indicated values of the parameters.

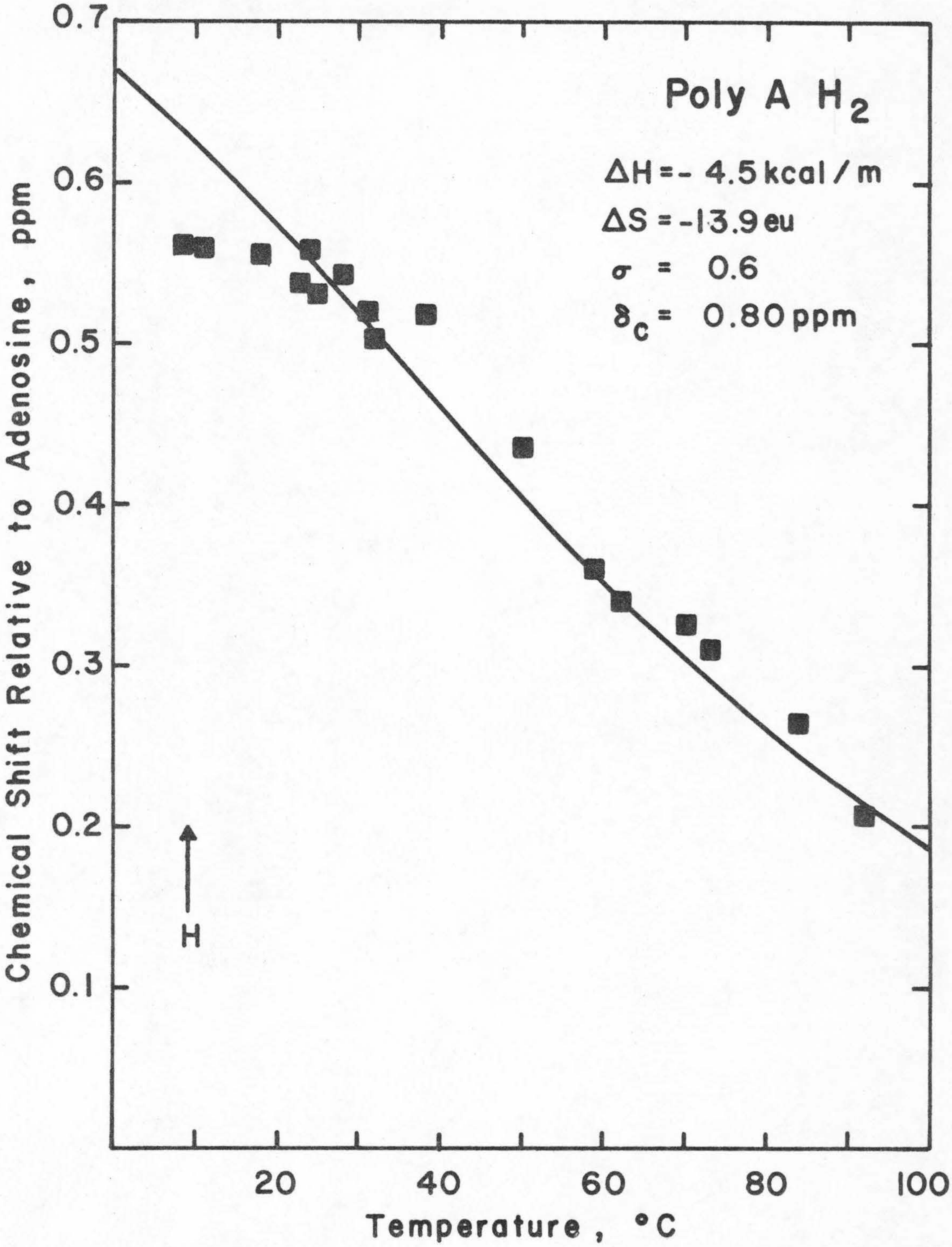
Poly A H_2
ΔH = - 4.5 kcal / m
ΔS = -13.9 eu
σ = 0.6
δ_c = 0.80 ppm
H
Chemical Shift Relative to Adenosine, ppm
0.7
0.6
0.5
0.4
0.3
0.2
0.1
20
40
60
80
100
Temperature, °C

FIGURE 14

Temperature dependence of the H_8 resonances of the 5′ base in ApA and of the central base in ApApA.(15) In order to correct for the effect of the phosphate group 0.137 ppm has been added to the experimental results. The solid line represents the behavior predicted for the indicated values of the parameters.

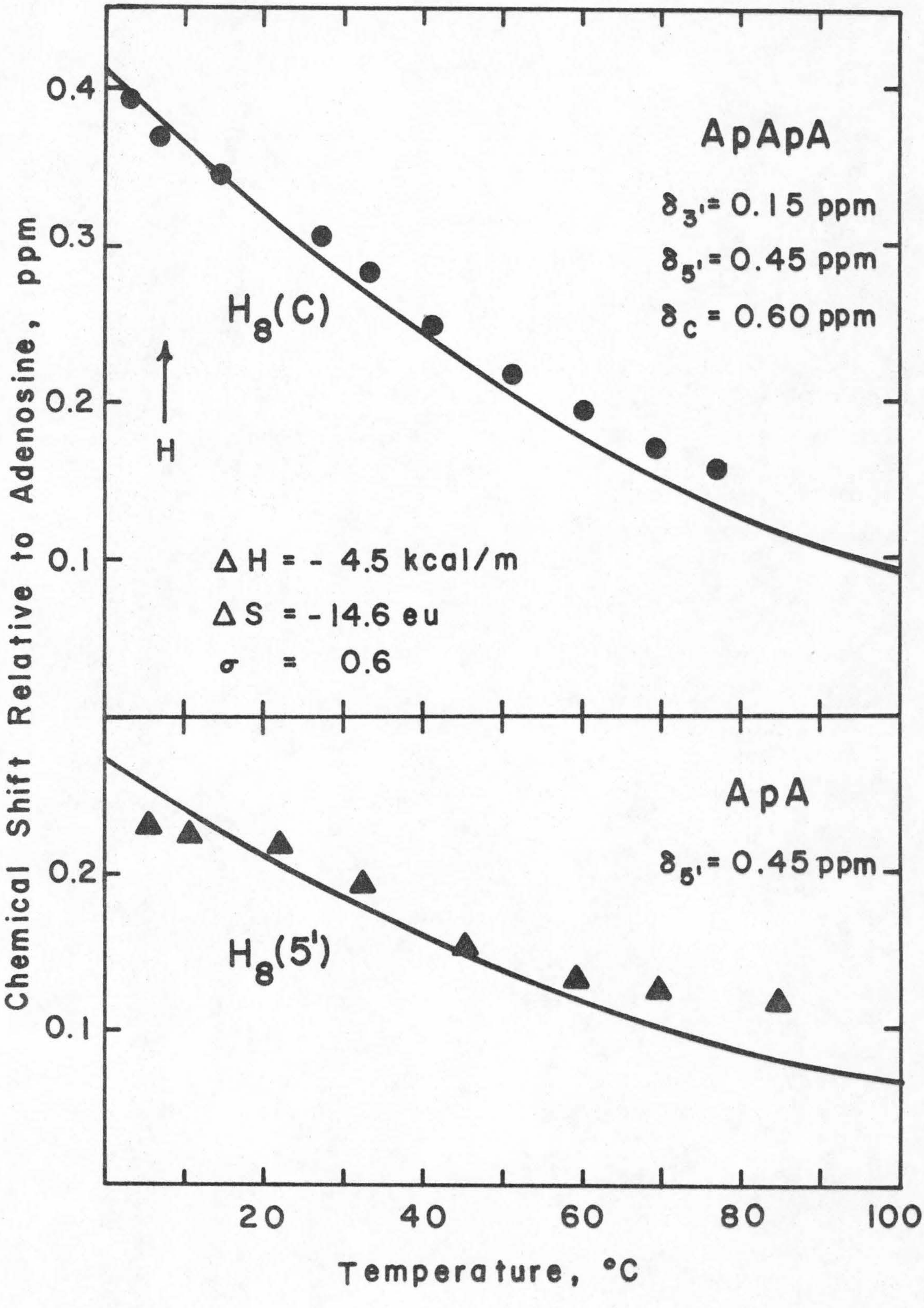
ApApA
$\delta_{3'}$ = 0.15 ppm
$\delta_{5'}$ = 0.45 ppm
δ_C = 0.60 ppm
$H_8(C)$
H
ΔH = - 4.5 kcal/m
ΔS = - 14.6 eu
σ = 0.6
ApA
$\delta_{5'}$ = 0.45 ppm
$H_8(5')$
0.4
0.3
0.2
0.1
0.2
0.1
20
40
60
80
100
Temperature, °C
Chemical Shift Relative to Adenosine, ppm

FIGURE 15

Temperature dependence of the H_8 resonances of the two central bases in ApApA.$^{(15)}$ The experimental results have been corrected for the effect of phosphate group by the addition of 0.137 ppm. The solid line represents the behavior predicted for the indicated values of the parameters.

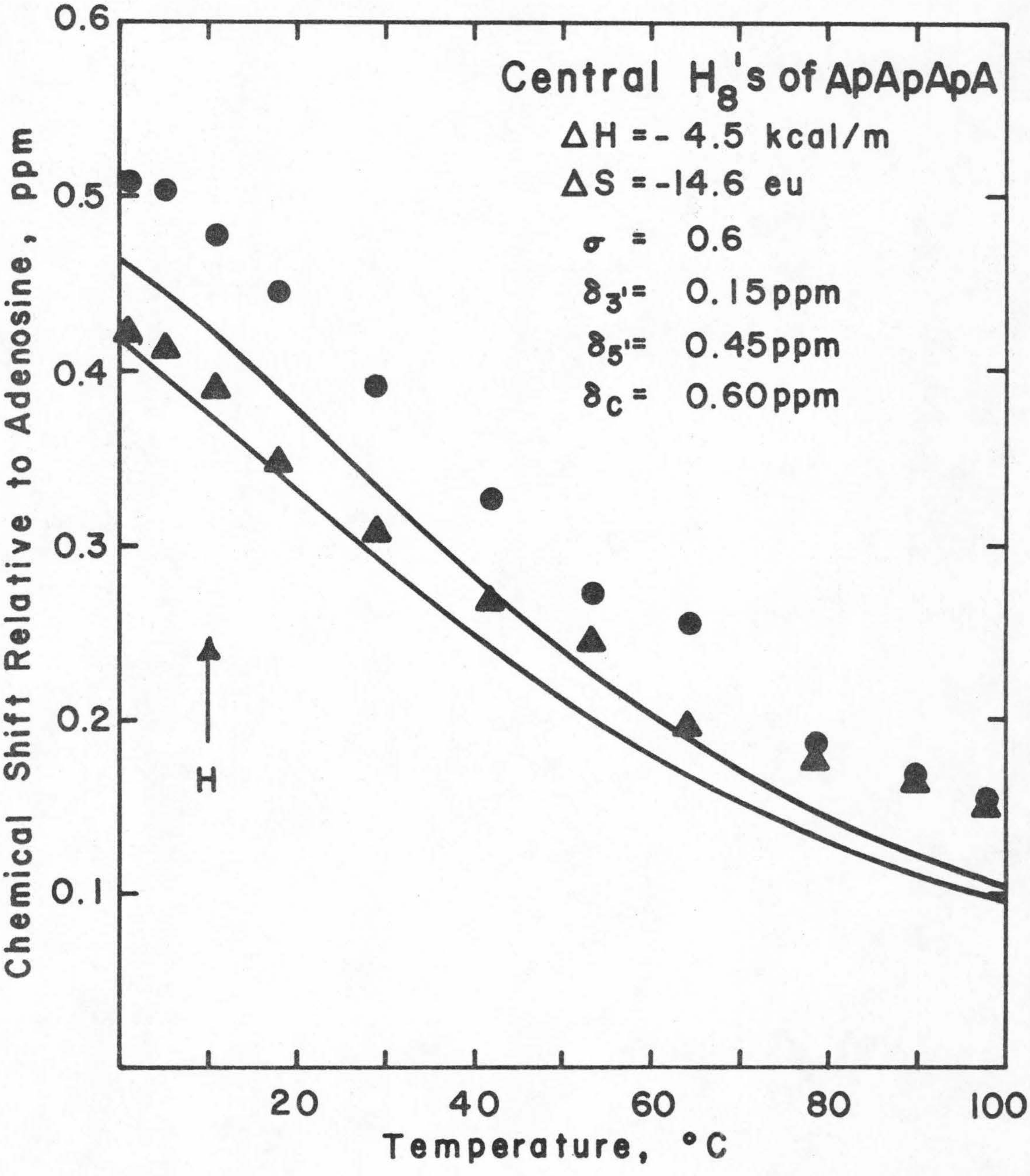
Central H_8's of ApApApA
ΔH = - 4.5 kcal/m
ΔS = -14.6 eu
σ = 0.6
$\delta_{3'}$ = 0.15 ppm
$\delta_{5'}$ = 0.45 ppm
δ_C = 0.60 ppm
H
0.6
0.5
0.4
0.3
0.2
0.1
20
40
60
80
100
Chemical Shift Relative to Adenosine, ppm
Temperature, °C

FIGURE 16

Temperature dependence of the H_8 resonances of poly A. The experimental results have been corrected for the effect of the phosphate group by the addition of 0.137 ppm. The solid line represents the behavior predicted for the indicated values of the parameters.

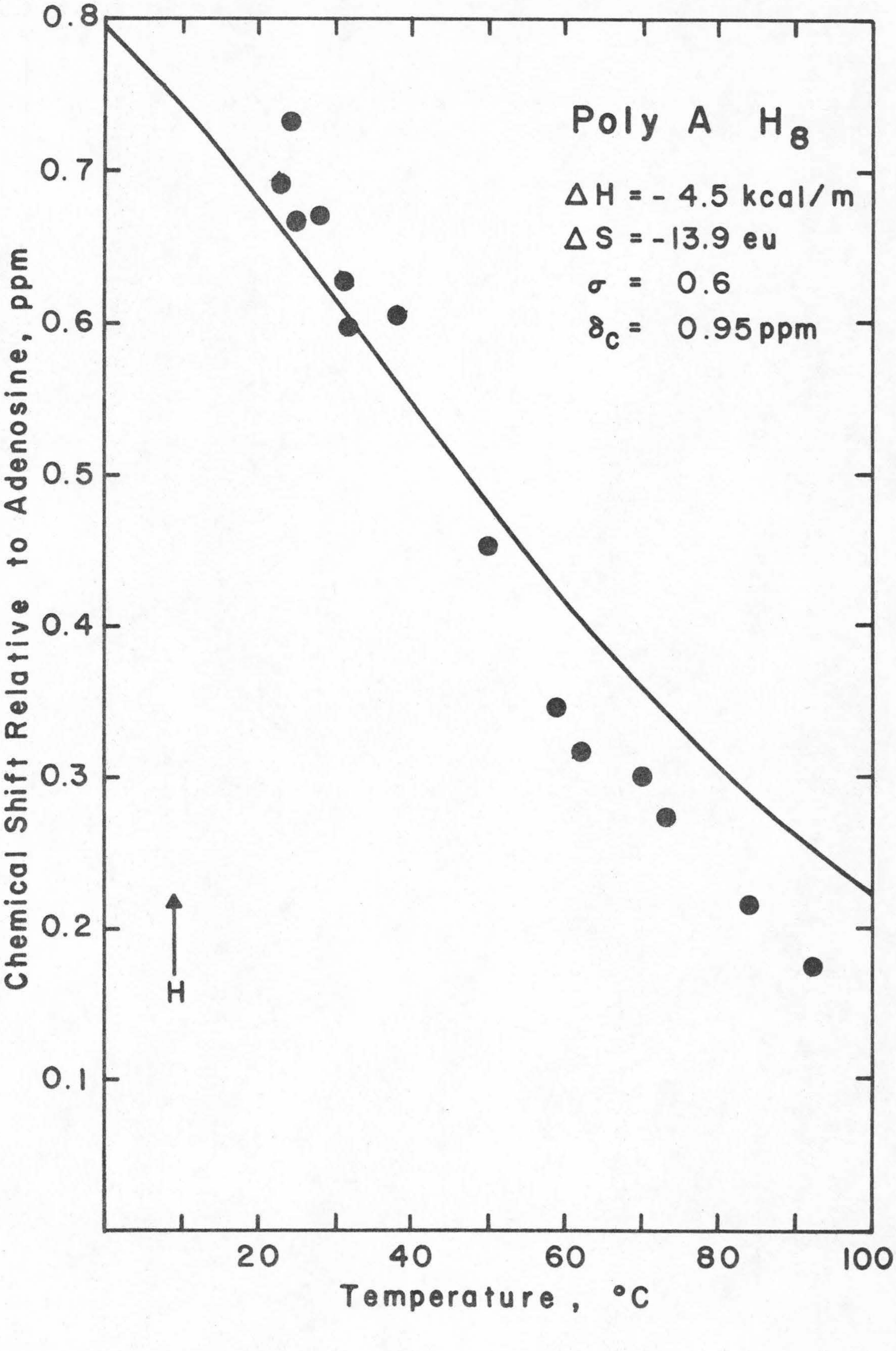
Poly A H_8
$\Delta H = -4.5$ kcal/m
$\Delta S = -13.9$ eu
$\sigma = 0.6$
$\delta_C = 0.95$ ppm
Chemical Shift Relative to Adenosine, ppm
Temperature, °C
H
0.8
0.7
0.6
0.5
0.4
0.3
0.2
0.1
20
40
60
80
100

TABLE III. The chemical shifts for the base protons in a stacked nucleotide chain.

	chemical shifts in ppm from adenosine		
	H_2	H_8	$H_{1'}$
oligoadenylates:			
3′ A in a stack	0.50	0.15	
5′ A in a stack	0.17	0.45	
central A in a stack	0.55	0.60	
poly A			
A in a stack	0.80	0.95	0.80
	max.shift in ppm from cytidine		
poly C	H_5	H_6	$H_{1'}$
C in a stack	0.30	0.20	0.30

TABLE IV. Base stacking predictions.

Oligonucleotides

number of bases in a stacked sequence	average number of stacked sequences of the given length per molecule at a given temperature					
	0°	20°	40°	60°	80°	100°
[Dinucleotide: ΔH = -4.5 kcal/mole, ΔS = -14.6 eu, $\sigma = 0.6$]						
2	0.61	0.47	0.35	0.26	0.19	0.14
[Trinucleotide: ΔH = -4.5 kcal/mole, ΔS = -14.6 eu, $\sigma = 0.6$]						
2	0.38	0.43	0.42	0.37	0.31	0.24
3	0.49	0.32	0.19	0.11	0.06	0.03
[Tetranucleotide: ΔH = -4.5 kcal/mole, ΔS = -14.6 eu, $\sigma = 0.6$]						
2	0.36	0.47	0.51	0.48	0.41	0.34
3	0.30	0.29	0.22	0.15	0.09	0.06
4	0.39	0.21	0.10	0.04	0.02	0.01

Polynucleotides

	fraction of bases stacked at a given temperature					
	0°	20°	40°	60°	80°	100°
[ΔH = -4.5 kcal/mole, ΔS = -13.9 eu, $\sigma = 0.6$]						
	0.83	0.72	0.58	0.44	0.32	0.24
[ΔH = -9.5 kcal/mole, ΔS = -29.5 eu, $\sigma = 0.6$]						
	0.96	0.87	0.65	0.36	0.17	0.08

not entirely satisfactory for this system. The chemical shift due to the stacking of two ring systems separated by a vertical distance, R, is approximately proportional to $|R|^{-3}$. Consequently, the pmr results can be interpreted as indicating that the stacked bases of poly A are closer together than those in a stacked tri- or tetranucleotide. By comparing the shift of 0.80 ppm for H_2 in poly A with 0.55 ppm for H_2 in the short chain nucleotides and comparing 0.95 ppm for H_8 in poly A with 0.60 ppm for H_8 in the oligonucleotides the ratio of the separation of the bases in the polymer and the separation of the bases in the short chains is found to be approximately 1.15. Assuming the axial separation of the stacked bases in poly A to be 3.62 Å, the separation of the bases in the short chains is 4.16 Å.

Further evidence that the distance between bases is larger in ApA than in a polynucleotide is provided by a study of the interaction of ApA with poly U.(46) In this study, the shifts of the ApA resonances induced by complex formation with poly U are interpreted as being due to enhancement of the intramolecular base stacking interaction within the ApA as it complexes with poly U. In free intramolecularly stacked ApA, there is, at a given temperature, a distribution of distances between the planes of the adenine bases but in the complex with poly U it is expected that the bases will be essentially in van der Waals contact.

The best fit (see Figure 17) of the poly C temperature data was obtained using an enthalpy of stacking, ΔH°, of -9.5 kcal/residue mole. The melting temperature is estimated to be 50°C from the pmr data and consequently, the entropy of stacking, ΔS°, is -29.4 e.u.

FIGURE 17

Temperature dependence of the H_5 and H_6 resonances of poly C. The experimental values for the H_6 resonance have been corrected for the effect of the phosphate group by the addition of 0.132 ppm. The solid lines represent the predicted behavior for the indicated values of the parameters.

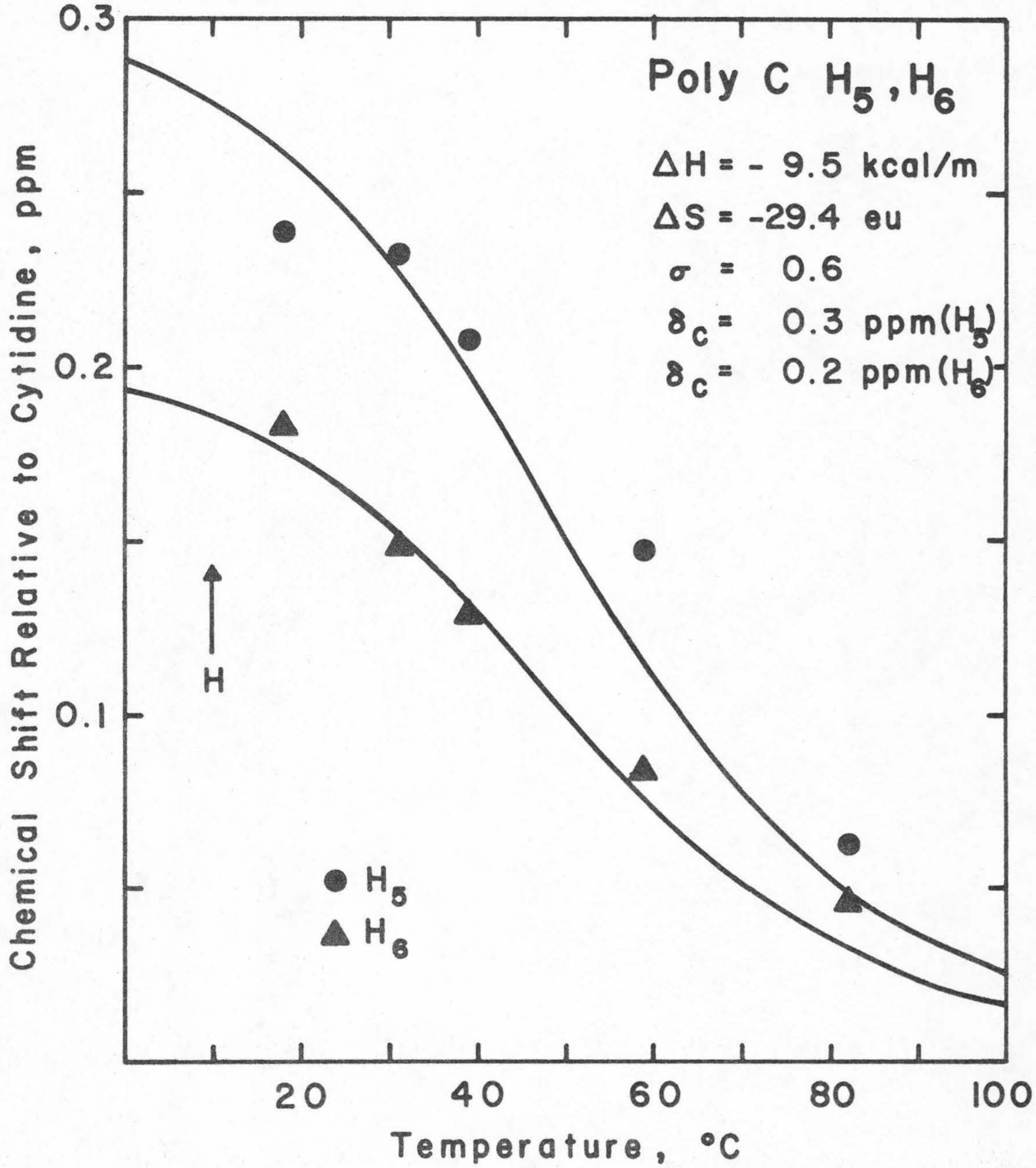
Poly C H_5, H_6
ΔH = - 9.5 kcal/m
ΔS = -29.4 eu
σ = 0.6
δ_c = 0.3 ppm(H_5)
δ_c = 0.2 ppm(H_6)
H
● H_5
▲ H_6
Chemical Shift Relative to Cytidine, ppm
0.3
0.2
0.1
20
40
60
80
100
Temperature, °C

The degree of cooperativeness was taken to be 0.6. Thermodynamic parameters derived from circular dichroic data by J. Brahms, J. C. Maurizot, and A. M. Michelson(20) are about 6.5 kcal/residue mole for the ΔH° of thermal denaturation and about 20 e.u. for ΔS° for a series of cytidine oligonucleotides.

The temperature variation of the pmr data of poly C indicates that the cytosine base does have a small but significant ring current magnetic anisotropy. The presence of this magnetic anisotropy was postulated previously(14) from the shifts observed for the adenine H_2 in ApC but was not observed in earlier work on the cytidine monomer.(7) In the CpC molecule, the average H_5 resonance is observed to shift 0.045 ppm downfield as the temperature is increased from 27°C to 72°C.(47) This small downfield shift is attributed to the magnetic anisotropy of the cytosine base. The larger shift observed for the H_5 protons of poly C can be interpreted as indicating that the cytosine bases are closer together in the poly C stack and consequently the small magnetic anisotropy of the cytosine base becomes more important in determining the resonance position of the neighboring cytosine protons.

The H_6 resonances in CpC move to slightly higher fields as the temperature is increased.(47) This shift is attributed to increased freedom of rotation of the cytosine bases relative to their ribose rings about the glycosidic bonds with increased temperature. In poly C, the H_6 resonance shifts downfield with increasing temperature. However, this shift is smaller than that of the H_5 resonance. As the temperature is increased the shift of the H_6 resonance is determined by at least two major factors: the downfield shift due to the decreased effect of the magnetic anisotropy of the neighboring cytosine base as the polymer unstacks, and the upfield shift due to the increased exposure of the H_6 to the furanose ether oxygen as the cytosine base becomes free to rotate about the glycosidic bond. Apparently in the poly C molecule, the first effect dominates while in CpC the second effect dominates. The difference can be attributed to closer stacking of the bases in poly C and possibly also to more restricted rotation of the base about its glycosidic bond.

2.3.3. Temperature Variation of the $H_{1'}$ Resonances. The $H_{1'}$ ribose proton provides further proton magnetic resonance data on the nucleotide systems. There are a number of factors which are involved in determining the $H_{1'}$ chemical shifts and consequently the interpretation of these shifts is not straightforward. The $H_{1'}$ resonances will be affected by changes in ribose ring conformation, by changes in the orientation of the base with respect to rotation about the glycosidic bond, by the ring currents of neighboring bases, and probably also by several other factors including the solvent structure and solvation of the various neighboring groups.

Bangerter and Chan(14) followed the shifts of the cytidine $H_{1'}$ resonances in ApC and CpA; the shifts are approximately 0.25 ppm upfield from $H_{1'}$ of cytidine at 10°C and approach 0.0 ppm and 0.07 ppm upfield from cytidine at 90°C. The observed temperature shifts are attributed to the conformational changes in the ribose rings and to possible changes in the conformation of the cytosine bases about the glycosidic bonds when the two bases in the dinucleotide become unstacked with increasing temperature. Both of these contributions are expected to lead to deshielding of the $H_{1'}$ as the temperature is increased. As the molecule unstacks with increasing temperature, the 3′-endo conformation of the ribose yields its predominance to the 2′-endo conformation (see Figure 18). Since the $H_{1'}$ is closer to the 2′-hydroxyl group when the ribose ring is in the 3′-endo conformation than when it is in the 2′-endo conformation, the $H_{1'}$ resonance is expected to shift downfield when the ribose conformation changes with increased temperature.(48) The conformation of the base about the glycosidic bond also is expected to yield an upfield shift with increased temperature because the keto group of cytidine appears to deshield the $H_{1'}$ proton and in the stacked configuration the conformation of the base about the glycosidic bond is expected to be restricted so that the 2-keto group of the cytidine base is rotated away from the $H_{1'}$.(48)

The temperature dependent shifts observed for the $H_{1'}$ of ApApA are shown in Figure 19. Because of the many factors involved in determining these shifts it is difficult to analyze this data in greater detail than to comment that the downfield shifts with increased temperature are expected due to the factors discussed in the preceding paragraph.

The temperature dependent shift of the $H_{1'}$ in poly A is considerably larger than those of ApApA. It is possible to fit the data for this proton using the method described in the preceding section and using the same thermodynamic values for the stacking of poly A. The fit of the data obtained when the maximum shift of the $H_{1'}$ proton

FIGURE 18

The 2′-endo and 3′-endo ribose conformations. In the 3′-endo conformation, the $C_{3'}$ and $C_{4'}$-$C_{5'}$ bond are on the same side of the plane formed by the $C_{1'}$, $O_{1'}$, and $C_{4'}$ atoms; in the 2′-endo conformation, the $C_{2'}$ is on the same side of the plane as the $C_{4'}$-$C_{5'}$ bond.

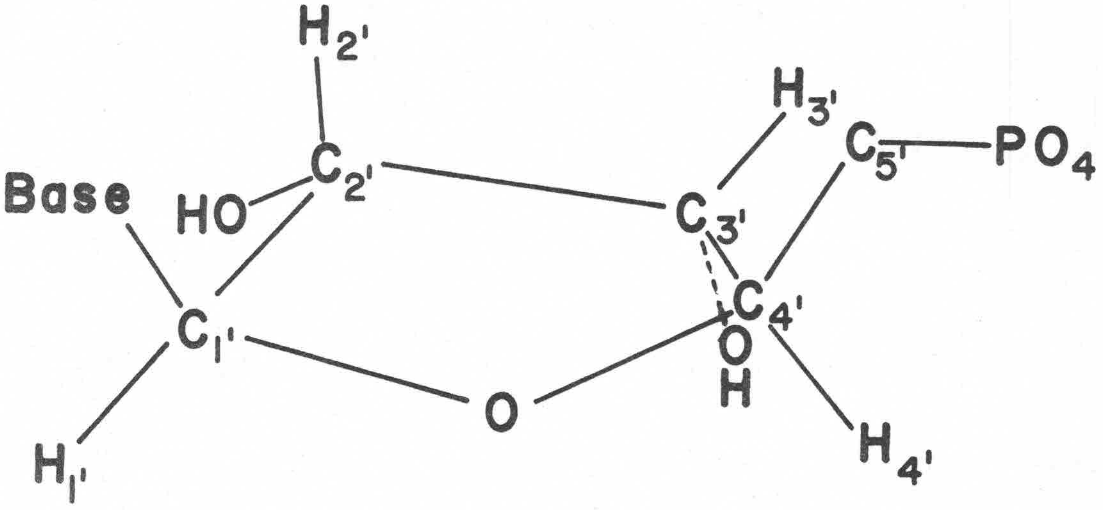
H2'
H3'
C5'
PO4
Base
HO
C2'
C3'
C4'
O
H
C1'
O
H1'
H4'

2'- endo

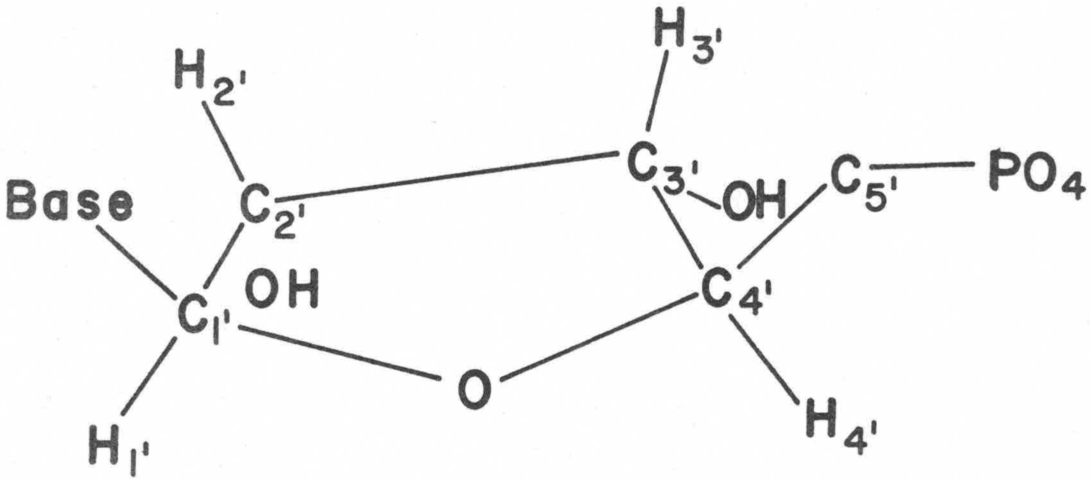
H3'
H2'
C3'
OH
C5'
PO4
Base
C2'
OH
C4'
C1'
O
H1'
H4'

3'- endo

FIGURE 19

Temperature dependence of the chemical shifts of the $H_{1'}$ resonances of ApApA.

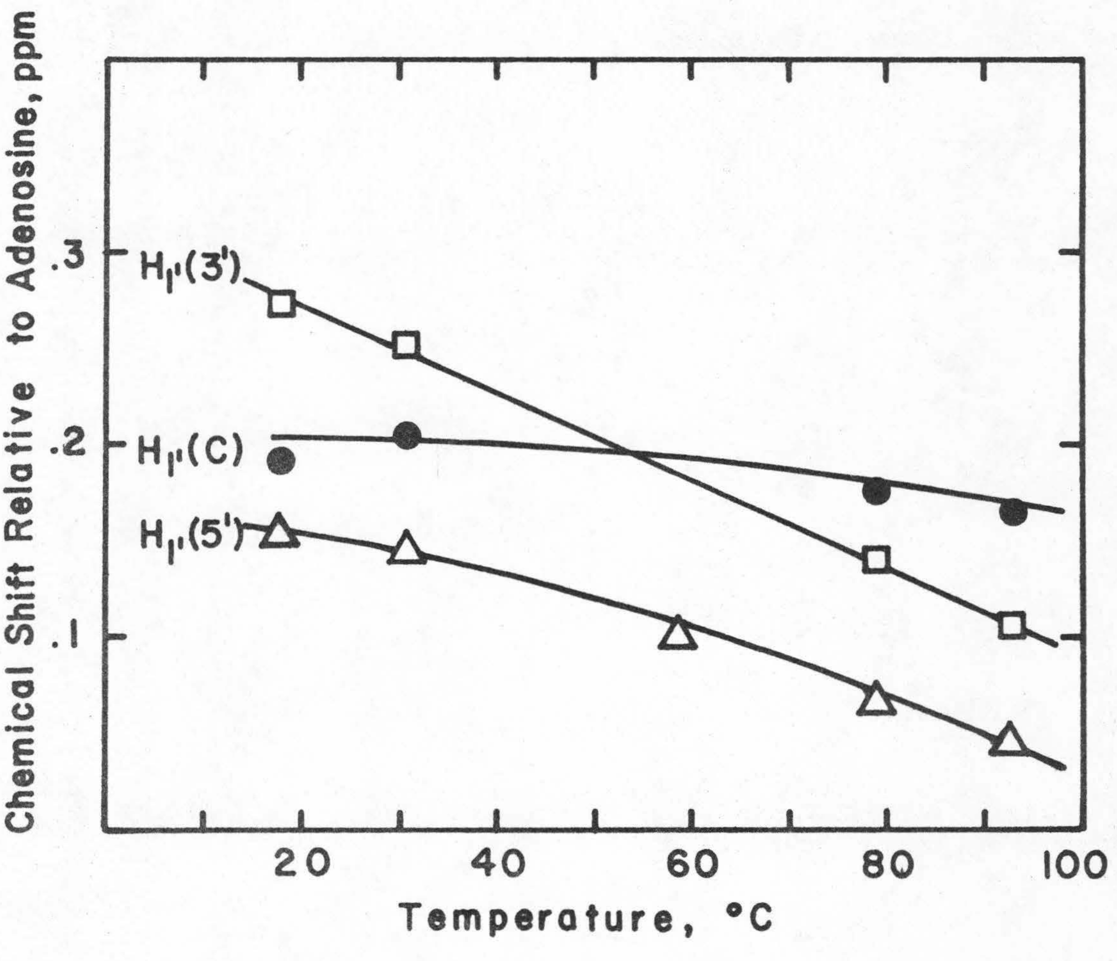
Chemical Shift Relative to Adenosine, ppm
.3
.2
.1
$H_{1'}(3')$
$H_{1'}(C)$
$H_{1'}(5')$
20
40
60
80
100
Temperature, °C

in the stacked conformation is taken to be 0.80 ppm relative to adenosine is shown in Figure 20. The size of this shift may provide additional evidence for the closeness of the bases in poly A as compared to ApApA. Conceivably, the closer stacking of the bases in the poly A molecule could be accompanied by conformational changes in the ribose which are causing additional shielding of the $H_{1'}$, and, as the bases come closer together, the ring current of the adjacent 3′ base could become a more important factor in the chemical shift determination.

The temperature dependent $H_{1'}$ shift of poly C is comparable to the shifts of the other observable protons on the cytidine. Again by applying the same method of predicting the temperature dependence as described previously and using the same thermodynamic values for the stacking of poly C, the data are fit reasonably well using a maximum shift of the proton on a base in a stack as 0.30 ppm relative to cytidine (see Figure 21). The temperature dependent shift of the $H_{1'}$ in poly C is larger than the shifts observed in CpC. In CpC, the $H_{1'}$ (5′) shifts 0.04 ppm and the $H_{1'}$ (3′) shifts 0.07 ppm when the temperature is varied from 27° to 72°C.(47) As in poly A, this larger shift in the poly C $H_{1'}$ resonance can be considered evidence for the closeness of the bases in the stack in the polymer and as additional evidence for a detectable magnetic anisotropy in the cytosine base.

A further feature of the proton magnetic resonance spectrum which can be used to follow the stacking process is the $H_{1'}$-$H_{2'}$ coupling constant which provides a sensitive indication of the average conformation of the ribose ring.(49) This coupling constant has been calculated

FIGURE 20

Temperature dependence of the chemical shift of the $H_{1'}$ resonance of poly A. The solid line indicates the behavior predicted for the values of the parameters shown.

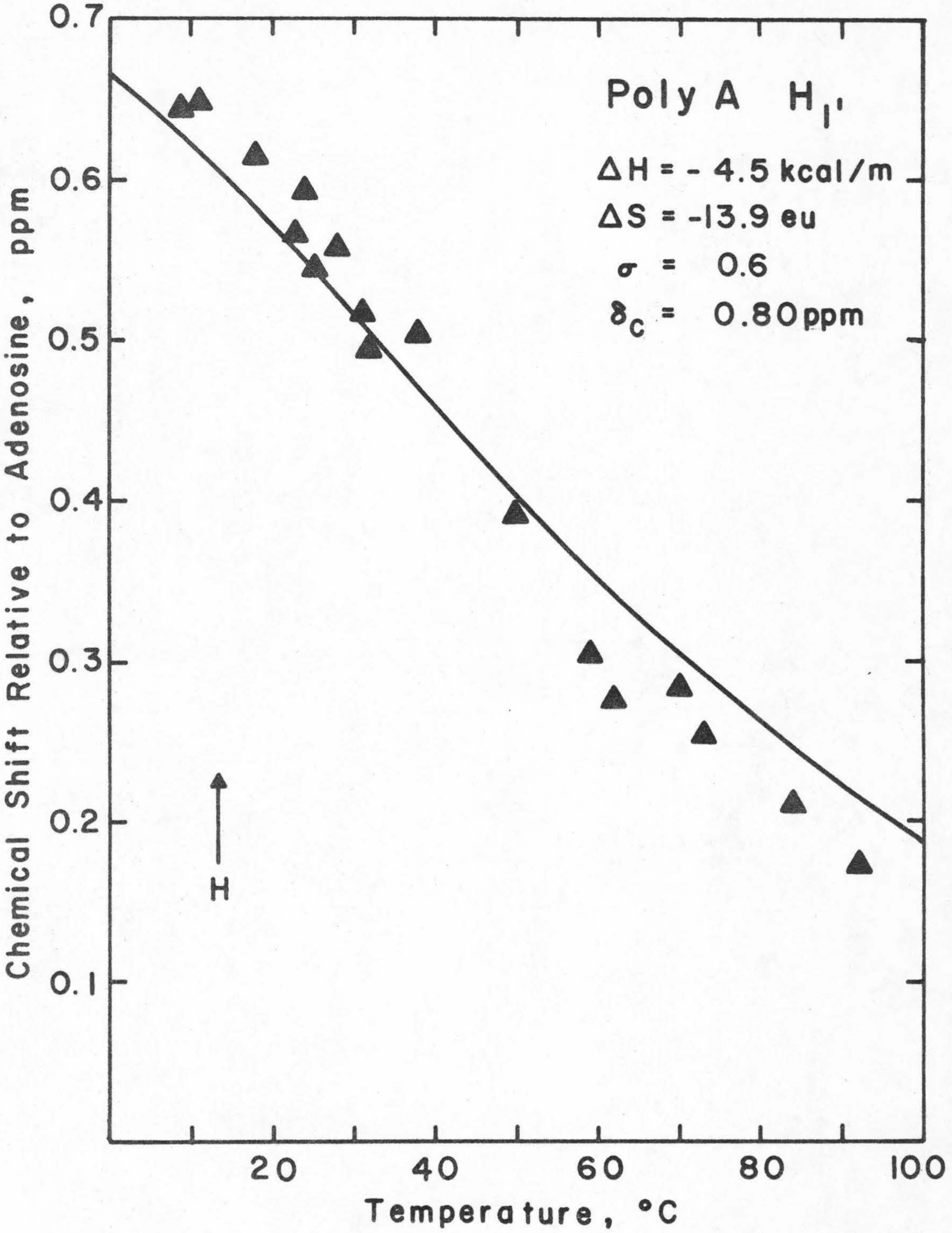
Poly A $H_{1'}$
$\Delta H = -4.5$ kcal/m
$\Delta S = -13.9$ eu
$\sigma = 0.6$
$\delta_c = 0.80$ ppm
Chemical Shift Relative to Adenosine, ppm
0.7
0.6
0.5
0.4
0.3
0.2
0.1
H
20
40
60
80
100
Temperature, °C

FIGURE 21

Temperature dependence of the $H_{1'}$ resonance of poly C. The solid line indicates the behavior predicted for the indicated values of the parameters.

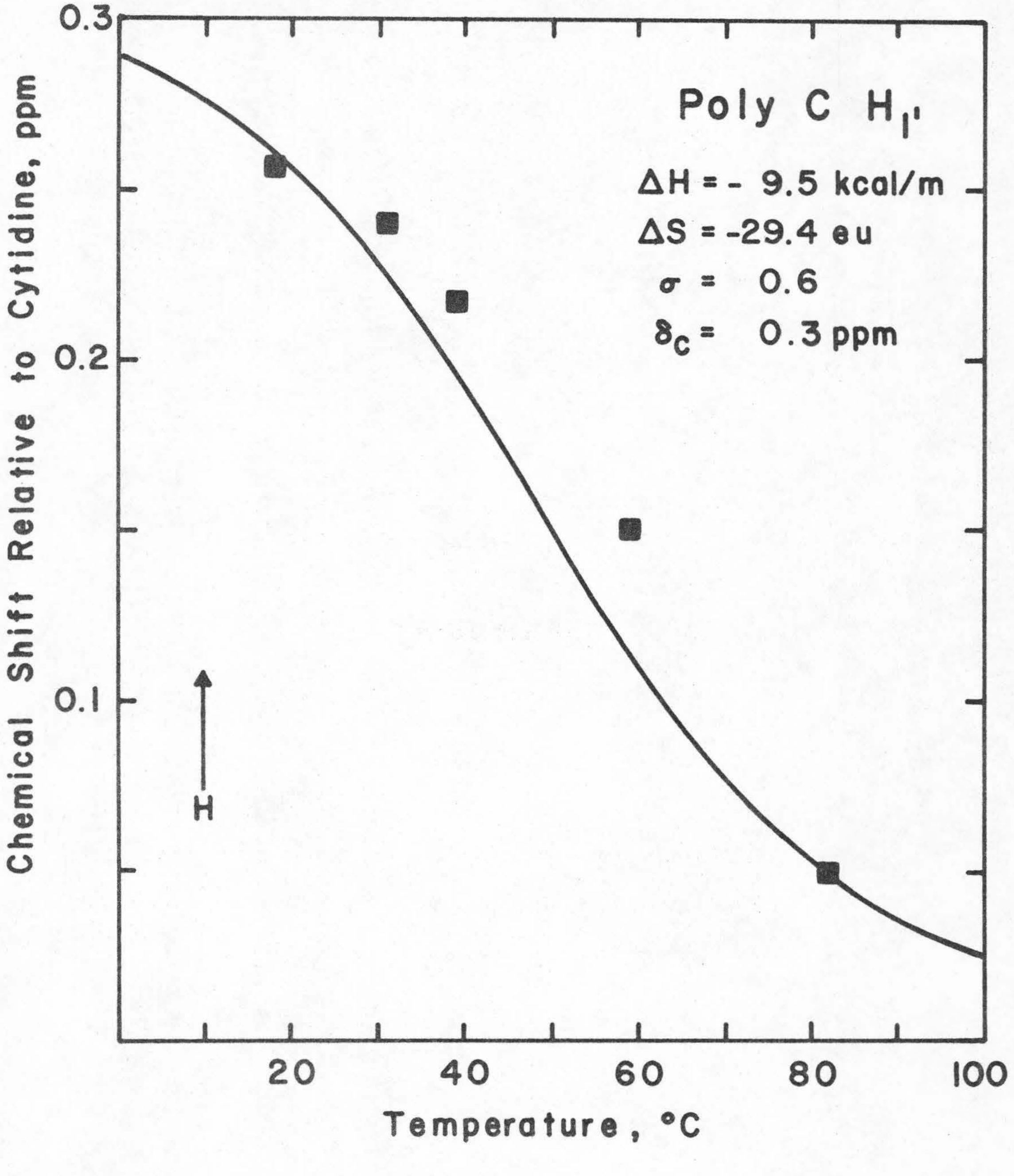
0.3
0.2
0.1
Chemical Shift Relative to Cytidine, ppm
H
Poly C $H_{1'}$
$\Delta H = -9.5$ kcal/m
$\Delta S = -29.4$ eu
$\sigma = 0.6$
$\delta_C = 0.3$ ppm
20
40
60
80
100
Temperature, °C

to be 6.9 Hz for the 2′-endo conformation and 1.7 Hz for the 3′-endo conformation.(50) The temperature variation of $|J_{H_{1'}-H_{2'}}|$ is shown for the three $H_{1'}$'s of ApApA and for that of poly A in Figure 22. The data for ApApA shown in Figure 22 are in agreement with data obtained by Nelson(15) on this system. The temperature variation is approximately the same for the $H_{1'}$ of poly A and for the $H_{1'}$'s of ApApA which indicates that the stacking tendencies in these two systems is about the same and that as the molecule becomes unstacked the dominant ribose conformation changes from 3′-endo to 2′-endo in both systems.

The $|J_{H_{1'}-H_{2'}}|$ of CpC changes from ~1.3 Hz to ~3.5 Hz over the temperature range of 14° to 63°C.(47) In poly C, due to the larger resonance widths and the small coupling constant, $|J_{H_{1'}-H_{2'}}|$ cannot be measured at low temperatures. However, by 82°C the value is still only ~2.9 Hz. These results indicate that the dominant ribose conformation is 3′-endo. A comparison of the coupling constants in the cytidine systems with those in the adenosine systems suggests that the 3′-endo conformation of the ribose predominates more in the cytidine systems than it does in the adenosine systems. This predominance may be evidence for more persistent stacking in the cytidine systems or it may be a consequence of the different geometries of the bases themselves.

2.3.4. Purine Interaction. Purine has been used as a probe molecule in pmr studies of several nucleotide systems.(13, 15, 47, 51-53) The purine has been shown to form complexes with the dinucleotide monophosphates and with polyuridylic acid which involves sandwiching

FIGURE 22

Temperature dependence of $|J_{H_{1'}-H_{2'}}|$ of the three $H_{1'}$ resonances of ApApA and of the $H_{1'}$ resonance of poly A.

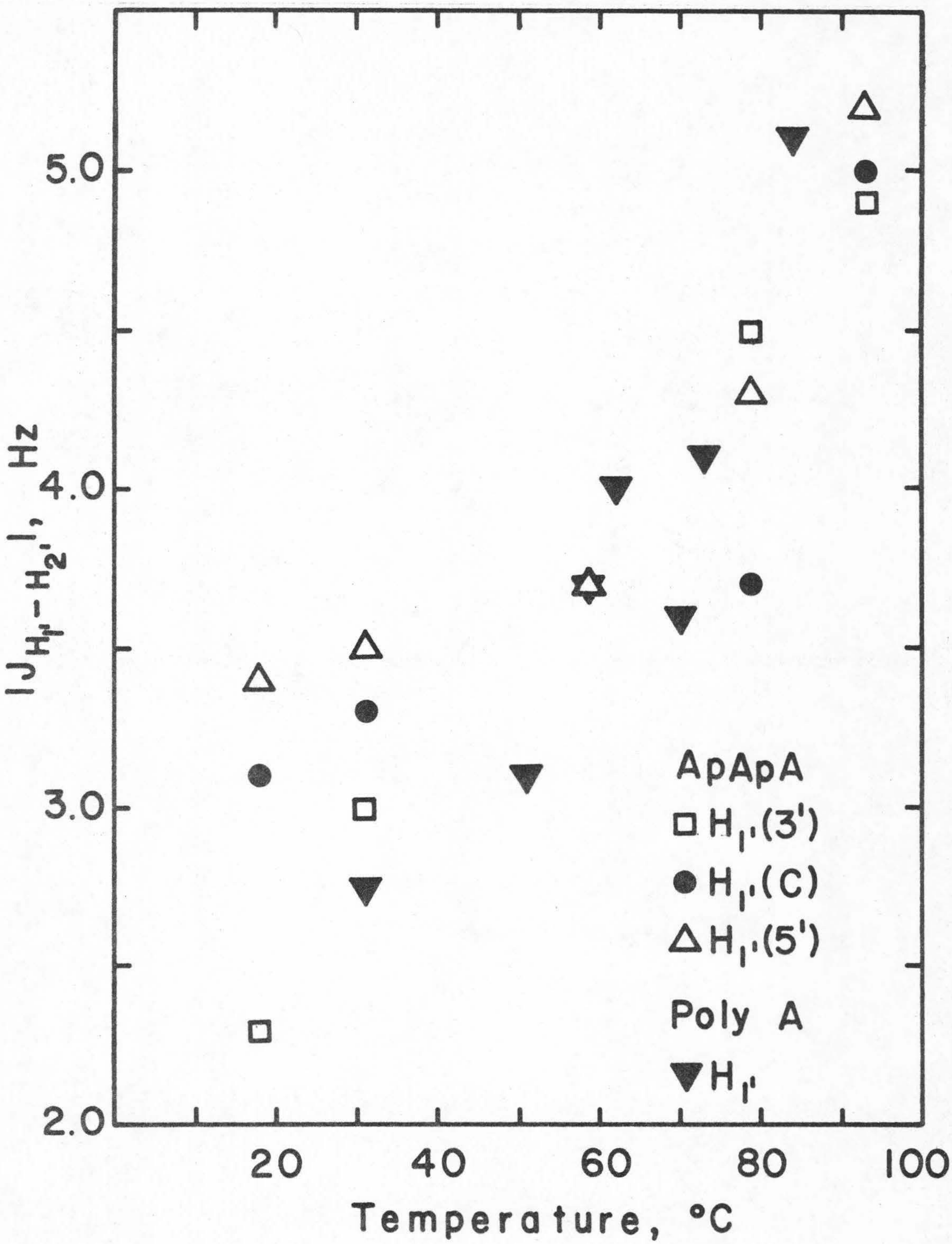
$|J_{H_{1'}-H_{2'}}|$, Hz
5.0
4.0
3.0
2.0
20
40
60
80
100
Temperature, °C
ApApA
□ $H_{1'}(3')$
● $H_{1'}(C)$
△ $H_{1'}(5')$
Poly A
▼ $H_{1'}$

a purine molecule between adjacent bases of the nucleotide chain. The formation of the complex is monitored by observing the shifts of the nucleotide proton resonances due to the ring current of the purine and by observing changes in the ribose $H_{1'}$-$H_{2'}$ coupling constants due to conformational changes in the ribose phosphate backbone. In addition, the purine proton resonances are broadened appreciably when the fraction of incorporated to unbound purine is high. (51, 52) The three purine resonances are broadened unequally. In the purine-poly U system the spin-lattice relaxation time (T_1) has been measured for the various purine protons and the nuclear Overhauser enhancement of the purine resonances upon strong irradiation of certain ribose protons has been observed. (53) This study suggests that the purine molecule in the purine intercalated complex is preferentially oriented with either the H_6 or H_8 directed toward the $H_{3'}$ or $H_{5'}$, $H_{5''}$ of the ribose moiety. Consequently, the purine proton resonances are broadened by nuclear spin relaxation induced by fluctuations of the local dipolar fields as suggested previously. (51)

The purine induced shifts in the H_8 and H_2 protons of ApApA and ApA were studied by Nelson. (15) In both molecules, the adenine H_8 resonances experience smaller upfield shifts than do the adenine H_2 resonances of the purine intercalated complex. This smaller shift is attributed to the closer proximity of the H_8 to the ribose-phosphate backbone of the molecule which means that it is less exposed to the ring current effects of an intercalated purine molecule.

The upfield shift of the $H_{1'}$ induced by 0.9 M purine in ApA (13) is approximately 0.1 ppm greater than that in ApApA. The ring currents of the intercalated purine would account for the upfield shifts of the $H_{1'}$ resonances. The shifts of the $H_{1'}$ resonances of ApApA are shown in Figure 23. The smaller shift of the $H_{1'}$ (3′) is expected since it is farthest away from the intercalated purine molecule.

The variation of the $H_{1'}$-$H_{2'}$ coupling constant shown in Figure 24 is again comparable to that observed in ApA.(13) The experimental values are difficult to obtain due to the overlapping of the resonances and the low concentration of the sample. However, the trends are clear. The coupling constant of the $H_{1'}$ of the central base changes less than the coupling constants of the end bases as purine intercalates into the molecule. Since this coupling constant is an indication of the ribose conformation, the change can be interpreted as indicating a tendency of the ribose conformation to become more 2′-endo as the purine complex is formed.

In the ApApA-purine complex, the purine resonances are broadened. Since the broadening of the resonances follows the same pattern as that observed in other systems, the orientation of the intercalated purine appears to be approximately the same. The trinucleotide, however, broadens each purine resonance to a greater extent than the dinucleotide under similar conditions.(15) This increased broadening is attributed to the formation of a more stable purine intercalated complex for the trinucleotide molecule or to differences in the kinetics of the two systems. Nelson(15) also studied the ApApA-purine system at 6°C and compared the results with those obtained at 30°C. It was observed that although the binding affinity of purine for the adenine base is increased at lower temperatures, the relative tendency

FIGURE 23

Purine-induced shift of the $H_{1'}$ resonances of ApApA.

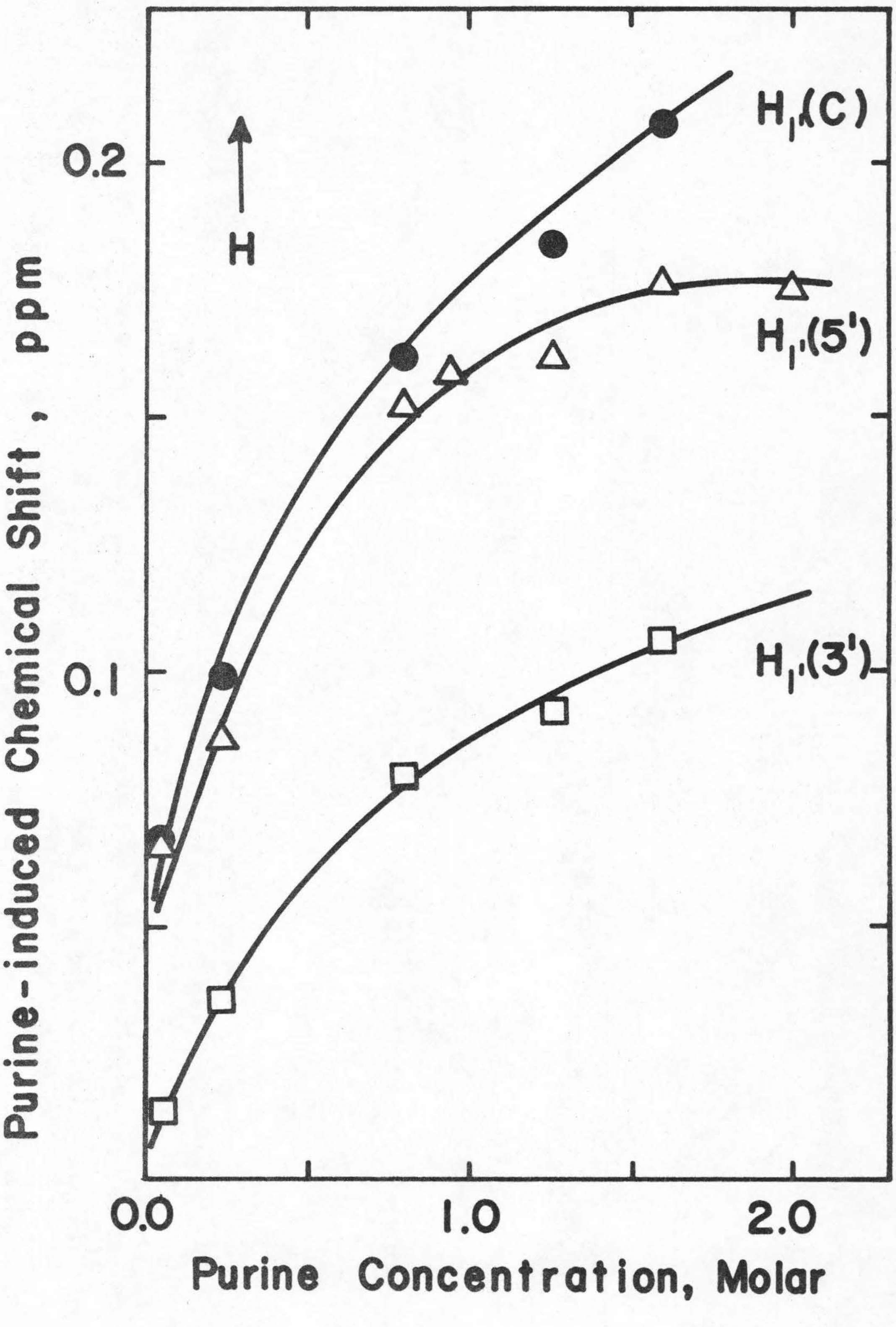

H$_{1'}$(C)
H$_{1'}$(5')
H$_{1'}$(3')
H
0.2
0.1
0.0
1.0
2.0
Purine-induced Chemical Shift, ppm
Purine Concentration, Molar

FIGURE 24

Dependence of the $|J_{H_{1'}-H_{2'}}|$ of the resonances of ApApA upon the purine concentration.

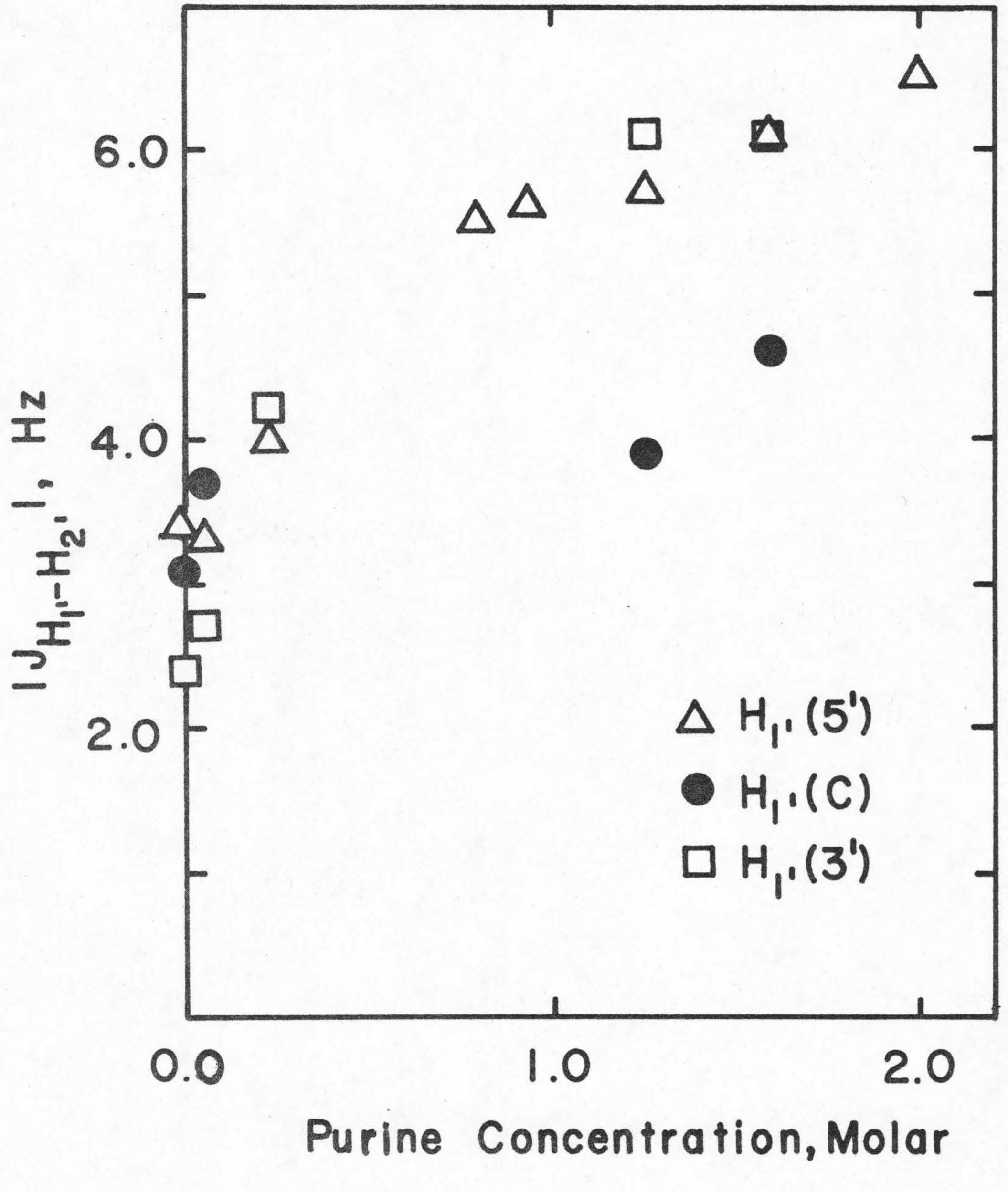
6.0
4.0
2.0
|J_{H_1'-H_2'}|, Hz
△ H_1'(5')
● H_1'(C)
□ H_1'(3')
0.0
1.0
2.0
Purine Concentration, Molar

of purine to form intercalated complexes is reduced due to the increased intramolecular adenine-adenine base stacking and the increased intermolecular purine association. The H_8 resonance of the central base in ApApA is shifted only 0.032 ppm with 0.8 M purine at 6°C while it is shifted 0.080 ppm with 0.8 M purine at 30°C. This small shift at 6°C is a reflection of the effective steric shielding of the H_8 (C) proton under conditions which favor strong intramolecular base stacking interactions.

When purine is added to a poly A solution, the results are somewhat different as shown in Figure 25. The purine interaction with poly A is indicated by a shifting of the H_8, H_2 and $H_{1'}$ resonances of the poly A molecule. The H_2 and $H_{1'}$ resonances are shifted upfield by approximately the same amount. This upfield shift can be attributed to the ring current of the complexing purine molecule as in the other systems. In the ApA and ApApA purine complexes, the H_2 resonances are shifted approximately twice the amount by which the $H_{1'}$ resonances are shifted. The differences in the relative magnitudes of the H_2 and $H_{1'}$ shifts seem to indicate that the purine ring current is being felt equally by the $H_{1'}$ and H_2 in the purine-poly A complex while, in the short chain adenosine-purine complexes, the H_2 of adenine is influenced more by the purine than is the $H_{1'}$. Thus, these results imply that the purine is positioned differently when it interacts with poly A than when it interacts with the short chain adenosines.

The H_8 resonance of poly A is shifted downfield when purine is added to the solution. This result can be explained by the disruptive effect of purine on the adenine-adenine intramolecular base

FIGURE 25

Purine-induced shifts of the H_2, H_8 and $H_{1'}$ resonances of poly A.

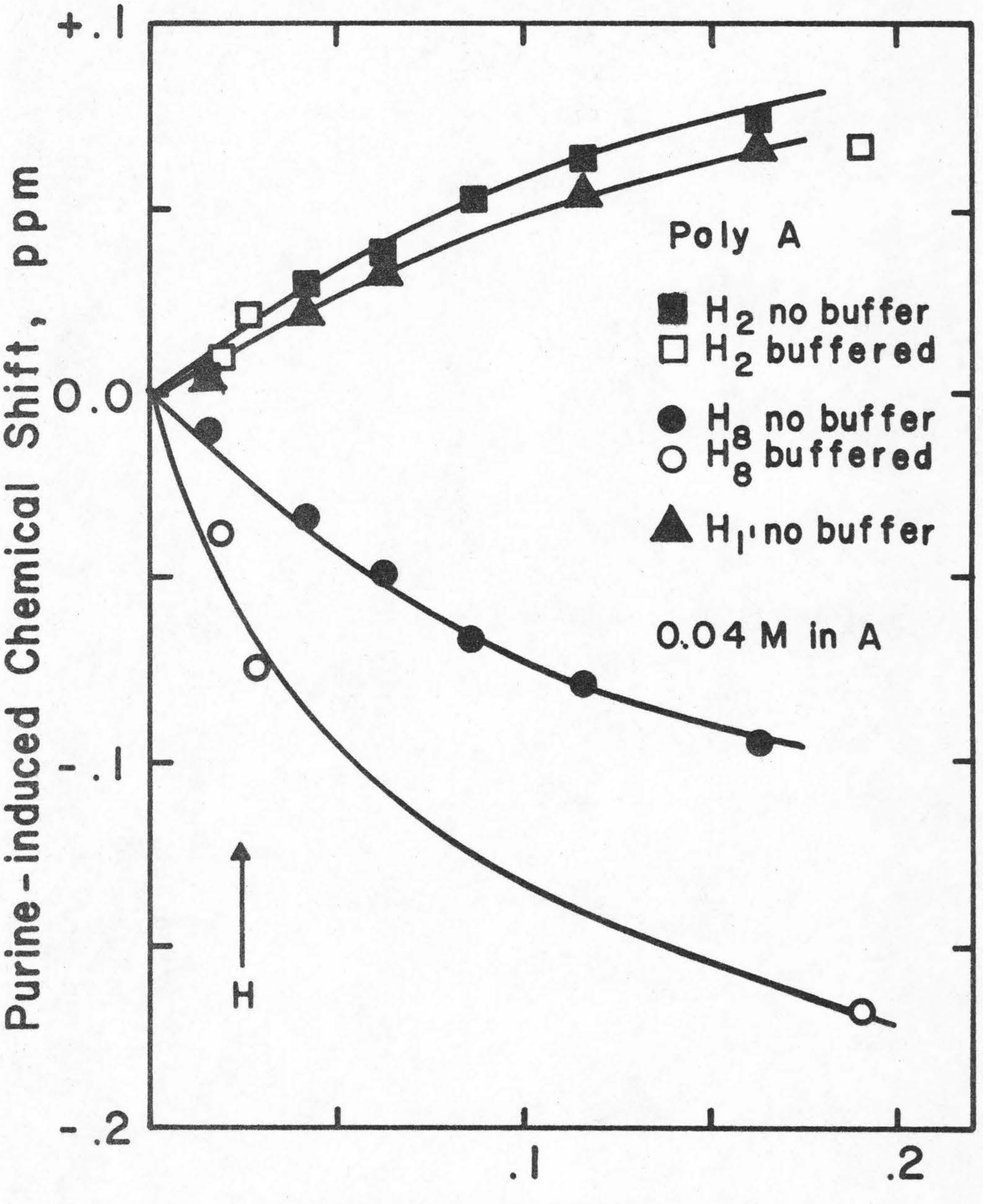
Purine-induced Chemical Shift, ppm
+.1
0.0
-.1
-.2
.1
.2
Purine Concentration, Molar
Poly A
■ H_2 no buffer
□ H_2 buffered
● H_8 no buffer
○ H_8 buffered
▲ $H_{1'}$ no buffer
0.04 M in A
H

stacking. Apparently, as noted above, the position of the purine in the poly A-purine complex is different from the position in the short chain complexes and the H_8 is sterically shielded from the purine ring currents. Taken all together, the results seem to indicate that when purine interacts with poly A, it is unable to intercalate as far into the molecule as it is able to in the short chain molecules. This hindered intercalation is further evidence that the bases in the poly A molecule are stacked closer together than the bases in ApA or ApApA.

The interaction of purine with poly A has recently been studied by C. Sander and P. O. P. Ts'o.(54) Their optical rotation and viscosity measurements showed that the addition of purine resulted in an unstacking of the adenosine bases in the poly A molecule. The rotation studies are interpreted as indicating that the poly A solution with 0.3 M purine at 25 °C contains approximately the same degree of stacking as the solution of poly A alone at 60 °C. The H_8 proton resonance of the adenosine in poly A is shifted approximately 0.1 ppm in the unbuffered solution by 0.16 M purine; the shift of the H_8 resonance induced by heating the poly A solution from 25° to 60 °C is approximately 0.2 ppm. Thus, it would seem that the downfield shift of the H_8 resonance can easily be accounted for by the unstacking induced by the interaction with purine.

Additional support of the positioning of the purine suggested above is provided by the failure of the purine resonances to be broadened appreciably by its interaction with poly A. In the ApApA system, the purine H_6 and H_8 resonances are approximately 20 Hz wide when the purine concentration is 0.048 M.(15) Under similar conditions in the poly A-purine system, the purine H_6 and H_8 resonances are under 5 Hz wide. These results imply that the purine H_6 and H_8 are not coming close to the phosphate-ribose backbone. In the interaction of purine with poly A, the purine is thus positioned more on the exterior of the molecule than in the sandwich type complex proposed for purine and poly U.

The difference in the shift observed for the H_8 proton in the buffered and unbuffered poly A solutions can be attributed to the larger ionic strength of the buffered solution. The chemical shifts relative to $(CH_3)_4N+$ are shown in Figure 26. From examining Figures 25 and 26, it becomes apparent that the larger purine-induced shift in the buffered system is attributable to the higher field position of the H_8 resonance in the buffered solution as compared to the unbuffered solutions. It is reasonable that the ionic strength of the solution would have an effect on the resonance positions and that the effect would be largest for the H_8 resonance due to the proximity of this proton to the phosphate group. At the higher ionic strength, the effect of the phosphate would be lessened due to at least partial shielding of the charge by counter-ions. Such a lessening of the phosphate effect would shift the resonance of the H_8 to higher fields. The purine induced shift observed for the H_8 is a combination of the downfield shift due to the decreased adenosine ring current effect which accompanies the unstacking of the poly A molecule and of the upfield shift due to the increased distance between the H_8 and the phosphate group as the molecule unstacks. Consequently, in the buffered solution the first factor predominates more completely than in the unbuffered solution.

FIGURE 26

Purine dependence of the H_2 and H_8 resonances of poly A.

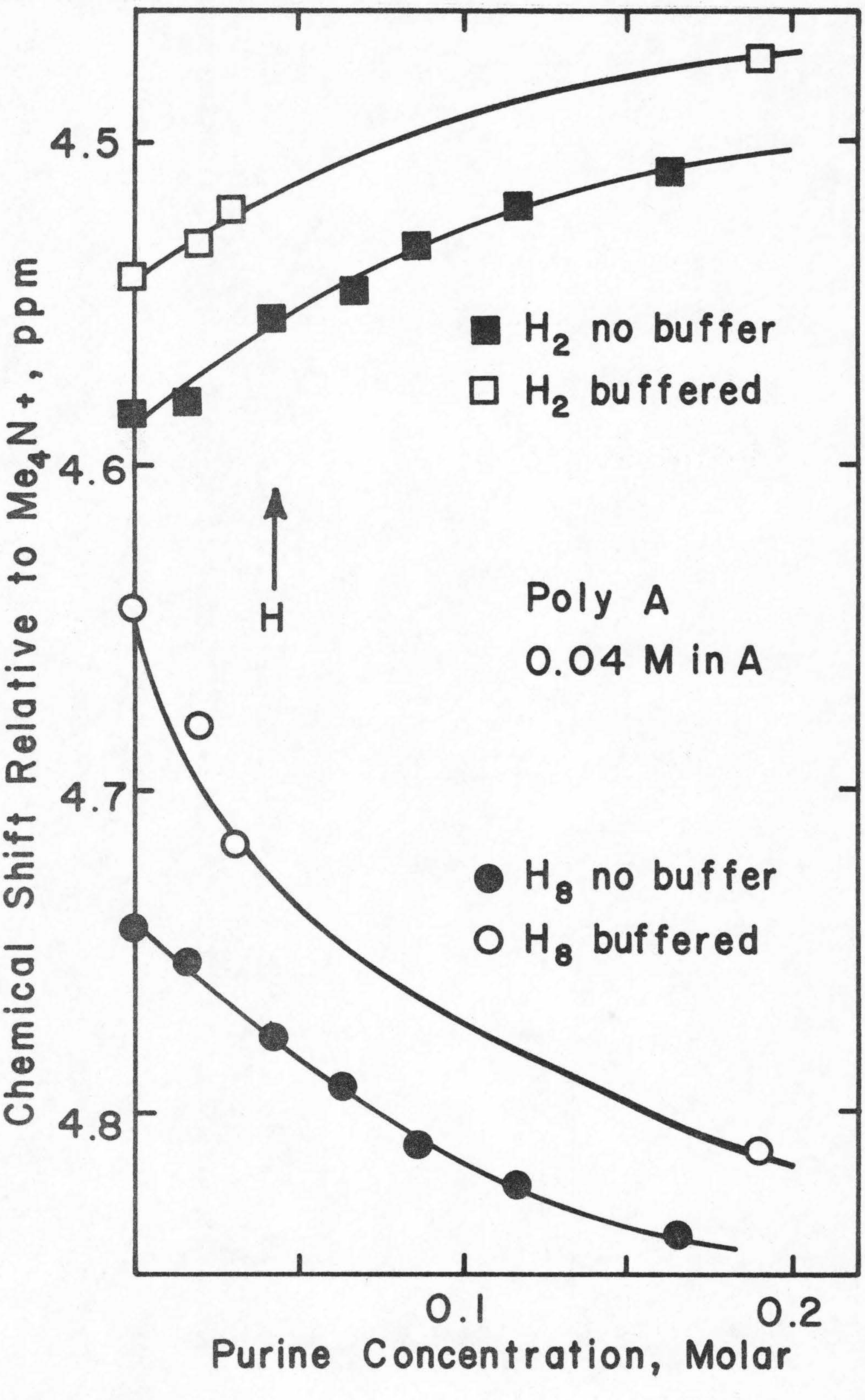
Chemical Shift Relative to Me_4N^+, ppm
4.5
4.6
4.7
4.8
0.1
0.2
Purine Concentration, Molar
■ H_2 no buffer
□ H_2 buffered
H
Poly A
0.04 M in A
● H_8 no buffer
○ H_8 buffered

The pmr resonances of the purine proton move upfield with concentration due to the intermolecular stacking of the purine molecules. This concentration dependence of the purine resonances has been studied previously.(6) In Figures 27 and 28, the concentration dependence of the shifts of the purine resonances are compared for a solution of purine alone and for solutions of 0.04 M poly A with purine. In all cases, the purine resonances are shifted to slightly higher field in the presence of the poly A. Such a shift is expected from the complexing of the purine with the adenosine bases which have large ring currents.

When purine is added to a 0.01 M CpC solution, the H_6 and H_5 resonances of the cytosines are shifted approximately 0.30 ppm upfield and the $H_{1'}$ resonances are shifted approximately 0.18 ppm upfield by 1.0 M purine.(47) The shifts are attributed to the formation of a sandwich complex with the purine molecule intercalating between the two cytidine bases. The shifts then are due to the ring current magnetic anisotropy of the intercalated purine molecule. The linewidths of the purine protons are broadened as in the short chain adenosine systems. For a 0.08 M CpC solution, the H_6 resonance of the purine is approximately 12 Hz, the H_8 resonance of purine is approximately 9 Hz and the H_2 resonance is 3.0 Hz when the purine concentration is 0.16 M.(47) These results indicate that the intercalated complex is approximately the same as that observed in the poly U system.(53)

When the purine is added to a poly C solution neither significant purine dependent shifts of the poly C protons nor severe broadening of the purine proton resonances are observed (see Table V). The effect

FIGURE 27

Concentration dependence of the purine H_2 and H_6 resonances with and without poly A in the solution.

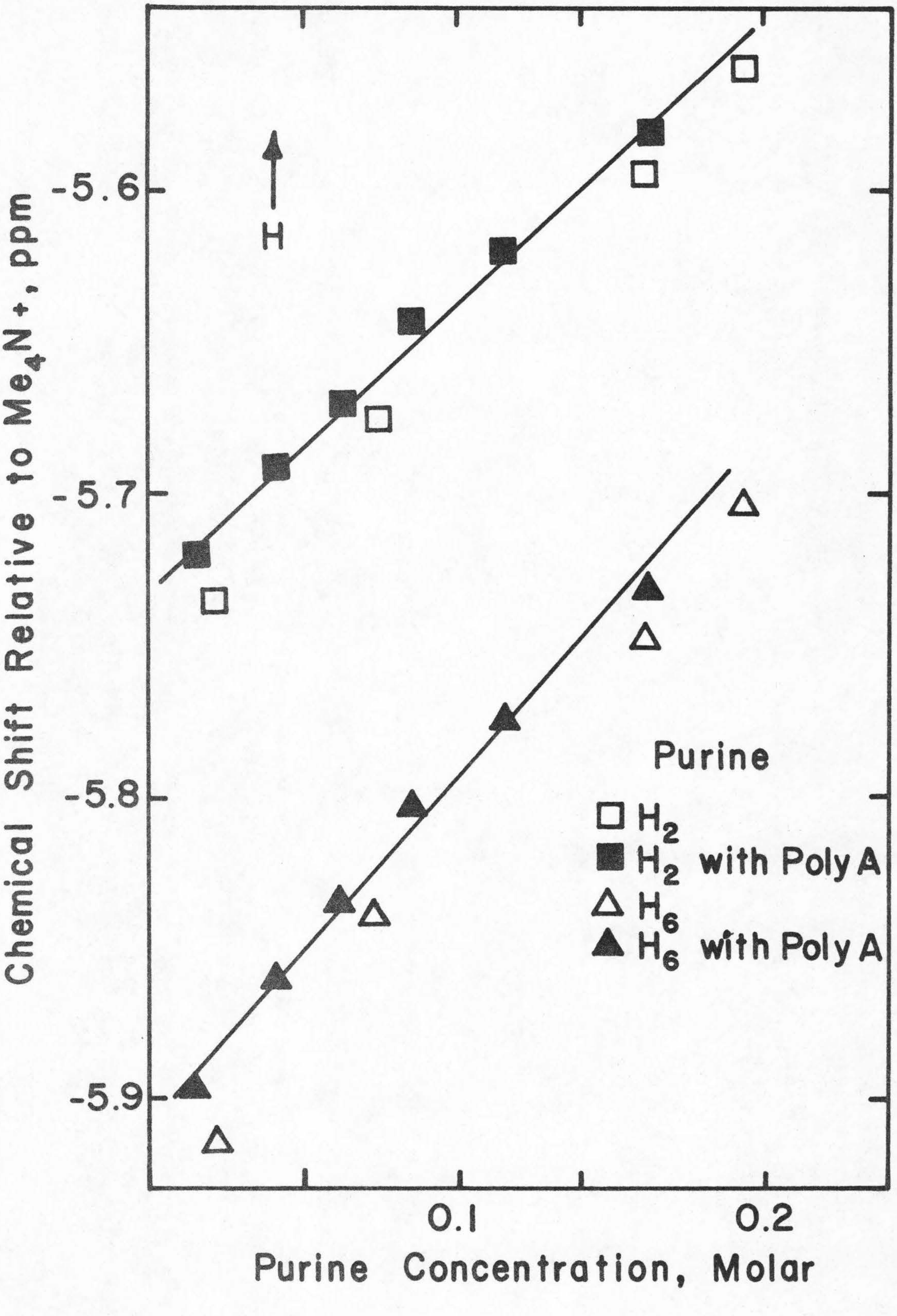
Chemical Shift Relative to Me_4N^+, ppm
-5.6
-5.7
-5.8
-5.9
H
Purine
□ H_2
■ H_2 with Poly A
△ H_6
▲ H_6 with Poly A
0.1
0.2
Purine Concentration, Molar

FIGURE 28

Concentration dependence of the purine H_8 resonance with and without poly A in the solution.

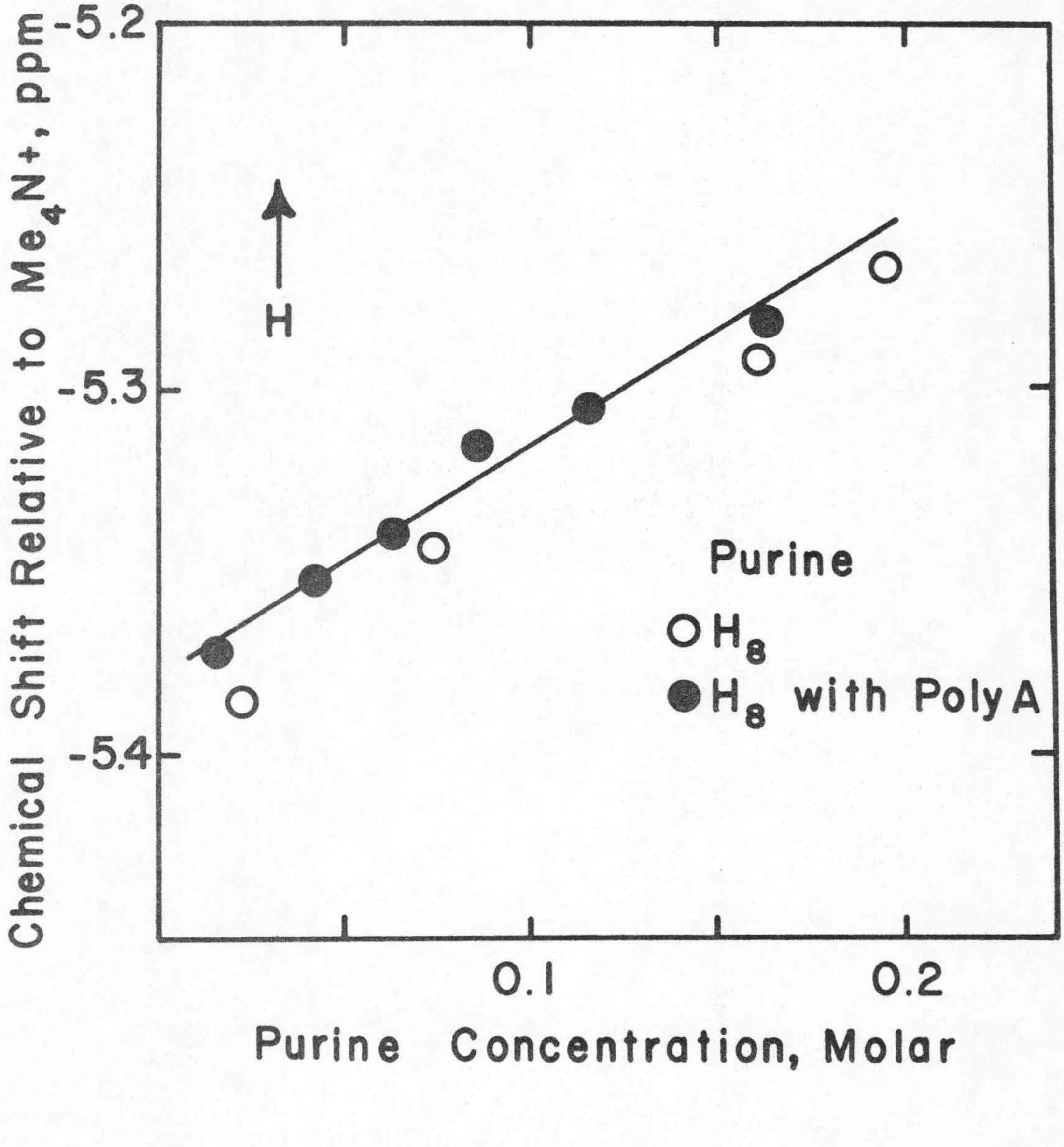
Chemical Shift Relative to Me_4N^+, ppm
-5.2
-5.3
-5.4
H
Purine
○ H_8
● H_8 with Poly A
0.1
0.2
Purine Concentration, Molar

TABLE V. Poly C and Purine.

pD = 6.6 0.04 M in C

Purine Con	Purine chemical shifts (ppm), linewidths (Hz)						Poly C chemical shifts (ppm)		
	H_6		H_2		H_8		H_6	H_5	$H_{1'}$
0.00							-4.612	-2.623	-2.465
0.03	-5.922		-5.743		-5.393		-4.634	-2.660	-2.495
0.05	-5.890	2.0	-5.714	1.7	-5.373	2.3	-4.636	-2.663	-2.500
0.11	-5.814	1.3	-5.651	1.3	-5.332	1.5	-4.639	-2.670	-2.510
0.37	-5.633	1.0	-5.496	1.1	-5.224	1.1	-4.633	-2.672	-2.507
0.62	-5.537	1.1	-5.411	1.2	-5.168	1.3	-4.630	-2.674	-2.517
1.09	-5.424	1.6	-5.313	1.7	-5.102	1.7			

chemical shifts in ppm from Me_4N+

of the purine on the resonances of the poly C protons, if any, is to shift them to lower field. Such an effect could be the result of a slight unstacking of the cytidine bases in the polymer when purine is added. The absence of an appreciable purine resonance broadening also indicates that the purine is not intercalating into the molecule as it does in poly U for example. The lack of measurable intercalation is in agreement with the preceding analysis of the temperature dependence of the poly C resonances which was interpreted as indicating that the cytosine bases are stacked closer together in the polymer than in the dinucleotide.

The pmr results are in general agreement with optical work. Sander and Ts'o(54) studied the poly C-purine system. Their measurements of the optical rotation show that purine interacts less strongly with poly C than with poly A and that at 25 °C poly C still possesses a considerable degree of stacking in a 0.3 M purine solution.

2.4. Conclusions

A two state model was used to predict the pmr results for the thermal unstacking of the oligo- and polynucleotides of adenosine and of the polynucleotide of cytidine. This analysis yielded an enthalpy of stacking of -4.5 kcal/residue mole for the adenosine system and -9.5 kcal/residue mole for the cytidine system. Since the temperature dependent shifts of the base resonances are due to the ring current magnetic anisotropies of the bases, the pmr results depend on $|R|^{-3}$. In order to fit the pmr data using the two state model, it is necessary to predict a decrease in the distance between the bases for the polynucleotide chain as compared to the short chain nucleotides. The results obtained using purine as a probe molecule in these nucleotide systems agree with this dependence of the distance between the bases upon the chain length.

The temperature dependent shifts observed for polycytidylic acid indicate that the cytosine base does possess a small ring current magnetic anisotropy.

In the following section, pmr is used to study two specific transfer RNA molecules.

3. PROTON MAGNETIC RESONANCE OF TRANSFER RNA

3.1. Introduction

Transfer RNA performs two major functions: it recognizes a particular aminoacyl-tRNA synthetase where it bonds to the appropriate amino acid and it codes with the messenger RNA at the ribosome in a manner to ensure the correct placement of the amino acid in the growing polypeptide chain.

The process of synthetase recognition is a very active area of research. The prominent ideas concerning the recognition process are discussed in a recent review article.(55) It is not yet understood whether the recognition is localized to a particular region of the molecule, whether it involves the complete three-dimensional structure of the tRNA molecule, or whether it is some combination of both a specific region and the overall structure.

The role of the anticodon in the tRNA interaction at the ribosome is to pair by hydrogen bonding with the codon on the messenger RNA. In this manner, the information carried by the messenger RNA from the DNA is translated into the synthesis of polypeptide chains. The three-dimensional structure of the tRNA positions the amino acid so that it can be transferred to the growing polypeptide chain.

The sequence of at least thirteen tRNA molecules are now known.(55) The homology found in these sequences is fairly high with certain bases occurring in specific positions in the accepted cloverleaf structure. These homologies are illustrated in Figure 29 in a

FIGURE 29

tRNA homologies. A^* represents a derivative of adenine; I^{Me} represents a methylated inosine; ψ represents pseudouridine.

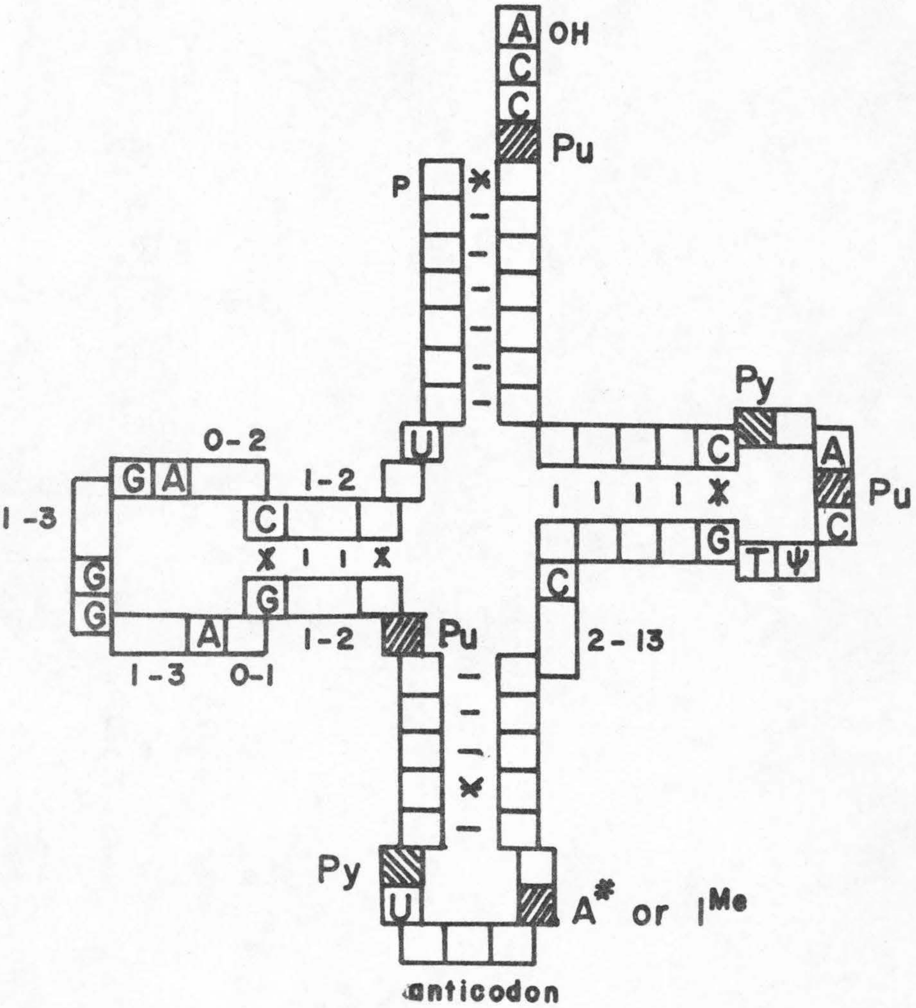
A OH
C
C
Pu
P
U
0-2
G A
1-2
1-3
C
G
G
G
A
1-2
Pu
1-3 0-1
Py
C
A
Pu
C
G
T Ψ
C
2-13
Py
U
A* or I^Me
anticodon

tRNA Homologies

*	G - C pairing
Pu	a purine
Py	a pyrimidine

generalized clover-leaf form published in a recent review article.(56)

It seems reasonable that in the relatively near future, high resolution x-ray diffraction data will reveal the details of the structure of transfer RNA in the crystalline form. A number of groups have been able to obtain crystals of purified tRNA(57-65) and some x-ray diffraction data(66-69) has been gathered. The x-ray diffraction data gathered recently indicate that the molecule is long. One study(66) approximates the length as being 80 Å and the cross section as being somewhat irregular and approximately 25 by 35 Å. A recent small-angle x-ray scattering study of four different species of tRNA in solution indicate that the molecules are of very similar size and shape.(70) A model proposed in this study has the arms of the clover-leaf form folded tightly around a helical core and has a molecular dimension of 25 by 35 by 85 Å. Several other groups have also proposed three dimensional structures for tRNA.(71-76)

The pmr spectra of aqueous solutions of tRNA has been observed previously at 220 MHz(77) and at lower frequencies.(29, 30, 77-81) There is no improvement in resolution in going from 60 or 100 MHz to 220 MHz. Even in the study at 220 MHz(77) of alanine tRNA, among the common bases, it is possible to assign only the resonances due to the H_8 of adenine. Weak high field resonances are tentatively assigned to protons on several modified nucleosides: 1-methylguanosine, N_2-dimethylguanosine, dihydrouridine and thymidine. The lack of resolution of the resonances of the common bases is indicative of large intrinsic resonance widths and of considerable chemical shift homogeneity among each type of base proton due to nearest neighbor interactions.

The large intrinsic resonance widths found in tRNA can be attributed to slow rotational motion of the molecule in solution. The rotational correlation time is on the order of 10^{-8} seconds for a molecule with the dimensions estimated for tRNA in crystals. When a small molecule rotates rapidly in solution, the magnetic dipolar interactions of the various magnetic nuclei are averaged out. A large molecule such as tRNA which retains a three dimensional structure in solution does not rotate rapidly enough to average out the intramolecular magnetic dipolar interactions and consequently these magnetic dipolar couplings control the resonance widths. In contrast, the resonances in the polynucleotides of adenine, cytosine and uracil are relatively narrow indicating that, even though they may be highly stacked, these molecules retain a large amount of flexibility in solution.

In aqueous solution, the tRNA resonances are sufficiently broad to make a quantitative study of the temperature dependence of the proton chemical shifts of the molecule impossible. There are, however, other studies involving the tRNA molecule which can take advantage of the pmr technique. For example, the introduction of a small probe molecule such as purine into the system allows one to study the interaction between the probe molecule and tRNA by observing the resonances of the probe molecule itself. Purine has been shown to be a powerful denaturant(82) for nucleic acids. Previous studies involving purine(13, 15, 47, 51-54) indicate that the denaturing effect is probably due to hydrophobic and stacking interactions. More direct knowledge of the details of the interaction of purine with tRNA should lead to a better understanding of the mechanism of denaturation of a nucleic acid.

Modified nucleosides have been found in all of the tRNA molecules sequenced so far.(55) The function of these nucleosides is not understood fully at this time. The presence of the various modified nucleosides can give rise to changes in hydrogen-bonding, base-stacking, and covalent bonding capabilities. Such changes can control the stability and the three-dimensional structure of the molecule. The use of a denaturing solvent, such as dimethylsulfoxide, disrupts the structure of the molecule sufficiently to allow the observation of reasonably sharp pmr resonances from the various base protons.(79) Consequently, the observation of the resonances of the modified nucleosides during the "melting" of the structure of the tRNA by the titration of an aqueous solution with dimethylsulfoxide has the potential of yielding information concerning the structure in the region of the modified nucleoside. Thus, some understanding of their role in the tRNA molecule may result.

One of the tRNA's used in this work was N-formylmethionine tRNA (tRNA_f^{Met}) from E. coli. The primary sequence of this molecule(83) is shown in Figure 30.

The tRNA_f^{Met} has been shown to initiate protein synthesis in bacteria and bacteriophages.(84-88) Thus, the first amino acid in a polypeptide chain is methionine with a formyl group attached to the amino end. In bacterial cells, the formyl group is subsequently removed by peptide deformylases.(89) The methionine may remain at

FIGURE 30

The sequence for $tRNA_f^{Met}$ is shown in the usual clover-leaf form. The modified nucleosides are 4-thiouridine (4tU), dihydrouridine (D), 2′-O-methylcytidine (2′OmC), 7-methylguanosine (7mG), ribothymidine (T), pseudouridine (ψ). Approximately 75 per cent of $tRNA_f^{Met}$ contains 7 mG in the position indicated while the remaining 25 per cent contains A in this position.

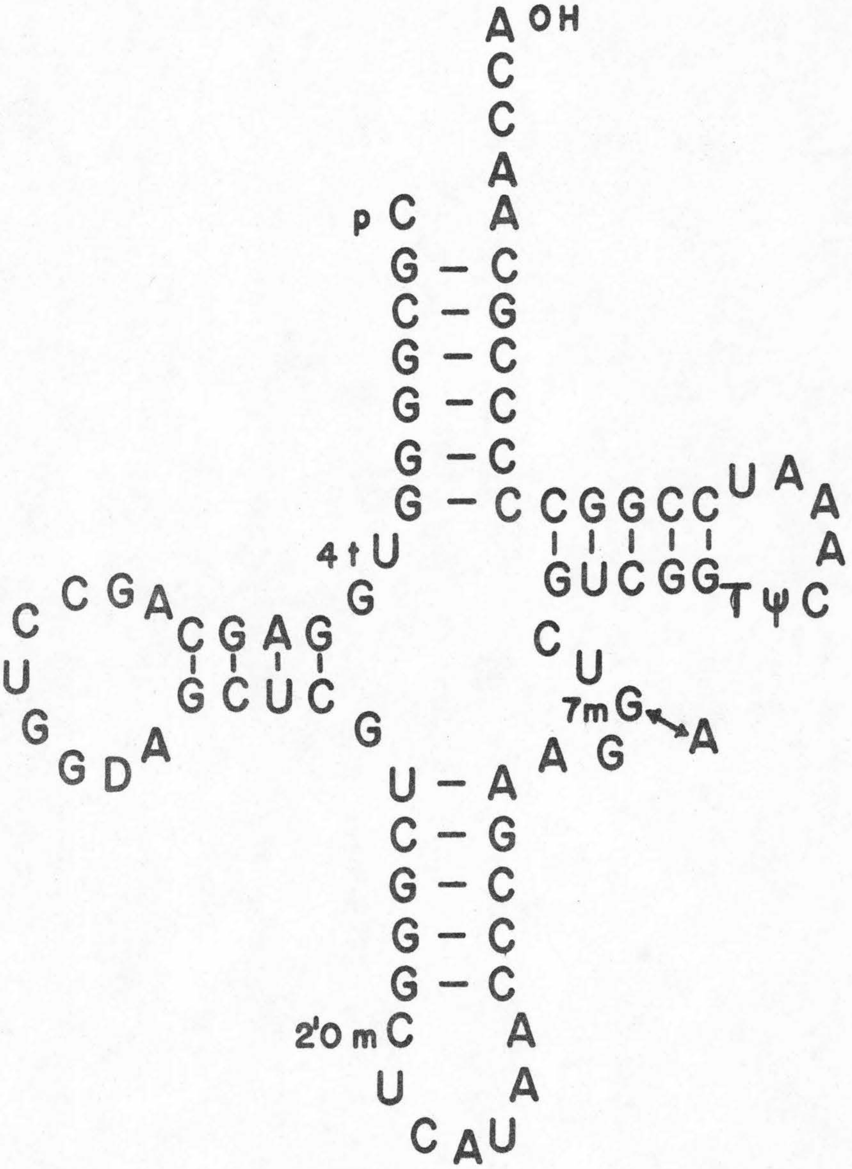
A OH
C
C
A
p C A
G – C
C – G
G – C
G – C
G – C
G – C C G G C C U A A
4 t U A
G G U C G G T ψ C
C C G A C G A G
C U
U G C U C 7mG A
G G A G
G D A
U – A
C – G
G – C
G – C
G – C
2'0 m C A
U A
C A U

Formylmethionine tRNA

E. Coli

the amino end of the polypeptide chain or it may be removed. A recent study showed that chain initiation of certain histones in mammalian tissues is performed in an analogous manner by N-acetyl-seryl-tRNA. (90)

The other tRNA reported on here is phenylalanine tRNA ($\mathrm{tRNA}^{\mathrm{Phe}}$) from yeast. The primary sequence of this molecule(91) is shown in Figure 31. This molecule contains a number of modified bases including the "Y" base which occurs next to the anticodon. A structure has not yet been reported for this base although it appears to be a rather hydrophobic purine derivative and is strongly fluorescent. (92-94)

In our study, the advantage of the 220 MHz pmr instrument is principally the increased sensitivity which reduces the amount of time-averaging required. However, the larger separation of chemical shifts was helpful in the purine binding study.

The application of pmr to the study of the complete tRNA molecule in aqueous solution seems of limited success. However, pmr may prove useful in studying specific portions of the molecule such as the uncommon bases which have resonances in regions away from the major resonances of tRNA. Also, the techniques can be applied to studying the interaction of tRNA with small molecules which have resonances away from those of tRNA, and to studying broken segments of the tRNA molecule itself.

3.2. Experimental.

The N-formylmethionine tRNA from E. coli came from Oak

FIGURE 31

Primary sequence of phenylalanine tRNA. The modified nucleosides are 2-methylguanosine (2mG), dihydrouridine (D), N_2-dimethylguanosine (2 dim G), 2′-O-methylcytidine (2′OmC), 2′-O-methylguanosine (2′OmG), unknown base (Y), psueoduridine (ψ), 5-methylcytidine (5mC), 7-methylguanosine (7mG), and 1-methyladenosine (1mA).

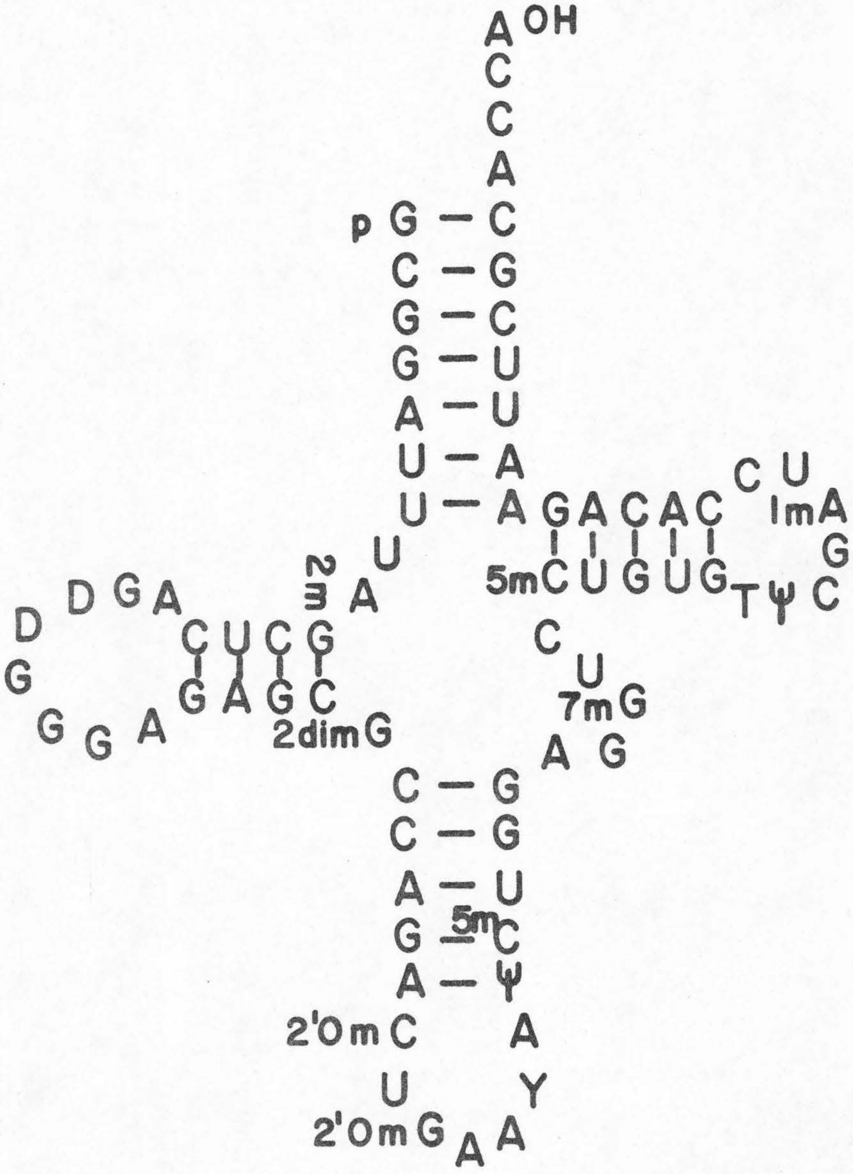
A OH
C
C
A
pG — C
C — G
G — C
G — U
A — U
U — A
U — A G A C A C
C U
ImA
G
5mC U G U G T ψ C
U
2m A
D G A
D
C U C G
G
G A G C
G G A
2dimG
C
U
7mG
A G
C — G
C — G
A — U
G — C
5m
A — ψ
2'OmC
A
U
Y
2'OmG A A

Phenylalanine tRNA

yeast

Ridge National Laboratory and was given to us by Dr. Barbara Vold of Scripps Clinic at La Jolla. The activity of the sample was reported to be 97%.

The sample was dialyzed against a solution so that the final concentrations were 0.01 M $MgCl_2$, 0.01 M tris buffer, 0.002 M $Na_2S_2O_3$ and the concentration of tRNA was approximately 34 mg/ml. The sample was lyophilized three times with 100 atom % D D_2O and the final solution was prepared with the 100 atom % D D_2O and sealed under vacuum.

The 100 atom % D_2O was obtained from Diaprep, Inc., Atlanta, Georgia and was stored under vacuum.

The purine was obtained from Sigma Chemical Company. It was deuterated in the H_8 position by heating a D_2O solution and was sublimed _in vacuo_. The tRNA sample was opened and sealed with a plastic cap during the purine study.

The phenylalanine tRNA was supplied by Dr. M. P. Schweizer of the Nucleic Acid Research Institute, International Chemical and Nuclear Corporation, Irvine, California, in the form of the lithium salt. It was enriched 9-10 fold in phenylalanine acceptance over bulk yeast tRNA.

The dimethylsulfoxide (DMSO) used in these experiments was 100.0 atom % deuterated and was obtained from Diaprep, Inc., Atlanta, Georgia.

The phenylalanine tRNA solutions were prepared and sealed under vacuum. The tRNA was lyophilized from D_2O. The DMSO concentrations are given in volume per cent.

The modified nucleosides studied here were also supplied by Dr. M. P. Schweizer.

The pmr spectra were taken on a Varian HR-220 NMR spectrometer. The sample temperature was controlled to ± 1°C by a Varian V-4343 variable temperature unit. The temperature was measured by observing the spectrum of ethylene glycol and using a calibration curve supplied by Varian.

A Hewlett-Packard 200 ABR audio oscillator was used to produce frequency side bands for chemical shift measurements and for triggering a Varian C-1024 time-averaging computer when additional signal-to-noise was necessary. The frequency of the side bands was counted with a Hewlett-Packard 5221 B electronic counter.

Measurements of pH were made with a Leeds and Northrup 7401 pH meter equipped with a miniature electrode assembly. The system was standardized to read pH. The standard correction was applied to determine the pD (18): pD = pH (meter reading + 0. 40).

3. 3. Results and Discussion of Experiments with $\mathrm{tRNA_f}^{\mathrm{Met}}$.

3. 3. 1. Temperature Study. The complete 220 MHz proton magnetic resonance spectrum of N-formylmethionine tRNA is shown in Figure 32. The low field region, I, contains the contributions from the H_8 and H_2 of adenine, H_8 of guanine, H_6 of cytosine and uracil. The region marked II contains the resonances of the H_5 protons of cytosine and uracil and the $H_{1'}$ protons of all the ribose moieties. The high field region, III, contains the remaining resonances of the ribose protons. The narrow high field resonance is due to tris which

FIGURE 32

A single scan of the complete proton magnetic resonance spectrum of $tRNA_f^{Met}$ at 220 MHz.

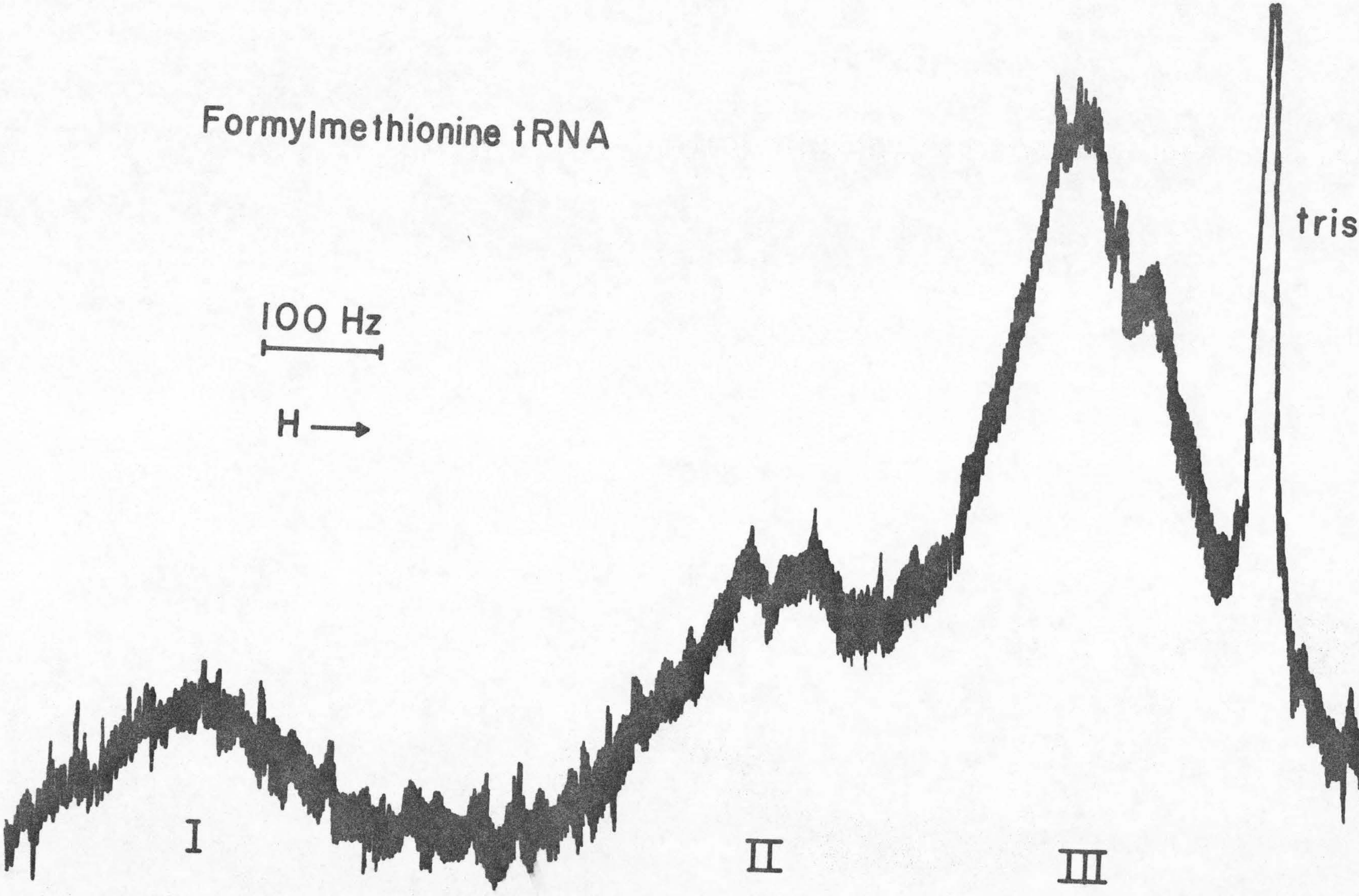
Formylmethionine tRNA
100 Hz
H ⟶
tris
I
II
III

was used as a buffer and as a standard for referencing chemical shifts.

The temperature variation of regions I and II is shown in Figure 33. From these spectra, it is seen that the broad envelope of the resonances changes only slightly when the temperature is varied from 31°C to 71°C. In contrast, I. C. P. Smith, et al.(77) observed three distinguishable peaks in the lowest field resonance of alanine tRNA at 68°C. The difference in these observations can be attributed to two possible sources. In the experiments with $tRNA_f^{Met}$, the solution contained 0.01 M $MgCl_2$ while the alanine tRNA solution contained 0.5 M NaCl. It is known that Mg^{++} aggregates tRNA;(95, 96) however, aggregation studies are usually made with at least 0.02 M Mg^{++}. Aggregation can also occur in Na^+ solutions; some aggregation has been reported in a solution with 0.1 M NaCl and about 100 mg tRNA per milliliter.(81) Thus, it is possible that either or both tRNA solutions contain some aggregates. The formation of aggregates would result in broadening of the resonances due to the larger size and slower tumbling rate.

Another difference in the two tRNA experiments is the transfer RNA itself. The sequence (see Table VI) of both of these molecules is known.(83, 97) It is expected from experiments with the homoribonucleotides at these temperatures that the low field portion of region I will contain the adenine and guanine resonances while the high field side of this region will contain the uracil and cytosine resonances. From the sequences of these tRNA molecules, it is seen that the A + G: C + U ratio in the $tRNA_f^{Met}$ is 38:33 while in the alanine

FIGURE 33

The effect of temperature on the low field resonances of $tRNA_f^{Met}$ (regions I and II).

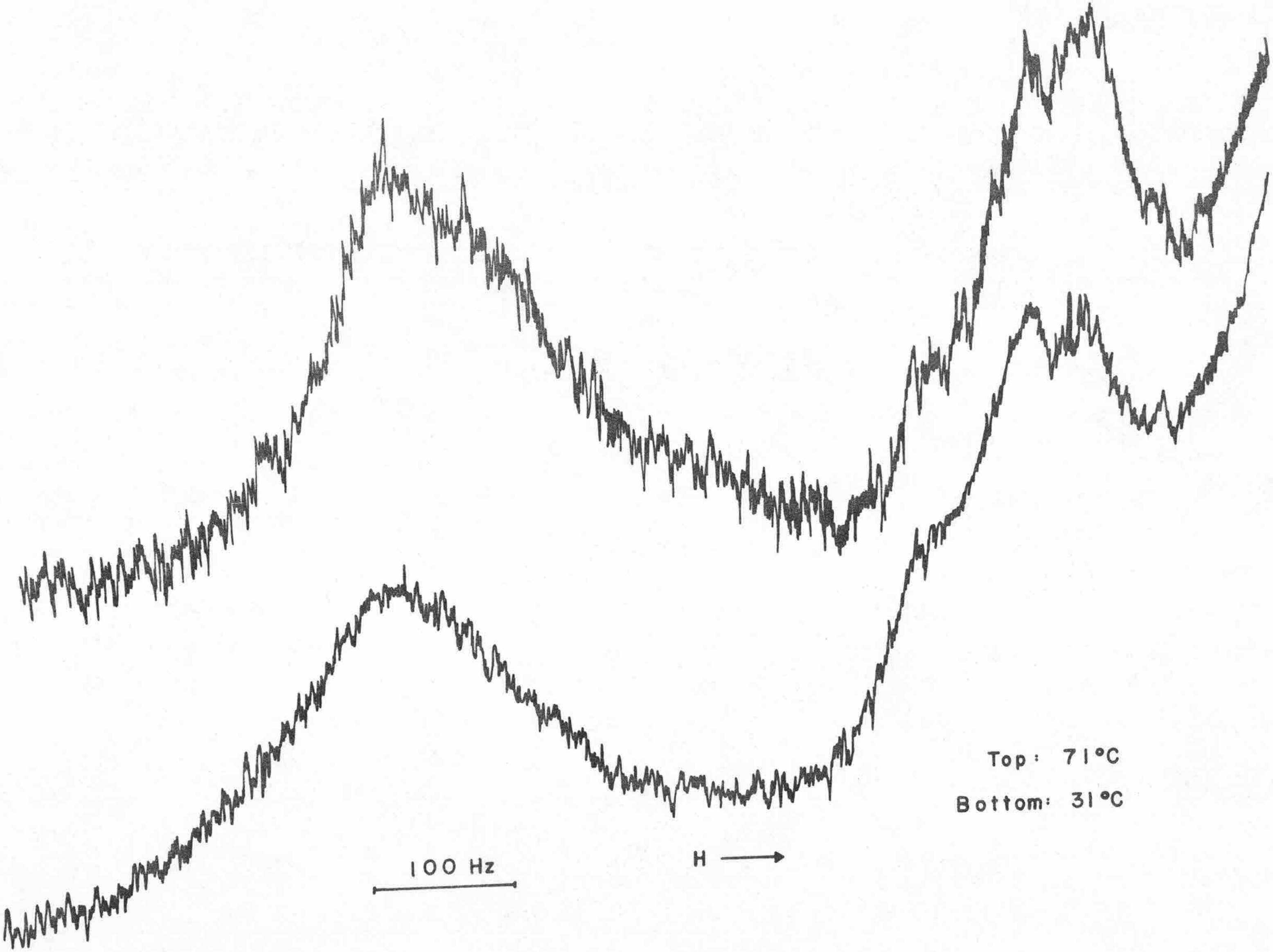
100 Hz
H ⟶
Top: 71°C
Bottom: 31°C

TABLE VI. Nucleoside Content of Formylmethionine, Alanine and Phenylalanine tRNA.

	Formyl-methionine (E. Coli)	Alanine (yeast)	Phenyl-alanine (yeast)
adenosine	14	7	17
guanosine	24	25	18
cytidine	25	24	15
uridine	8	12	12
pseudouridine	1	2	2
ribothymidine	1	1	1
dihydrouridine	1	2	2
4-thiouridine	1	0	0
2'-O-methylcytidine	1	0	1
7-methylguanosine	1	0	1
N_2-dimethylguanosine	0	1	1
1-methylinosine	0	1	0
inosine	0	1	0
2'-O-methylguanosine	0	0	1
1-methyladenosine	0	0	1
5-methylcytidine	0	0	2
2-methylguanosine	0	0	1
Y	0	0	1

tRNA it is 32:36. The higher proportion of adenine and guanine in $\text{tRNA}_f^{\text{Met}}$ as compared to alanine tRNA would be expected to cause the low field portion of this region to be more prominent in the $\text{tRNA}_f^{\text{Met}}$ than in the alanine tRNA. Thus, the presence of the higher proportion of adenine and guanine resonances could at least partially obscure the splitting observed in the alanine tRNA spectrum.

3.3.2. Purine Study. The interaction of purine with short chain nucleotides and with polyribonucleotides was discussed in section 2.3.4 of this thesis. It has been shown that purine intercalates between the bases of a short chain nucleotide(13, 15, 47, 51) and between the bases of the polynucleotides of uracil.(52, 53) However, purine does not seem to form an intercalated complex with the polyribonucleotides of adenine and cytosine. Apparently, as shown in this thesis, the bases are too close together in the stacked polynucleotide to readily allow the complete intercalation of a purine molecule.

In contrast, purine is able to intercalate into the tRNA molecule. When purine is added to the tRNA solution, the purine resonances are quite broad as shown in Table VII and in Figure 34. The widths are essentially invariant with temperature. Since the purine used in the experiment was deuterated in the H_8 position, no values could be measured for this resonance width. The width for the H_6 proton resonance is considerably larger than the width of the H_2 resonance. This width difference is the same as was found in the poly U and short chain nucleotide complexes with purine. Consequently, it indicates that the purine is intercalating between the nucleotide bases

TABLE VII. Purine linewidths in a solution with Formylmethionine tRNA

Purine Concentration	Purine Linewidths, Hz H_6	H_2
0.10	31	14
0.20	21	10
0.26	22	12

FIGURE 34

The broadening effect of tRNA on the purine proton resonances.

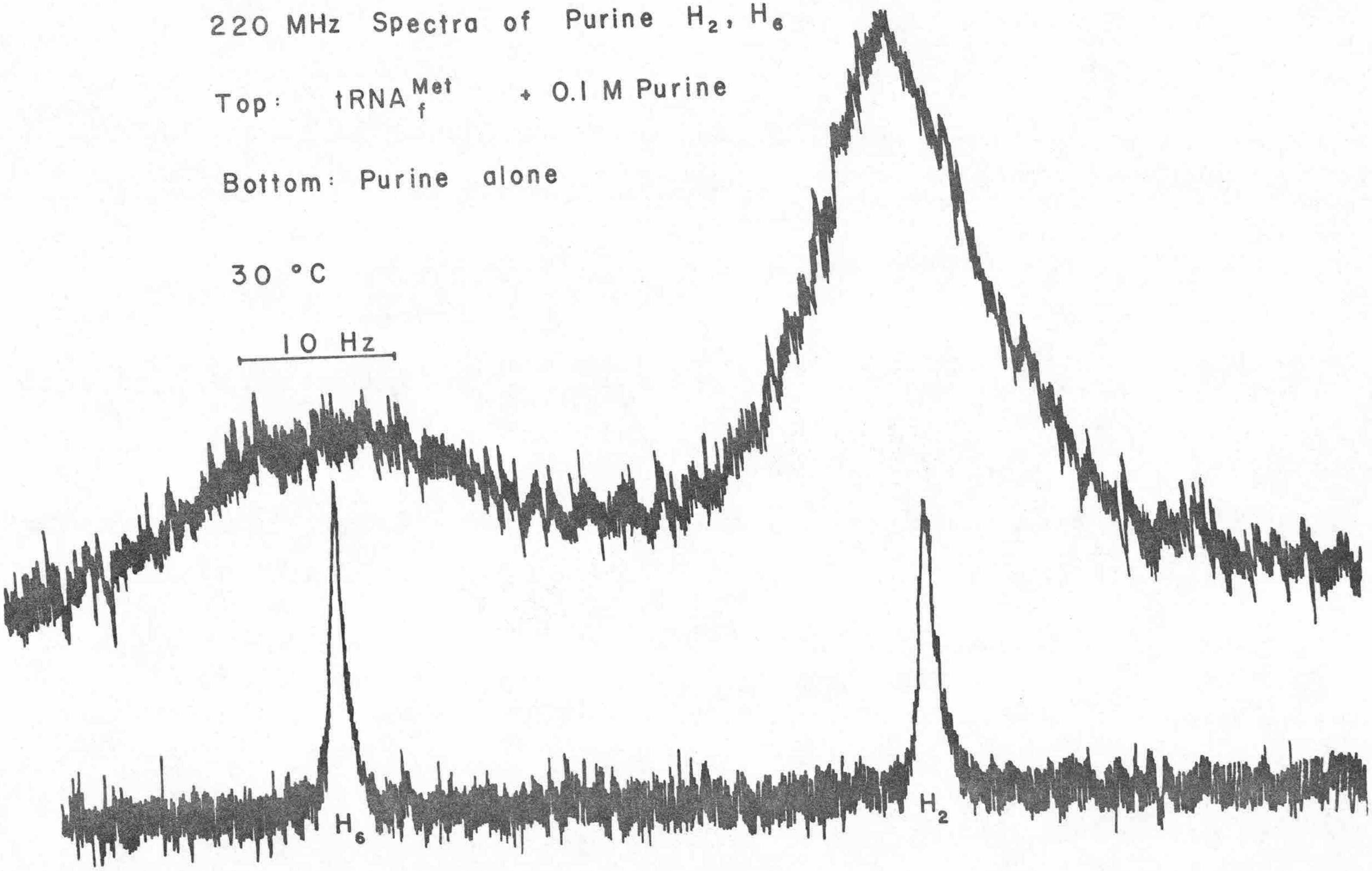
220 MHz Spectra of Purine H_2, H_6
Top: $tRNA_f^{Met}$ + 0.1 M Purine
Bottom: Purine alone
30 °C
10 Hz
H_6
H_2

in the tRNA in the same manner as it was shown to intercalate between the bases in poly U.(52, 53)

The work with the polynucleotides of adenine and cytosine indicate that purine is not capable of intercalating into closely stacked base systems. Examination of a CPK molecular model indicates that the bases in the loop regions would not be capable of stacking completely. Thus, it seems probable that the purine is intercalating into loop regions of the tRNA molecule.

The effect of purine on the low field region of the spectrum is shown in Figure 35. Although its effect cannot be measured quantitatively, it is apparent that the addition of purine has resulted in some changes in the resonances in this region.

3.4. Conclusions from the Study of Formylmethionine tRNA.

The low field region of the pmr spectrum of tRNA_f^{Met} differs slightly from that reported for alanine tRNA.(77) This difference may be explained by the base composition of the two molecules.

Even at 71°C, the proton resonances of the tRNA_f^{Met} remained too overlapped and too broad for assignment. The broadness of the resonances at this temperature indicates considerable retention of structure.

From the optical work, Sander and Ts'o(54) have shown that purine is a powerful denaturant for tRNA. Their optical rotation measurements indicate that the denaturing effect of 0.2 M-0.6 M purine is approximately equivalent to an elevation of 20°C to 40°C in temperature. The pmr results are in general agreement with

FIGURE 35

The effect of purine on the low field resonance of $tRNA_f^{Met}$. The bottom resonance is for the tRNA without purine at 67°C and the top spectrum shows the effect of 0.2 M purine at 61°C. The sharp resonances at low field in the top spectrum are a spinning sideband of the H_2 resonance of purine and the resonance of the protons remaining in the H_8 position of purine after deuteration.

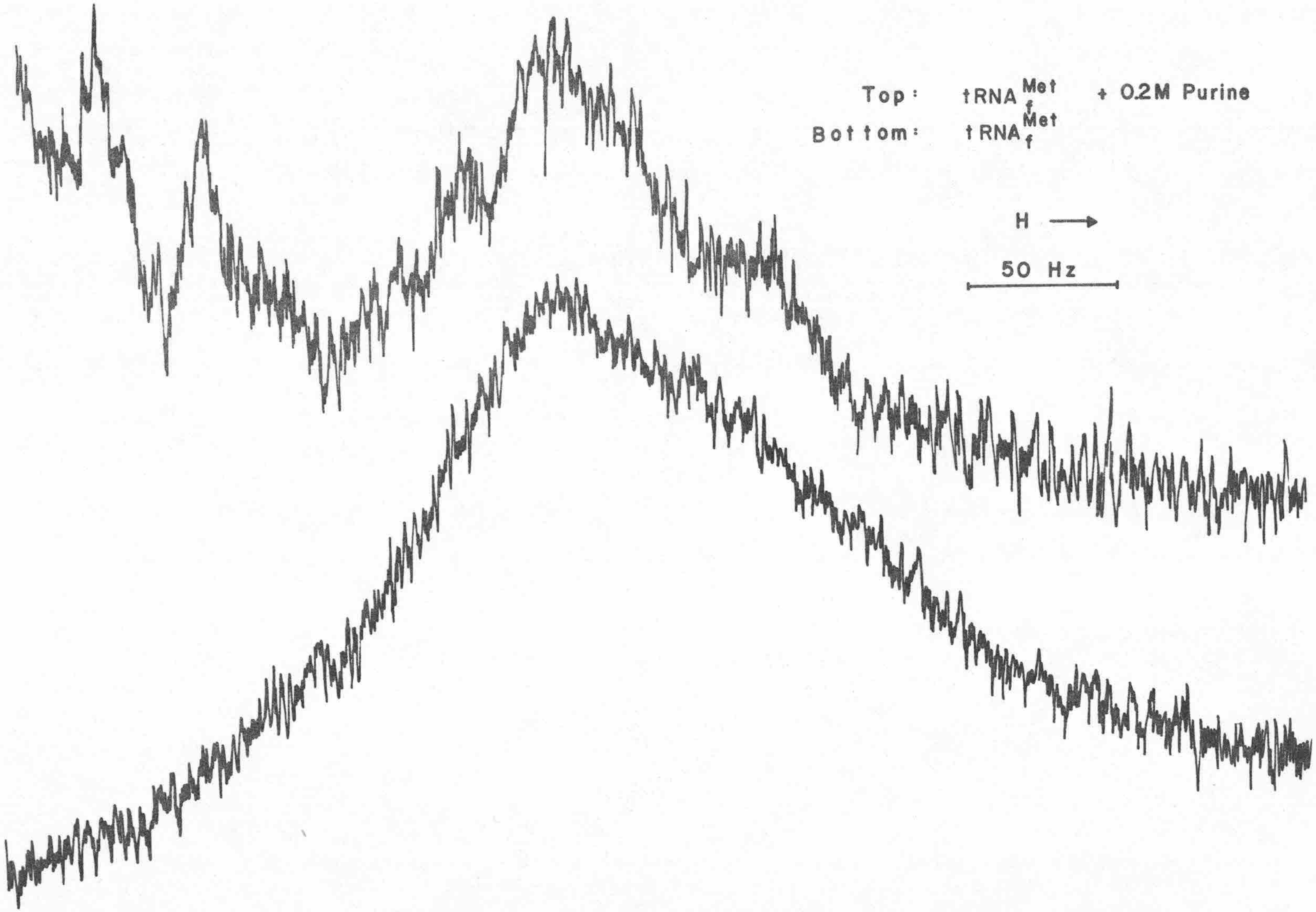
Top: $tRNA_f^{Met}$ + 0.2M Purine
Bottom: $tRNA_f^{Met}$
H →
50 Hz

these conclusions. In addition, they indicate that the denaturation effect of purine is probably due to disruption of stacking in the loop regions of the molecule where the purine is capable of intercalating between the bases.

3.5. Results and Discussion of Experiments on Phenylalanine tRNA.

The "melting" action of dimethylsulfoxide (DMSO) on double and single stranded nucleic acids has been demonstrated.(79, 98-101) DMSO has been shown to make the molecules quite flexible. The flexibility is presumably due to disruption of the ordered water structure by the DMSO and the interaction of the DMSO with the nucleic acids as a hydrogen bond acceptor.

DMSO is a strong proton acceptor. Consequently, the hydrogen bonding between complementary bases in the tRNA must compete with hydrogen bonding to the solvent. As shown in studies of the pairing of guanosine and cytidine,(102, 103) however, DMSO does not completely destroy this base pairing.

As the water structure is disrupted by the addition of DMSO, the hydrophobic vertical stacking of the bases becomes less important. Consequently, due to the disruption of base stacking and intramolecular hydrogen bonding, the structure of the tRNA is disrupted and the tRNA begins to resemble a randomly oriented, unstacked, single stranded polynucleotide chain. Due to the increased flexibility, the intramolecular dipolar interactions are averaged out more completely, and the pmr resonances become narrower. Also, the shielding effect of the nearest neighbor bases which causes the shifting of the positions of the resonances becomes much less important because the disruption of the stacking interaction means that the bases are on an average further apart. The shielding effect of the neighboring bases drops off as the reciprocal of the distance between the bases cubed. Thus, the addition of DMSO results in shifting the resonances to lower field just as it was shown(104) for the disruption of stacking by heating in the single stranded polynucleotides. The lessening of the nearest neighbor effects also contributes to a narrowing of the observed resonances of the common bases in the tRNA. Each adenine H_8 , for example, contributes a resonance to the same region of the spectrum. As the molecule loses its tertiary structure, the adenine H_8 's become more nearly equivalent. Thus, the resonance, which for the structured molecule is a broad envelope of lines of considerable chemical shift heterogeneity, becomes narrower due to the decrease in the shift differences of the various adenine H_8 's.

A rather abrupt decrease(105) in the optical rotation of the $tRNA^{Phe}$ occurs as DMSO is added; the largest change occurs between 50 and 60% DMSO. This study indicates that the DMSO continuously denatures the tRNA structure, but that the major structural transition is made in the region of 50-60% DMSO.

As a basis for assigning the resonances observed in the pmr of $tRNA^{Phe}$, spectra were taken of the various modified nucleosides which occur in this molecule. The observed resonances are given in Table VIII.

A single scan of a D_2O solution of a tRNA is shown in Figure 36. The spectrum is divided into regions. Region I contains the

TABLE VII. Proton Magnetic Resonances of Some Nucleosides.

Compound	Proton					
	H_8	H_2	H_6	H_5	$H_{1'}$	$-CH_3$
83% DMSO : 17% D_2O						
adenosine	-8.548	-8.369			-6.102	
guanosine	-8.089				-5.872	
N_2-methylguanosine						-3.027
2′-O-methylguanosine	-8.160				-5.990	-3.510
N_2-dimethylguanosine	-8.093				-5.915	-3.246
β-pseudouridine			-7.700		-4.647	
ribothymidine			-7.919		-5.987	-1.994
5-methylcytidine			-7.901		-5.957	-2.042
dihydrouridine				-3.73		
50% DMSO : 50% D_2O						
1-methyladenosine	-8.149	-8.019			-5.829	-3.472
7-methylguanosine					-5.603	-3.592

FIGURE 36

Proton magnetic resonance spectrum of DMSO-D_2O solution of a tRNA. Region I contains resonances from H_8 of guanine and adenine, H_2 of adenine and H_6 of cytosine and uracil. Region II contains resonances from H_5 of cytosine and uracil and $H_{1'}$ of all the ribose moieties. Region III and Region IV contain resonances from the modified nucleosides. The ribose resonances other than $H_{1'}$ and the residual resonance from water occur between Regions II and III; the residual resonance from DMSO occurs between Regions III and IV. The resonance of external TMS is at the high field end of the spectrum.

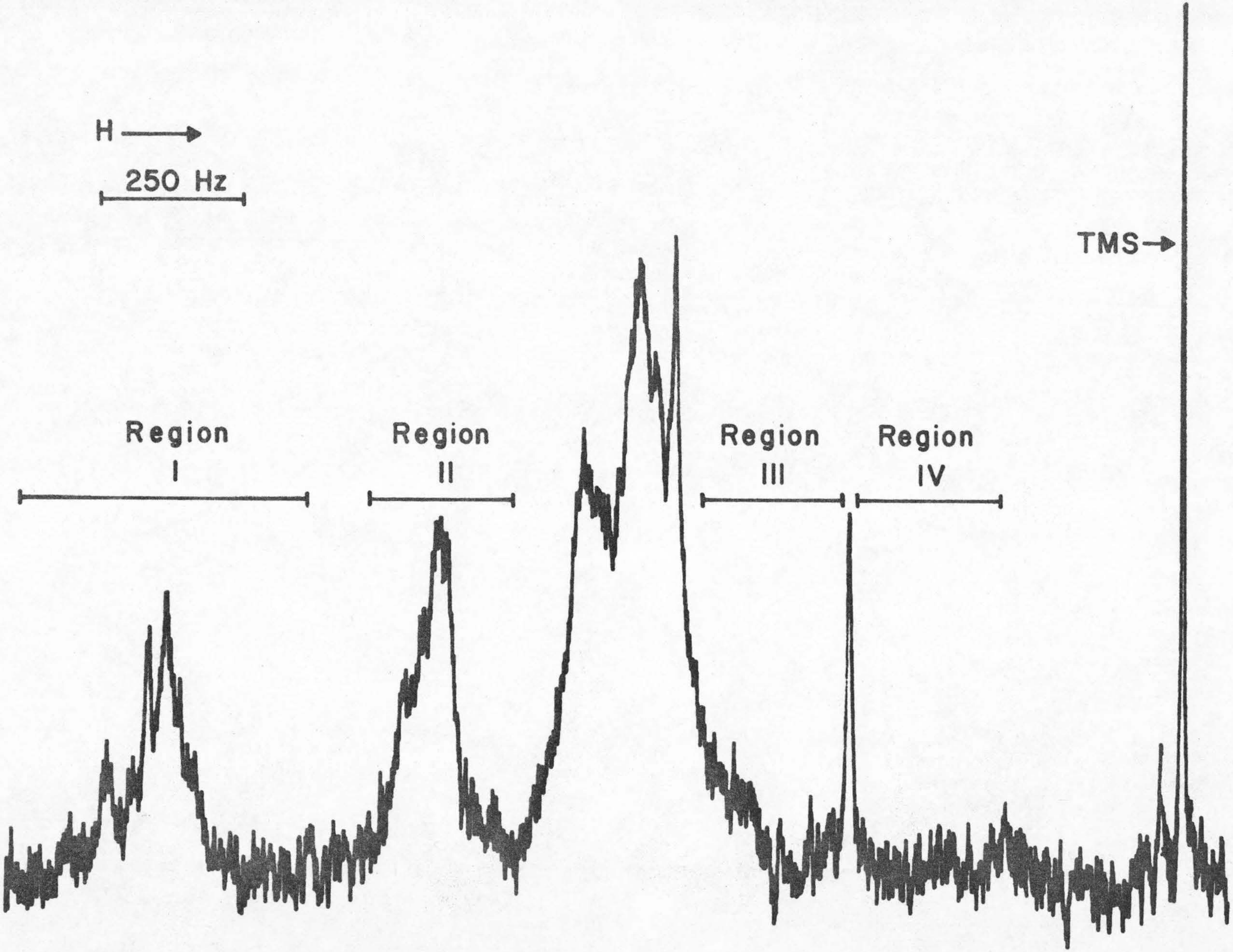
H →
250 Hz
Region I
Region II
Region III
Region IV
TMS →

aromatic resonances: adenine H_2 and H_2, guanine H_8 , and the pyrimidine H_6. Region II contains the pyrimidine H_5 and the ribose $H_{1'}$. Region III, IV, and V contain resonances from groups on the various modified nucleotides. Between Regions II and III, the sharp resonance is the residual water resonance and the strong-broad resonance is due to the ribose protons other than $H_{1'}$. A resonance due to the residual protons left in the deuterated DMSO occurs at the junction of Regions III and IV when DMSO is used in the solvent mixture.

The spectra of the aromatic resonances, Region I, are shown in Figure 37. The marked influence of DMSO on both the spectral resonance widths and the chemical shifts is apparent in going from 0 to 83% DMSO. By comparison of the $tRNA^{Phe}$ resonances with those observed for the various nucleosides, it is possible to make the following assignments (chemical shifts in ppm from external TMS) in the spectrum of 83% DMSO:

adenine H_8	-8.695	
adenine H_2	-8.356	
guanine H_8	-8.182	
pyrimidine H_6	-8.006	two doublets spin coupled with H_5; also ribothymine H_6
	-7.958	
pseudouracil H_6	-7.849	tentative

The other peaks were not assigned. There appears to be an additional pyrimidine H_6 resonance at -7.767 ppm. The difference in the purine H_8 resonances and those assigned to these protons in $tRNA^{Phe}$ (~0.15 ppm) is expected(9) due to the effect of the presence of the phosphate groups.

The resonance widths decrease by a factor of about 5 to 7

FIGURE 37

Spectra of the aromatic region, Region I, of tRNA^{Phe} upon addition of DMSO.

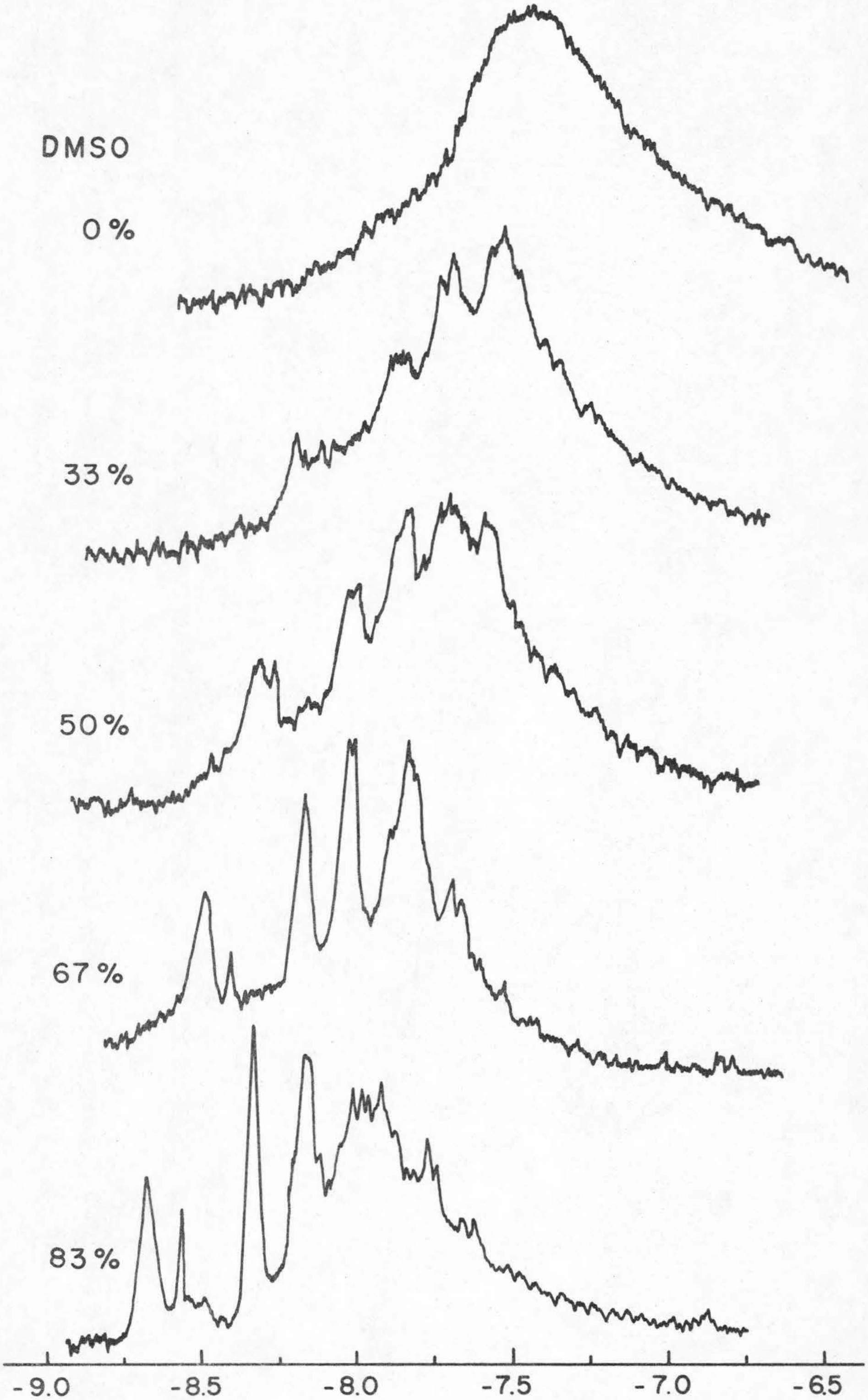
DMSO
0 %
33 %
50%
67 %
83 %
- 9.0
- 8.5
- 8.0
- 7.5
- 7.0
- 6.5
chemical shifts in ppm from TMS capillary

during the DMSO titration. For example, the adenine H_2 resonance is approximately 50 Hz in the spectrum with 33% DMSO, and about 8.0 Hz in the spectrum with 83% DMSO. The adenine H_8 is about 65 Hz with 33% DMSO and about 14 Hz with 83% DMSO.

The region of the pyrimidine H_5 and the ribose $H_{1'}$ resonances, Region II, is shown in Figure 38. The $H_{1'}$ resonances form the broad peak on the low field side of this region.

Region III is shown in Figure 39. This region extends from just to the high field side of the strong resonances of the five ribose protons to just to the low field side of the resonance due to the residual protons left on the DMSO. By examining the resonances of the modified nucleosides, it is possible to make the following assignments for the 83% DMSO solution:

H_5's of dihydrouridine	-3.620 ppm
$-CH_3$ of 2′-O-methylguanine	-3.473 ppm
$-CH_3$ of 2′-O-methylcytidine	-3.425 ppm
$-CH_3$'s of N_2-dimethylguanine	-3.162 ppm
$-CH_3$ of N_2-methylguanine	-2.972 ppm

The resonance at -3.660 ppm in the spectrum at 50% DMSO may be due to the methyl group of 7-methylguanosine.

For the methyl group of N_2-dimethylguanine, the resonance width decreases from 20 Hz to 10 Hz as the DMSO concentration is changed from 33 to 83%; for the same DMSO change, the width of the resonance assigned to the H_5's of dihydrouridine goes from 25 Hz to 11 Hz.

Region IV is shown in Figure 40. This region begins just to

FIGURE 38

Spectra of Region II upon addition of DMSO to the solution.

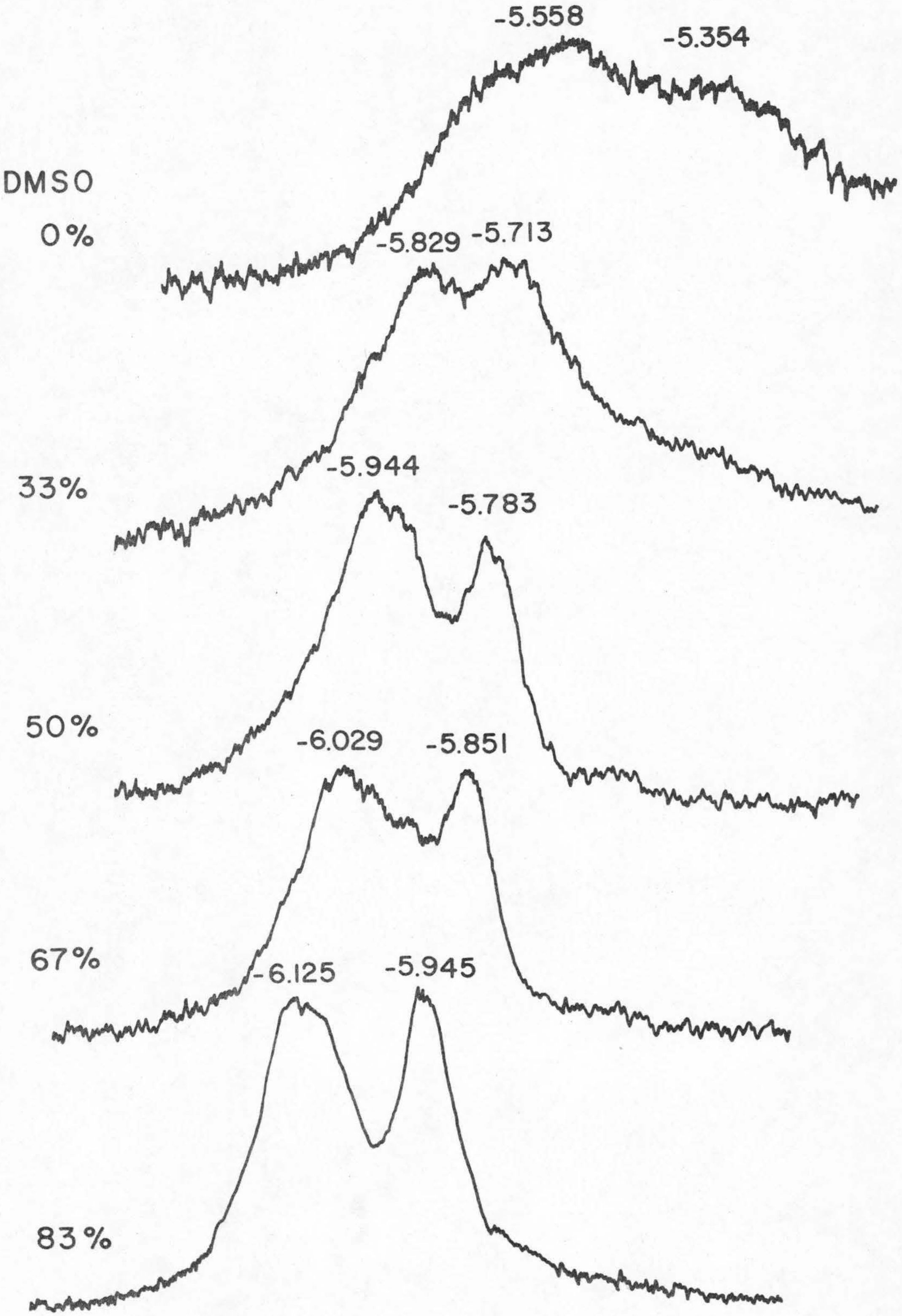

chemical shifts in ppm from TMS capillary

FIGURE 39

Spectra of Region III upon the addition of DMSO to the solution.

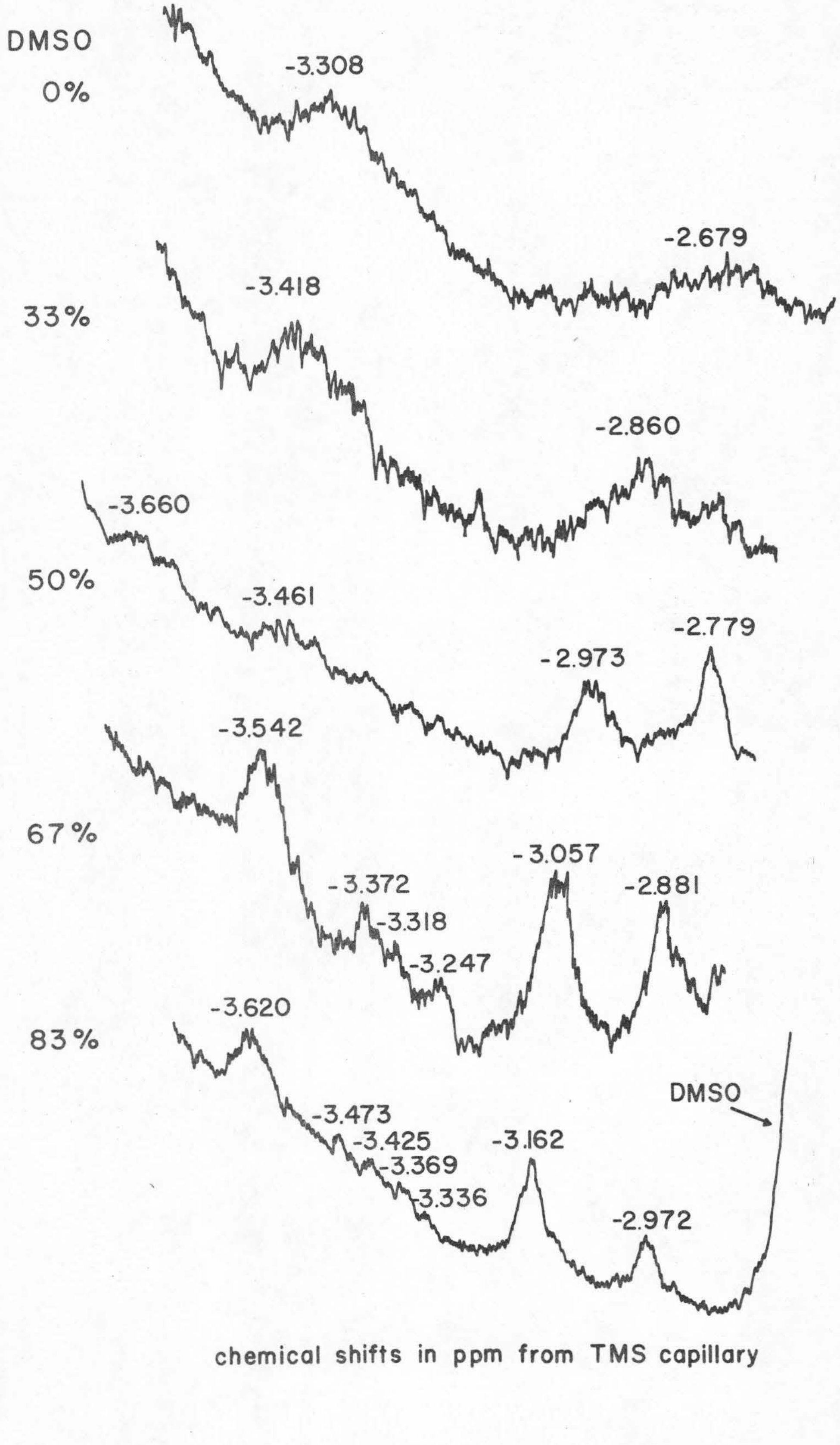

chemical shifts in ppm from TMS capillary

FIGURE 40

Spectra of Region IV upon the addition of DMSO to the solution.

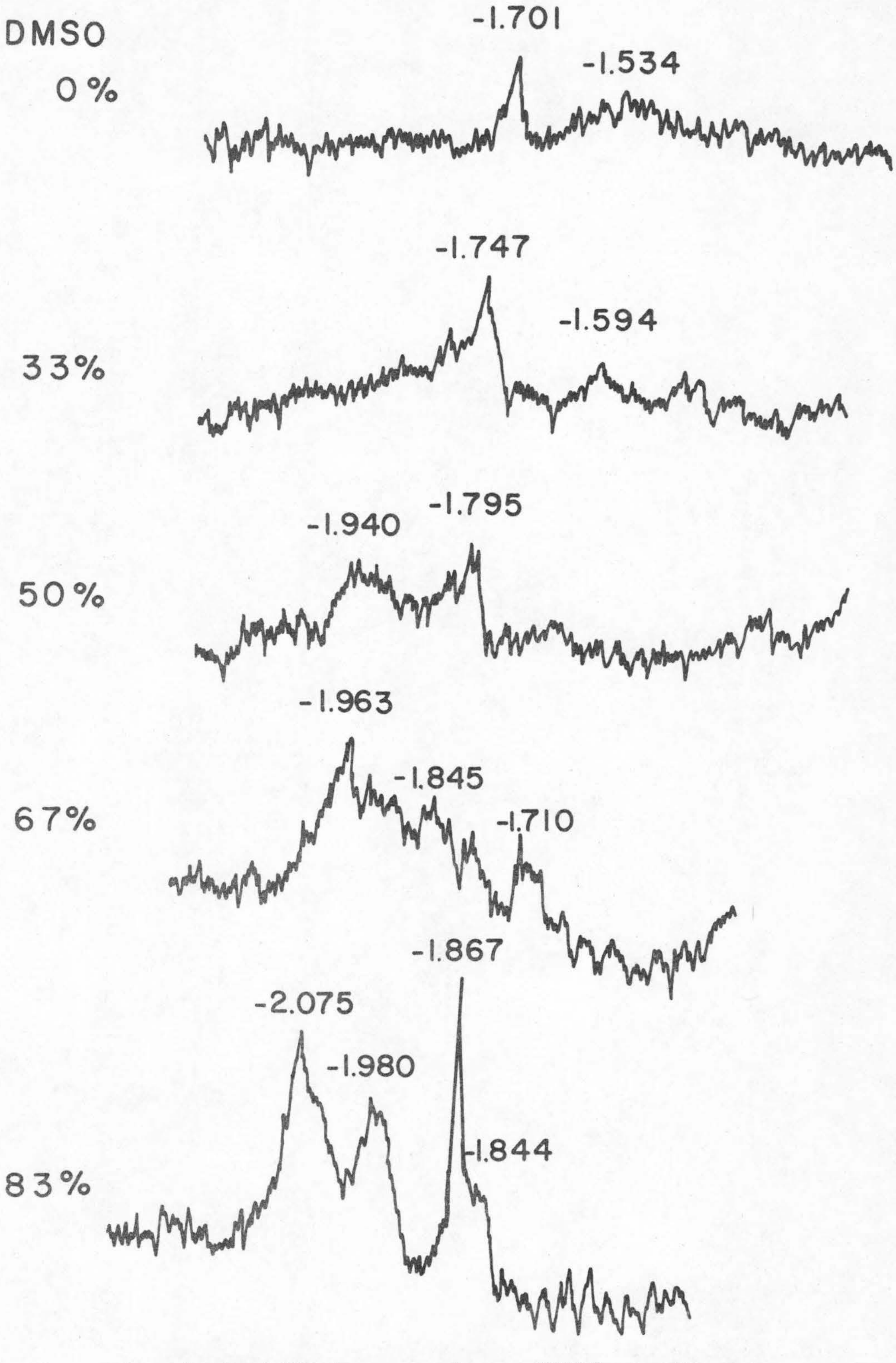

chemical shifts in ppm from TMS capillary

the high field side of the DMSO resonance. For the 83% DMSO solution, two resonances can be tentatively assigned:

-CH_3's of 5-methylcytidine	-2.075 ppm
-CH_3 of ribothymidine	-1.980 ppm

The source of the sharp resonance at -1.867 ppm in 83% DMSO and at ~-1.7 in 0 and 33% DMSO remains unexplained at this time.

Relatively intense, high field resonances were observed. These resonances are probably not attributable to the transfer RNA. In 83% DMSO, their position is approximately -1.35 ppm downfield from external TMS.

So far, no resonances can be positively assigned to the Y base. The Y base can be specifically removed(106) by incubating the tRNA for about two hours at pH 2.9 and 37°C. The sugar phosphate backbone is not disrupted and the acid treated tRNA can still be charged with phenylalanine. However, the ability to recognize the codon is completely destroyed.

The $tRNA^{Phe}$ used in the DMSO study has now been subjected to the acid treatment. We are preparing to take its spectrum to see if any of the resonances observed in $tRNA^{Phe}$ can be attributed to the Y base.

3.6. Conclusions from the Study of Phenylalanine tRNA.

The addition of dimethylsulfoxide to a deuterium oxide solution of transfer RNA renders the RNA molecule sufficiently flexible to allow the observation of proton magnetic resonances from individual base residues. The $tRNA^{Phe}$ molecule is known to contain a number of modified nucleotides. Resonances from these units can be observed and identified by comparison with spectra of the mononucleosides.

The use of dimethylsulfoxide as a denaturing solvent is currently being extended to studies on other specific tRNA molecules of known primary sequence. Preliminary results on $\mathrm{tRNA}_f^{\mathrm{Met}}$ from E. Coli indicate that this molecule is not as flexible as $\mathrm{tRNA}^{\mathrm{Phe}}$ in a solution containing 83% dimethylsulfoxide. This result may be a reflection of the high proportion of guanine-cytosine which occurs in the $\mathrm{tRNA}_f^{\mathrm{Met}}$ (Table VI). The guanine-cytosine pair with three hydrogen bonds is more stable than the adenine-uracil pair which has two hydrogen bonds. In support of this result, it has been noted(107) that $\mathrm{tRNA}_f^{\mathrm{Met}}$ has a higher melting temperature than $\mathrm{tRNA}^{\mathrm{Met}}$ which has a lower guanine-cytosine content.

REFERENCES

1. D. Baltimore, Nature, **226**, 1209 (1970).
2. H. M. Temin and S. Mizutani, Nature, **226**, 1211 (1970).
3. J. D. Watson and F. H. C. Crick, Nature, **171**, 737, 964 (1953).
4. P. O. P. Ts'o, I. S. Melvin and A. C. Olson, J. Am. Chem. Soc., **85**, 1289 (1963).
5. P. O. P. Ts'o and S. I. Chan, J. Am. Chem. Soc., **86**, 4176 (1964).
6. S. I. Chan, M. P. Schweizer, P. O. P. Ts'o and G. M. Helmkamp, J. Am. Chem. Soc., **86**, 4182 (1964).
7. M. P. Schweizer, S. I. Chan and P. O. P. Ts'o, J. Am. Chem. Soc., **87**, 5241 (1965).
8. A. D. Broom, M. P. Schweizer and P. O. P. Ts'o, J. Am. Chem. Soc., **89**, 3612 (1967).
9. M. P. Schweizer, A. D. Broom, P. O. P. Ts'o and D. P. Hollis, J. Am. Chem. Soc., **90**, 1042 (1968).
10. M. M. Warshaw and I. Tinoco, Jr., J. Mol. Biol., **20**, 29 (1966).
11. J. Brahms, J. C. Maurizot and A. M. Michelson, J. Mol. Biol., **25**, 481 (1967).
12. R. C. David and I. Tinoco, Jr., Biopolymers, **6**, 223 (1968).
13. S. I. Chan and J. H. Nelson, J. Am. Chem. Soc., **91**, 168 (1969).
14. B. W. Bangerter and S. I. Chan, J. Am. Chem. Soc., **91**, 3910 (1969).

15. J. H. Nelson, Thesis, California Institute of Technology, 1969.

16. G. D. Fasman, C. Lindblow and L. Grossman, *Biochem.*, **3**, 1015 (1964).

17. D. N. Holcomb and I. Tinoco, Jr., *Biopolymers*, **3**, 121 (1965).

18. K. E. Van Holde, J. Brahms and A. M. Michelson, *J. Mol. Biol.*, **12**, 726 (1965).

19. A. M. Michelson and C. Monny, *Proc. Nat. Acad. Sci. U.S.*, **56**, 1528 (1966).

20. J. Brahms, J. C. Maurizot and A. M. Michelson, *J. Mol. Biol.*, **25**, 465 (1967).

21. J. A. Pople, W. G. Schneider and H. J. Bernstein,"High-resolution Nuclear Magnetic Resonance," McGraw-Hill, New York, 1959, pp. 176-183.

22. Reference 20, pp. 407-415.

23. J. W. Emsley, J. Feeney and L. H. Sutcliffe, "High Resolution Nuclear Magnetic Resonance Spectroscopy," Pergamon Press, Oxford, 1965, pp. 66-99.

24. J. Applequist and V. Damle, *J. Am. Chem. Soc.*, **88**, 3895 (1966).

25. D. Poland, J. N. Vournakis and H. A. Scheraga, *Biopolymers*, **4**, 223 (1966).

26. R. M. Epand and H. A. Scheraga, *J. Am. Chem. Soc.*, **89**, 3888 (1967).

27. D. Glaubiger, D. A. Lloyd and I. Tinoco, Jr., *Biopolymers*, **6**, 409 (1968).

28. P. K. Glasoe and F. A. Long, *J. Phys. Chem.*, **64**, 188 (1960).

29. C. C. McDonald, W. D. Phillips and S. Penman, Science, **144**, 1234 (1964).

30. J. P. McTague, V. Ross and J. H. Gibbs, Biopolymers, **2**, 163 (1964).

31. O. Jardetzky, Biopolymers Symposia, **1**, 501 (1964).

32. A. E. V. Haschemeyer and A. Rich, J. Mol. Biol., **27**, 369 (1967).

33. J. Donohue and K. N. Trueblood, J. Mol. Biol., **2**, 363 (1960).

34. I. Feldman and R. P. Agarwal, J. Am. Chem. Soc., **90**, 7329 (1968).

35. C. D. Jardetzky and O. Jardetzky, J. Am. Chem. Soc., **82**, 222 (1960).

36. L. Gatlin and J. C. Davis, Jr., J. Am. Chem. Soc., **84**, 4464(1962).

37. C. E. Johnson, Jr. and F. A. Bovey, J. Chem. Phys., **29**, 1012 (1958).

38. C. Giessner-Prettre and B. Pullman, Compt. Rend., **261**, 2521 (1965).

39. J. T. Finch and A. Klug, J. Mol. Biol., **46**, 597 (1969).

40. H. DeVoe, Theory of the Conformations of Biological Macromolecules in Solution, in "Structure and Stability of Biological Macromolecules," S. N. Timasheff and G. D. Fasman, eds., Marcel Dekker, New York, 1969, pp. 1-63.

41. M. Leng and G. Felsenfeld, J. Mol. Biol., **15**, 455 (1966).

42. J. Brahms, A. M. Michelson and K. E. Van Holde, J. Mol. Biol., **15**, 467 (1966).

43. J. Applequist, J. Chem. Phys., **38**, 934 (1963).

44. B. H. Zimm and J. K. Bragg, *J. Chem. Phys.*, **31**, 526 (1959).

45. A. M. Michelson, Oligonucleotide Interactions, in "Molecular Associations in Biology," B. Pullman, ed., Academic Press, New York, 1968, pp. 93-106.

46. G. P. Kreishman and S. I. Chan, *Biopolymers*, in press.

47. B. W. Bangerter, Thesis, California Institute of Technology, 1969.

48. J. H. Prestegard and S. I. Chan, *J. Am. Chem. Soc.*, **91**, 2843 (1969).

49. F. E. Hruska and S. I. Danyluk, *J. Am. Chem. Soc.*, **90**, 3266 (1968).

50. C. D. Jardetzky, *J. Am. Chem. Soc.*, **82**, 229 (1960).

51. S. I. Chan, B. W. Bangerter and H. H. Peter, *Proc. Nat. Acad. Sci. U.S.*, **55**, 720 (1966).

52. B. W. Bangerter and S. I. Chan, *Biopolymers*, **6**, 983 (1968).

53. S. I. Chan and G. P. Kreishman, *J. Am. Chem. Soc.*, **92**, 1102 (1970).

54. C. Sander and P. O. P. Ts'o, *Biopolymers*, **9**, 765 (1970).

55. H. G. Zachau, *Angew. Chem.*, **81**, 645 (1969); *Angew. Chem., Internat. Edit.*, **8**, 711 (1969).

56. M. J. Waring, *Annual Reports, The Chem. Soc.*, **65 B**, 551 (1968).

57. B. F. C. Clark, B. P. Doctor, K. C. Holmes, A. Klug, K. A. Marcker, S. J. Morris, H. H. Paradies, *Nature*, **219**, 1222 (1968).

58. A. Hampel, M. Labanauskas, P. G. Connors, L. Kirkegard,

U. L. RajBhandary, P. B. Sigler and R. M. Bock, *Science*, **162**, 1384 (1968).

59. F. Cramer, F. von der Haar, W. Saenger and E. Schlimme, *Angew. Chem.*, **80**, 969 (1968); *Angew. Chem., Internat. Edit.*, **7**, 895 (1968).

60. J. R. Fresco, R. D. Blake and R. Langridge, *Nature*, **220**, 1285 (1968).

61. H. H. Paradies, *F. E. B. S. Letters*, **2**, 112 (1968).

62. J. D. Young, R. M. Bock, S. Nishimura, H. Ishikura, Y. Yamada, U. L. RajBhandary, M. Labanauskas, P. G. Connors, *Science*, **166**, 1527 (1969).

63. S. H. Kim and A. Rich, *Science*, **162**, 1381 (1968).

64. B. S. Vold, *Biochem. Biophys. Res. Comm.*, **35**, 222 (1969).

65. C. D. Johnson, K. Adolph, J. J. Rosa, M. D. Hall and P. B. Sigler, *Nature*, **226**, 1246 (1970).

66. S. H. Kim and A. Rich, *Science*, **166**, 1621 (1969).

67. M. Labanauskas, P. G. Connors, J. D. Young, R. M. Bock, J. W. Anderegg and W. W. Beeman, *Nature*, **166**, 1530 (1969).

68. R. D. Blake, J. R. Fresco and R. Langridge, *Nature*, **225**, 32 (1970).

69. F. Cramer, F. von der Haar, K. C. Holmes, W. Saenger, E. Schimme and G. E. Schulz, *J. Mol. Biol.*, **51**, 523 (1970).

70. P. G. Connors, M. Labanauskas and W. W. Beeman, *Science*, **166**, 1528 (1969).

71. F. Cramer, H. Doepner, F. von der Haar, E. Schlimme and H. Seidel, *Proc. Nat. Acad. Sci. U.S.*, **61**, 1384 (1968).

72. F. Cramer, *Angew. Chem.*, **79**, 653 (1967); *Angew. Chem. Internat. Edit.*, **6**, 642 (1967).

73. J. Ninio, A. Favre and M. Yaniv, *Nature*, **223**, 1333 (1969).

74. M. Levitt, *Nature*, **224**, 759 (1969).

75. G. Melcher, *F. E. B. S. Letters*, **3**, 185 (1969).

76. J. A. Lake and W. W. Beeman, *J. Mol. Biol.*, **31**, 115 (1968).

77. I. C. P. Smith, T. Yamane and R. G. Shulman, *Canadian J. Biochem.*, **47**, 480 (1969).

78. M. Cohn, A. Danchin and Grunberg-Manago, *J. Mol. Biol.*, **39**, 199 (1969).

79. M. P. Schweizer, *Biochem. Biophys. Res. Comm.*, **36**, 871 (1969).

80. C. C. McDonald, W. D. Phillips and J. Penswick, *Biopolymers*, **3**, 609 (1965).

81. I. C. P. Smith, T. Yamane and R. G. Shulman, *Science*, **159**, 1360 (1968).

82. P. O. P. Ts'o, G. K. Helmkamp and C. Sander, *Proc. Nat. Acad. Sci. U.S.*, **48**, 686(1962).

83. S. K. Dube, K. A. Marcker, B. F. C. Clark and S. Cory, *Nature*, **218**, 232 (1968).

84. B. F. C. Clark and K. A. Marcker, *J. Mol. Biol.*, **17**, 394 (1966).

85. R. E. Webster, D. L. Engelhardt and N. D. Zinder, *Proc. Nat. Acad. Sci. U.S.*, **55**, 155 (1966).

86. J. M. Adams and M. R. Capecchi, *Proc. Nat. Acad. Sci. U.S.*, **55**, 147 (1966).

87. B. F. C. Clark and K. A. Marcker, *Nature*, **211**, 378 (1966).

88. K. A. Marcker and F. Sanger, *J. Mol. Biol.*, **8**, 835 (1964).

89. M. S. Bretscher, *J. Mol. Biol.*, **34**, 131 (1968).

90. C. C. Liew, G. W. Haslett and V. G. Allfrey, *Nature*, **226**, 414 (1970).

91. U. L. RajBhandary, S. H. Chang, A. Stuart, R. D. Faulkner, R. M. Hoskinson and H. G. Khorana, *Proc. Nat. Acad. Sci. U.S.*, **57**, 751 (1967).

92. D. Yoshikami, G. Katz, E. B. Keller and B. S. Dudock, *Biochim. Biophys. Acta*, **166**, 714 (1968).

93. L. M. Fink, T. Goto, F. Frankel and I. B. Weinstein, *Biochem. Biophys. Res. Comm.*, **32**, 963 (1968).

94. B. S. Dudock, G. Katz, E. K. Taylor and R. W. Holley, *Fed. Proc.*, **27**, 342 (1968).

95. D. B. Millar and R. F. Steiner, *Biochem.*, **5**, 2289 (1966).

96. D. B. Millar, *Nature*, **211**, 1088 (1966).

97. R. W. Holley, J. Apgar, G. A. Everett, J. T. Madison, M. Marquisee, S.H. Merrill, J. R. Penswick and A. Zamir, *Science*, **147**, 1462 (1965).

98. G. K. Helmkamp and P. O. P. Ts'o, *J. Am. Chem. Soc.*, **83**, 138 (1961).

99. L. Katz and S. Penman, *Biochem. Biophys. Res. Comm.*, **23**, 557 (1966).

100. J. H. Strauss, Jr., R. B. Kelly and R. L. Sinsheimer, *Biopolymers*, **6**, 793 (1968).

101. P. O. P. Ts'o, N. S. Kondo, M. P. Schweizer and D. P.

Hollis, Biochem., 8, 997 (1969).

102. R. A. Newmark and C. R. Cantor, J. Am. Chem. Soc., 90, 5010 (1968).

103. F. K. Schweighardt, C. Moll and N. C. Li, J. Magnetic Res., 2, 35 (1970).

104. Part I, Section 2 of this thesis.

105. M. P. Schweizer, private communication.

106. R. Thiebe and H. G. Zachau, European J. Biochem., 5, 546 (1968).

107. T. Seno, M. Kobayashi and S. Nishimura, Biochim. Biophys. Acta, 169, 80 (1968).

PART II

ELECTRON SPIN RELAXATION STUDIES OF MANGANESE (II) COMPLEXES IN ACETONITRILE

The following section of this thesis is being submitted for publication under joint authorship with Lahmer Lynds, Sunney I. Chan and Ruth M. Lynden-Bell.

1. INTRODUCTION

The electron paramagnetic resonance spectra of $\mathrm{Mn}[(\mathrm{CH_3CN})_6]^{+2}$, $[\mathrm{MnCl_4}]^{-2}$ and $[\mathrm{MnBr_4}]^{-2}$ in $\mathrm{CH_3CN}$ have been reported[1] by Chan, Fung and Lütje. The electron structure of these complexes have been characterized by the comparison of their electron paramagnetic and optical spectra. A clear relationship between the $^{55}\mathrm{Mn}$ nuclear hyperfine constant and the symmetry of the complex is apparent. In the tetrahedral ligand field, the nuclear hyperfine constant, $|<A>|$, equals 75-79 gauss; in an octahedral ligand field, $|<A>|$ equals 93-95 gauss.

In contrast to the relatively sharp electron paramagnetic resonance spectra of the $[\mathrm{Mn}(\mathrm{CH_3CN})_6]^{+2}$ and $[\mathrm{MnCl_4}]^{-2}$ complexes, the spectrum of the $[\mathrm{MnBr_4}]^{-2}$ complex has unusually broad $^{55}\mathrm{Mn}$ nuclear hyperfine components. The width of the components becomes more pronounced[1] with increasing bromide ion concentration. A detailed study of this phenomenon[2] suggested that bromide ligand exchange provides a relaxation channel leading to resonance broadening. From an analysis of the bromide dependent resonance widths, it is possible to extract the bimolecular rate constant characterizing the exchange of bromide ions in solution with those coordinated with the manganese.

The objective of this paper is to further elucidate the dynamical processes which lead to the resonance broadening of the tetrahedral manganese complex. For comparison purposes, we have studied the linewidths of the hyperfine components of $[\mathrm{Mn}(\mathrm{CH_3CN})_6]^{+2}$, $[\mathrm{MnCl_4}]^{-2}$ and $[\mathrm{MnBr_4}]^{-2}$ as a function of manganese concentration, ion concentration, temperature, and the frequency of the H_1 field.

1.1. Spectral Analysis

The line positions of ${}^6S_{5/2}\,Mn^{+2}$ ions can be located by the eigenvalues of the spin Hamiltonian:

$$\mathcal{H} = \langle g \rangle \beta H_0 S_Z + \langle A \rangle \vec{I} \cdot \vec{S} \qquad (1)$$

where H_0 is the resonance magnetic field, g is the electron spectroscopic splitting factor, β is the Bohr magneton and A is the hyperfine coupling constant. The electronic spin, S, and nuclear spin, I, are both 5/2 for ${}^{55}Mn$. Consequently, the selection rules ($\Delta M_S = \pm 1$, $\Delta M_I = 0$) allow thirty paramagnetic resonance transitions with positions given by the well-known second-order expression:

$$\frac{\hbar \omega}{\langle g \rangle \beta} = H_0 + \langle A \rangle M_I + \frac{\langle A \rangle^2}{2 H_0} \left[I(I+1) - M_I^2 + M_I (2 M_S + 1) \right]$$

Since the experiments are conducted at a fixed frequency (ω) with a varying magnetic field, it is convenient to rearrange the above expression and solve it for the resonance magnetic field:

$$H_0\,(\text{gauss}) = \frac{1}{2} \left[\frac{\hbar \omega}{\langle g \rangle \beta} - \langle A \rangle M_I \right] \pm \frac{1}{2} \left\{ \left[\langle A \rangle M_I - \frac{\hbar \omega}{\langle g \rangle \beta} \right]^2 - 2 \langle A \rangle^2 \left[I(I+1) - M_I^2 + M_I (2 M_S + 1) \right] \right\}^{\frac{1}{2}} \qquad (2)$$

where $M_I = -I, -I + I, \cdots I - 1, I$ and $M_S = -S, -S + 1, \cdots S - 1, S$. From the selection rules, it is apparent that there are five $|M_S, M_I\rangle \longrightarrow |M_{S+1}, M_I\rangle$ transitions for every M_I and from the above expression it is apparent that each transition occurs at a slightly different field.

Since the second-order effects are M_I dependent, the over-all resonance width of each hyperfine component will vary with M_I. The second-order effects are sufficiently small so that the $| M_S, M_I > \rightarrow | M_{S+1}, M_I >$ transitions can be considered to be symmetrically disposed about the $| -1/2, M_I > \rightarrow | 1/2, M_I >$ transitions. The locations of the $| -1/2, M_I > \rightarrow | 1/2, M_I >$ transitions are, to a very good approximation, given by the observed line centers of the hyperfine components. Thus, in the case of $[Mn(CH_3CN)_6]^{+2}$ and $[MnCl_4]^{-2}$, the spin Hamiltonian parameters, $< g >$ and $< A >$, can be extracted from the position of this hyperfine component. In the case of $[MnBr_4]^{-2}$, the hyperfine components overlap appreciably. Consequently, the $< g >$ and $< A >$ values must be determined by comparing the observed spectra with computer-simulated spectra.

2. EXPERIMENTAL

Anhydrous $MnCl_2$ and $MnBr_2$ are rendered soluble in acetonitrile by tetraalkylammonium halides to form the corresponding tetrahalomanganese (II) complexes, $[MnCl_4]^{-2}$ and $[MnBr_4]^{-2}$. The solvated complex, $Mn[(CH_3CN)_6]^{+2}$ was formed by a 2:1 metathetical reaction between $AgClO_4$ and $MnBr_2$ conducted in acetonitrile. Care was taken to avoid the uncertainties imposed by contact with air and moisture. Accordingly, these solutions were prepared under vacuum in a pyrex transfer apparatus suited for mixing and deployment of the solution into capillaries which were subsequently sealed off.

The anhydrous manganese halides (Research Inorganic Co.) were prepared from their hydrates by heating under continuous evacuation. In the case of $MnBr_2$, the solid was redissolved in acetonitrile, filtered, vacuum pumped, redissolved in water, filtered, and finally recrystallized from the aqueous medium. The dehydration procedure was then repeated. Anhydrous $AgClO_4$ was prepared by a similar technique.

Tetra-n-butylammonium bromide and tetraethylammonium chloride were analytical grade materials obtained from the Eastman Kodak Co. Tetra-n-butylammonium perchlorate was obtained from both Matheson-Bell and Southwestern Analytical Chemical Co. Prior to use these compounds were recrystallized from acetonitrile and dried in a vacuum oven.

Matheson spectroscopic grade acetonitrile was used exclusively in this work. In cases where minute quantities of water were known to influence the results, the solvent was dried with P_2O_5, degassed and transferred under vacuum onto the solute.

The electron spin resonance system consisted of a standard V-4502 spectrometer suited for both 9 GHz (X-band) and 35 GHz (K-band) operation. Initially, a high impedance Varian V-4007 six-inch electromagnet driven by a V-2200A regulated magnet power supply was used for experiments at 9 GHz. Most of the work, however, was performed with a twelve-inch low impedance Varian V-3603 electromagnet with a Fieldial Magnetic Field Regulator Mark II. Accurate magnetic field intensities were measured with an Alpha Scientific Laboratory NMR Gaussmeter (Al 675) containing a solid-state broad band amplifier to provide sufficient output to drive a Hewlett-Packard 5245-L counter. ^1H and ^7Li resonances were used to calibrate the

9 GHz (3400 gauss) and 35 GHz (12400 gauss) regions, respectively.

X and K-band experiments were conducted in cylindrical microwave cavities operated in a TE 011 mode with 100 K Hz Zeeman modulation. In this mode of operation an electric (E) field null runs axially through the cavity. At 9 GHz, sample tubes (pyrex) were typically 1-2 mm in outside diameter and were positioned axially to take advantage of the electric (E) field null. Rather minor dielectric losses permitted the solution length to transverse the entire cavity. However, at 35 GHz sample requirements were much more demanding with respect to volume and positioning. Samples were contained in ~1 mm outside diameter capillaries and solution lengths were on the order of 1-3 mm.

At X-band frequencies, temperature studies were performed with a standard Varian V-4540 temperature controller and quartz dewar. A variable temperature dewar was designed for the K-band cavity; modification of the microwave cavity was necessary to accommodate the dewar and allow tuning from the top. Temperature regulated nitrogen from the V-4540 was swept around the entire cavity. Temperatures in both cavities were monitored with an iron-constantan thermocouple having an estimated ± 2°C tolerance.

A Weld specific gravity bottle was used to determine densities at room temperature; a set of hydrometers for other temperatures. Viscosity was measured in a standardized Ostwald viscometer suspended in a temperature regulated water bath.

3. RESULTS AND DISCUSSION

The results from the three manganese systems are summarized in this section. Comparisons of their behavior indicate their relative stability and their principal spin relaxation mechanisms in acetonitrile solution.

3.1. $[Mn(CH_3CN)_6]^{+2}$

The effect of ion-pairing and ligand exchange with the first and second coordination sphere on resonance widths is considered in this section as a prelude to the more detailed work on $[MnCl_4]^{-2}$ and $[MnBr_4]^{-2}$.

Irreproducibility of resonance widths after brief exposure to air prompted an additional investigation into the role of water as a possible source of broadening. The comparison was made with $Mn[(CH_3CN)_6]^{+2}$ solutions prepared in air without special precautions toward moisture other than starting with dry reactants. Upon addition of water K-band resonance widths became steadily larger than X-band widths and an increasing g shift was observed. This probably reflects the presence of a new paramagnetic component having a different g-value. Under these circumstances the logical candidate is the complex, $[Mn(H_2O)_6]^{+2}$ ($g = 2.0023$). In any event, special precautions against the presence of water are required to obtain meaningful spin Hamiltonian constants and resonance widths for the solvated complex, $[Mn(CH_3CN)_6]^{+2}$.

Electron spin resonance spectra of $[Mn(CH_3CN)_6]^{+2}$ taken at

X and K-band frequencies are compared in Fig. 1. The K-band spectrum has six hyperfine components with nearly the same amplitude and thus clearly reflects the reduction in the second-order effect obtained by going to higher frequencies. The spin Hamiltonian parameters and resonance widths are presented in Table I. The g value reported in this work represents an average of a number of measurements and is definitely lower than the value reported by Chan, Fung and Lütje ($g = 2.003 \pm 0.001$).[1] The hyperfine constant was within the limits of error compared to the former work.[1]

Experiments were conducted on vacuum prepared $Mn[(CH_3CN)_6]^{+2}$ to examine the response of the narrowest hyperfine component ($M_I = 1/2$) to changes in concentration and frequency. Results of this study are summarized in Fig. 2 and indicate that resonance widths are essentially independent of frequency. However, they do increase with concentration which suggests that manganese spin-spin dipolar interactions are operative in this system.

Since ClO_4^- provides the counterion for the paramagnetic complex, a brief study was made of the interaction between the two ionic components and its effect on the effective spin Hamiltonian constants and resonance widths. Excess Bu_4NClO_4, defined as $[ClO_4^-]/[Mn^{+2}] > 2$, was added to a solution containing 0.005 molar (M) $[Mn(CH_3CN)_6]^{+2}$ and the effects on the $M_I = 1/2$ hyperfine component resonance widths were observed. A slight increase in width with increasing excess Bu_4NClO_4 was observed. Above 0.10 m excess Bu_4NClO_4, the width is approximately 10.5 gauss. If there is any effect at all due to the excess counterion, it is small and definitive measurements would

FIGURE 1

Electron paramagnetic spectra of 0.0039 M $[Mn(CH_3CN)_6]^{+2}$ in acetonitrile at X-band (top) and K-band (bottom) frequencies. The sharp central line is a DPPH marker. The field increases to the left.

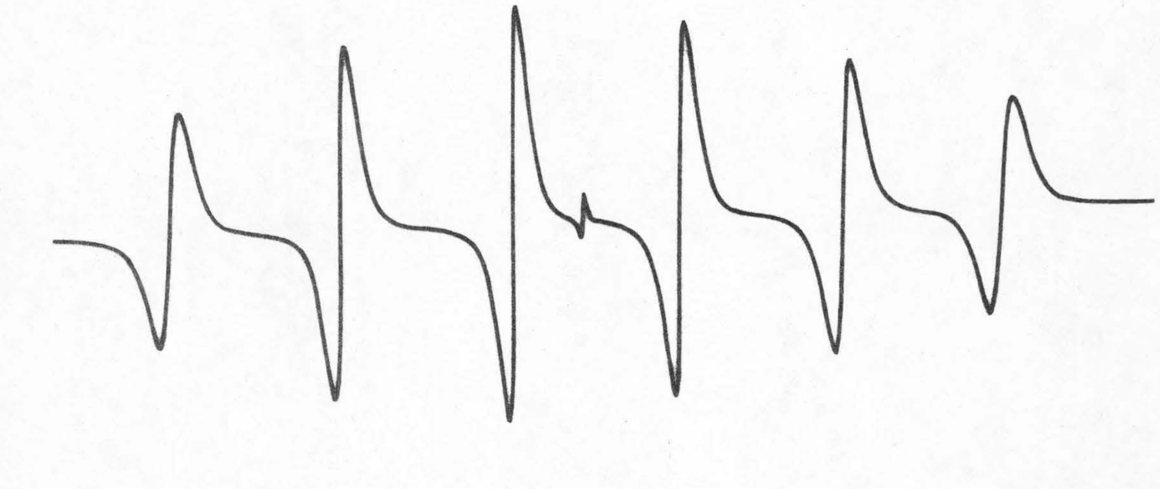
100 GAUSS

TABLE I. Spin Hamiltonian Constants for $[Mn(CH_3CN)_6]^{+2}$ in Acetonitrile.

Concentration (molal)				
$[Mn(CH_3CN)_6]^{+2}$	Excess Bu_4NClO_4	ΔH* Gauss ± 0.2	<g> ± 0.0005	<A> Gauss ± 0.2
0.005	0.000	8.7	2.0005	-93.1
0.005	0.110	9.8	2.0001	-93.0

* 4th line; $M_I = 1/2$ hyperfine component.

FIGURE 2

Resonance width of the $M_I = 1/2$ component as a function of $[Mn(CH_3CN)_6]^{+2}$ concentration at X (Δ) and K (O)-band frequencies. ClO_4^- is the counterion.

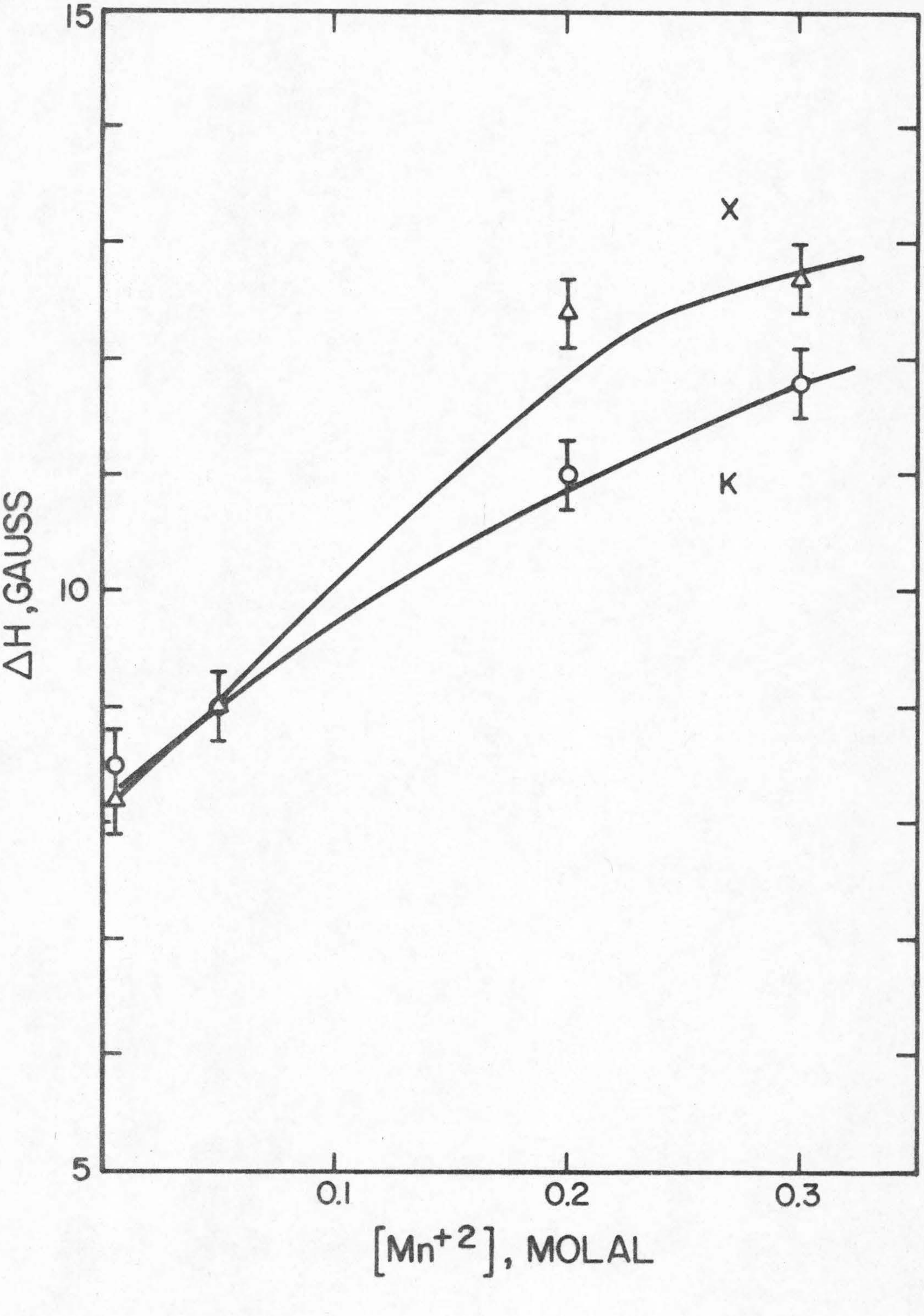
15
10
5
ΔH, GAUSS
0.1
0.2
0.3
[Mn+2], MOLAL
X
K

certainly be obscured by the tolerance of the measurements. Moreover, there are no significant changes observed on the effective spin Hamiltonian constants within the concentration range examined.

3.2. $[MnCl_4]^{-2}$

A study of the $[MnCl_4]^{-2}$ complex in acetonitrile was carried out to provide a comparison for the results obtained for $[MnBr_4]^{-2}$. Relaxation processes are frequently composed of several phenomena and it is sometimes helpful to have "chemical" arguments at hand to provide insight into the problem. On these grounds it is proposed that a parallel study between the tetrachloro and tetrabromomanganese (II) complexes in the same solvent can provide this type of information. Experiments on the chloride system were designed to investigate ion-pairing, chemical exchange, dipolar interactions and frequency or field effects under conditions similar to the bromide studies described in the next section.

Typical electron spin resonance spectra of $[MnCl_4]^{-2}$ with a tetraethylammonium, Et_4N^+, counterion taken at X and K-band frequencies are presented in Fig. 3. Spectra may be explained quite adequately on the basis of the effective spin Hamiltonian and its eigenvalues taken to second order as given in Eqs. (1) and (2). In this case also, the effective spin Hamiltonian parameters were extracted from the two central hyperfine components, M_I equal to -1/2 and 1/2. Resonance widths were determined from the $M_I = 1/2$ component which provides the least amount of $M_S \rightarrow M_S + 1$ overlap. Again, as in the solvated complex, the K band spectrum has six hyperfine

FIGURE 3

Electron paramagnetic resonance of 0.0039 m $[MnCl_4]^{-2}$ in acetonitrile at X-band (top) and K-band (bottom) frequencies. H_0 increases to the right.

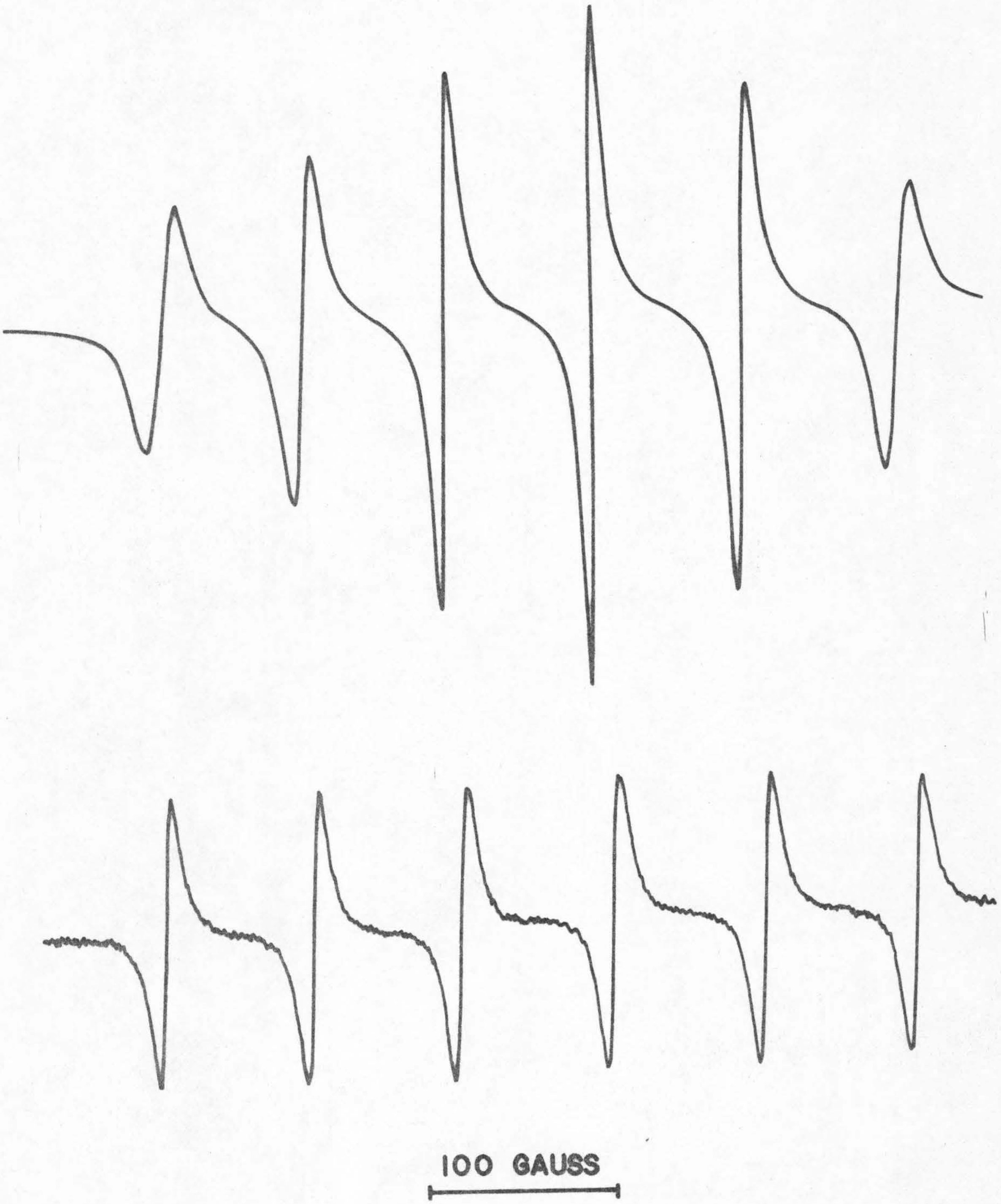
100 GAUSS

components with nearly the same amplitude which reflects the smallness of the second-order effects. A careful determination of the g-value was made by comparison with purified DPPH diluted with KCl and contained in sealed capillaries and by accurate field and frequency measurements. The evaluation of the spin Hamiltonian constants for $[MnCl_4]^{-2}$ yielded: $\langle A \rangle = -79.7 \pm 0.2$ gauss and $\langle g \rangle = 2.0027 \pm 0.0005$. Our g-value was considerably smaller than the one reported[1] earlier ($g = 2.007 \pm 0.001$) but the hyperfine constant was in agreement.

Due to the sharpness of the hyperfine components it is possible to study the influence of ion pairing ($Et_4N^+ \cdots [MnCl_4]^{-2}$ in this case) on the hyperfine coupling constant. We observed that the coupling constant, $\langle A \rangle$, decreased from -79.7 ± 0.2 gauss for dilute stoichiometric 0.005 m $[MnCl_4]^{-2}$ to -78.9 ± 0.2 gauss for 0.005 m $[MnCl_4]^{-2}$ containing 0.682 m excess Et_4NClO_4. Therefore, upon increasing the Et_4N^+ concentration to favor the presence of our hypothetical ion-pair, we observe a slight decrease in $\langle A \rangle$, greater than the limit of error. Assuming that ClO_4^- does not interact with the complex, the increase of Et_4N^+ counterion concentration may expand the complex slightly through an electrostatic interaction thus provoking a decrease in hyperfine coupling. In addition, the $\langle g \rangle$ values do not change under any experimental circumstance; consequently, any ion-pair which is formed has the same g-value as the manganese complex itself.

The variation of the resonance widths in solutions containing stoichiometric $[MnCl_4]^{-2}$ with tetraethylammonium counterions was examined over a wide manganese concentration range at both X and K-band frequencies. The results are plotted together in Fig. 4.

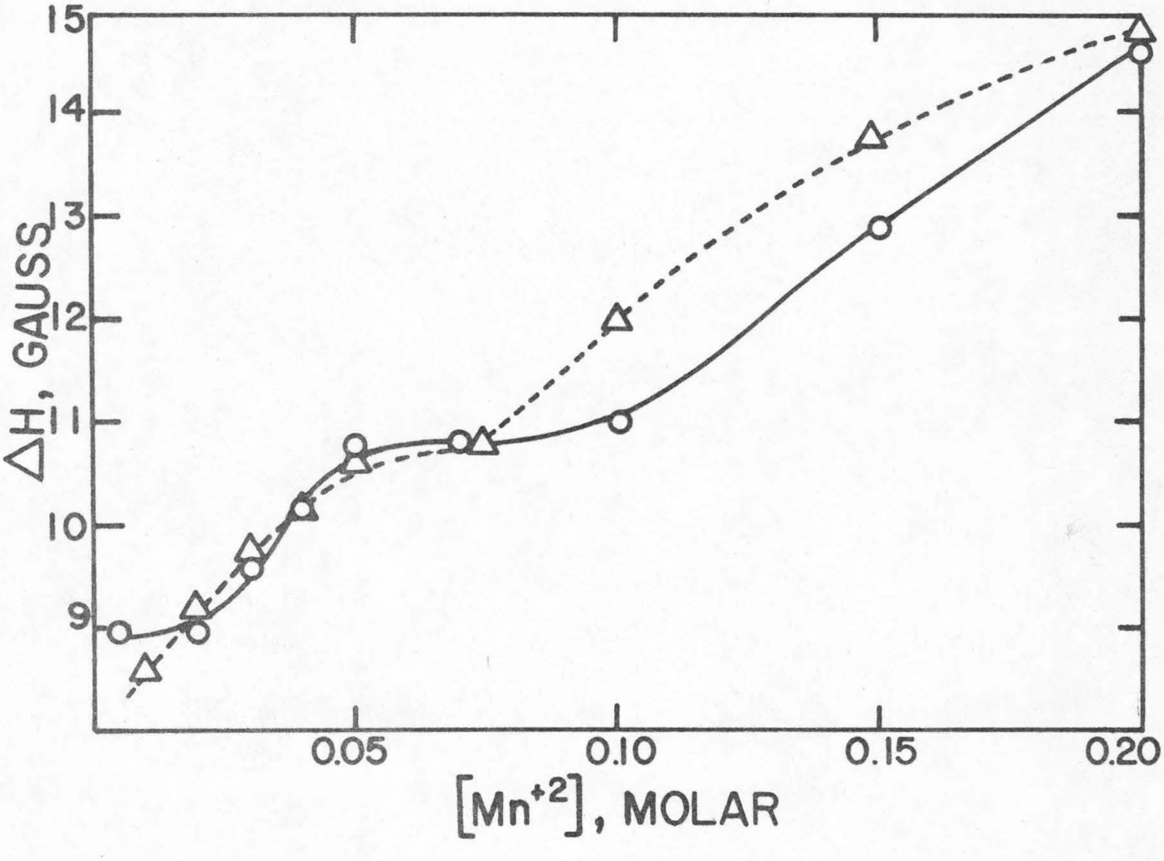

FIGURE 4

Variation of resonance width with manganese chloride concentration at X-band (Δ) and K-band (O) frequencies.

There were no significant changes in the hyperfine coupling constant or g-value over the entire concentration range and little, if any, resonance width dependency on frequency. Inspection of the two plots reveal the same general behavior. The initial rise in the observed resonance width, ΔH, commencing at about 0.01 M $[MnCl_4]^{-2}$ may be caused by the onset of a new paramagnetic component having a slightly smaller relaxation time. A possible candidate is an ion-pair consisting of a relatively short range electrostatic marriage between the paramagnetic anion and its counterion. Several additional experiments were aimed at establishing dynamical ion-pairing as a source of electron spin relaxation. We, first, explore the effect of Et_4N^+ counterion from two different sources on the resonance width by changing the counterion concentration relative to $[MnCl_4]^{-2}$. Second, we "freeze in" the anticipated broadening effect due to viscosity in order to get a better look at the ion-pairing.

The first study was performed with 0.05 m $[MnCl_4]^{-2}$ solutions and excess Et_4N^+ was provided by tetraethylammonium chloride. Chloride ion concentrations in excess of the stoichiometric 4:1 ratio were taken to be "excess" concentrations. A plot of the chloride curve compensated for the association of Et_4NCl in acetonitrile at 25°C ($K_d = 0.029$[3]) is shown in Fig. 5 and it is apparent that there is a small initial increase in the curve before straightening out. Recalling Fig. 4, it is noted that the stoichiometric 0.05 m (0.039 M) $[MnCl_4]^{-2}$ solutions are nearly converted to the ion-pair. Consequently, a large initial rise in ΔH upon addition of excess Et_4N^+ due to a "chemical-shove" in favor of the ion-pair would not be expected. The effect of excess Et_4 NCl on the resonance width is small amounting only to 3-4 gauss over a wide range of concentration and viscosity.

A parallel experiment using tetraethylammonium perchlorate in place of the chloride was superimposable with the curve in Fig. 5. If we assume that the ClO_4^- exchange rate to be slower than Cl^-, we may conclude that chemical exchange between Cl^- and $[MnCl_4]^{-2}$ is not on the electron spin resonance time scale and, as a result, does not significantly contribute to spin relaxation.

Garrett and Morgan [4] have established that electron spin relaxation of the unpaired electrons in solvated manganese (II) complexes arises principally through spin-orbit interaction caused by modulation of the ligand field resulting from transient distortions of the complex by solvent fluctuations in the immediate surroundings of the paramagnetic ion. If this mechanism were the only one operative here, the resonance widths would vary linearly with the correlation time characteristic of the solvent fluctuations and would not be strongly dependent upon excess chloride concentration. It has been suggested [4] that this correlation time is proportional to $\eta M/\rho T$, where η is the viscosity of the solution, M is the molecular weight of the solvent, and ρ is the density of the solvent at temperature T. In Fig. 6, we have shown the variation of the resonance widths as a function of $\eta M/\rho T$ for five solutions, each containing a different excess chloride concentration. It is significant to note that, whereas the resonance widths for each of these solutions do vary linearly with $\eta M/\rho T$ as the solvent structural correlation time is varied with temperature, the data points corresponding to different excess chloride concentrations fall into two

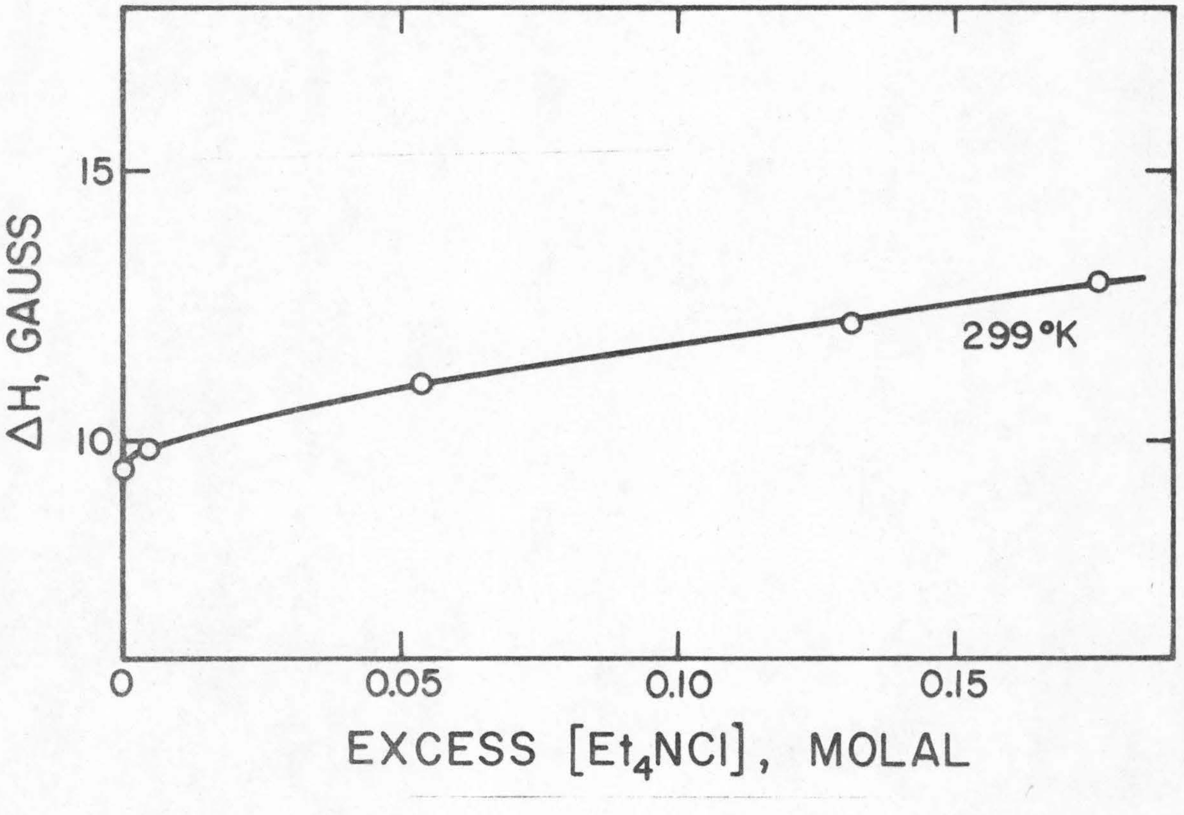

FIGURE 5

Variation in resonance width, ΔH, of the $M_I = 1/2$ hyperfine component of 0.05 m $[MnCl_4]^{-2}$ with excess molal Et_4NCl compensated for association at 25°C ($K_d = 0.029$).

major groups with one solution connecting the two groups. The points in the higher concentration group fall almost on the same line and, hence, appear to vary linearly with the correlation time characteristic of solvent fluctuations and are clearly not strongly dependent on excess chloride concentration. The lower, zero excess line displays the same general behavior; the 0.004 excess m line connects the two sets and intersects the resonance width axis approximately in the same region as the higher concentration lines at zero correlation. The latter may possibly be interpreted as a resonance width compensated for broadening imposed by solvent fluctuations. The lower "zero excess" line intersects the ΔH axis at about 8.1 gauss which is approximately 1.2 gauss lower than the other set of lines. This observation coupled with the results described previously and illustrated in Fig. 4 strongly suggests the existence of two paramagnetic components. The 0.004 m excess chloride line in Fig. 6 shows an intermediate case where considerable amounts of both components are present.

Based on experimental results, a plausible explanation for the two observable paramagnetic components would be a free or isolated $[MnCl_4]^{-2}$ anion at low manganese and counterion concentrations and a solvent separated or loosely bound ion-pair designated by $[Et_4N^+ \cdots MnCl_4^{-2}]$ at higher manganese concentration or counterion/manganese ratios. Equilibrium between the two states may be described by the simple reaction scheme

$$\underset{[A]}{[MnCl_4]^{-2}} + \underset{[C]}{Et_4N^+} \overset{K_a}{\rightleftharpoons} \underset{[B]}{[Et_4N^+ \cdots MnCl_4^{-2}]}$$

FIGURE 6

Variation of the resonance width, ΔH, of 0.05 m $[MnCl_4]^{-2}$ solutions containing different concentrations of excess Et_4NCl as a function of $\eta M/\rho T$: ●, 0.00 excess m Cl^-; △, 0.004 excess m Cl^-; ▽, 0.14 excess m Cl^-; ○, 0.610 excess m Cl^-; □, 0.98 excess m Cl^-.

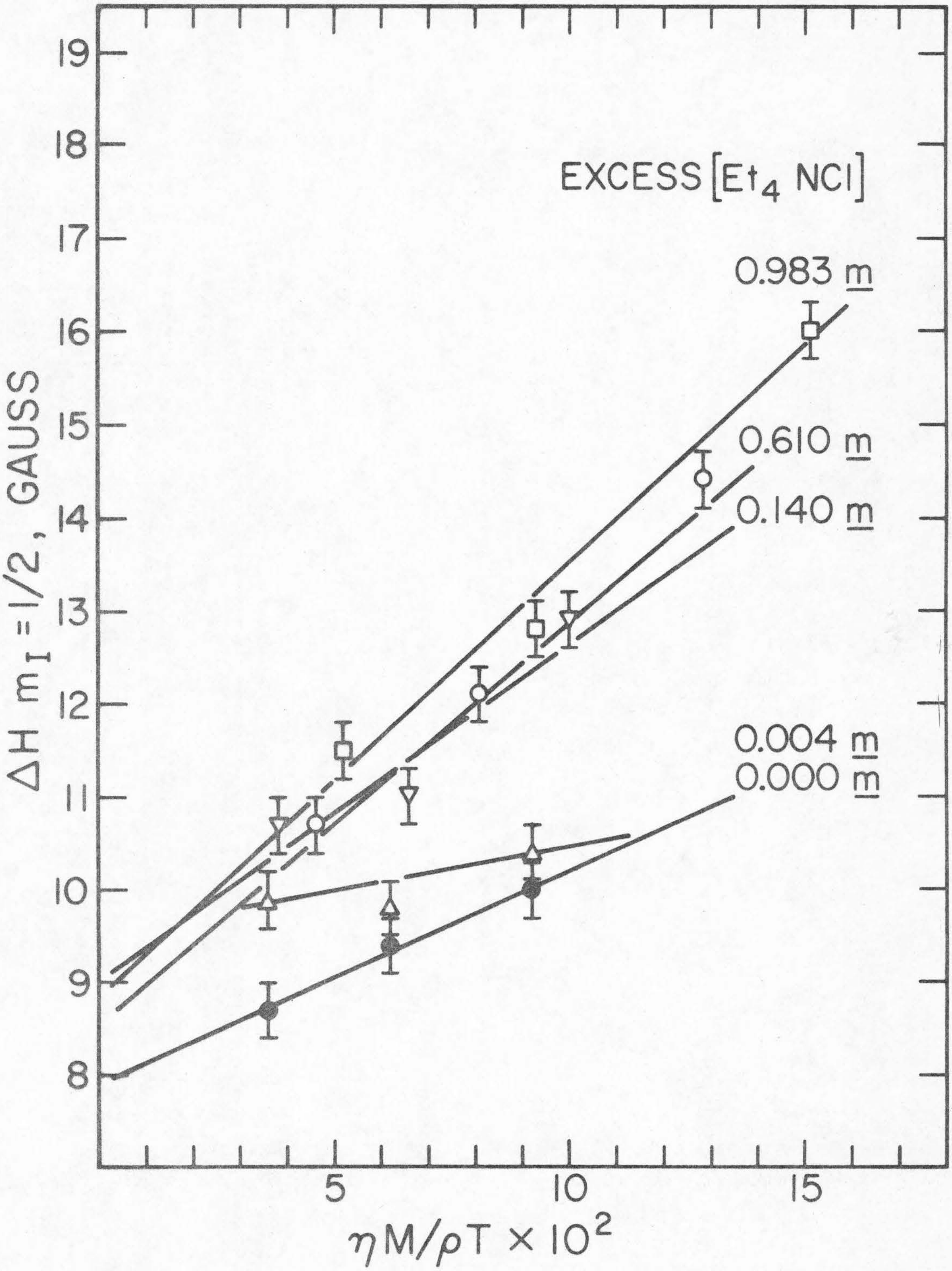
EXCESS [Et$_4$ NCl]
0.983 m
0.610 m
0.140 m
0.004 m
0.000 m
ΔH m_I = 1/2, GAUSS
$\eta M/\rho T \times 10^2$
19
18
17
16
15
14
13
12
11
10
9
8
5
10
15

and the mass action equilibrium constant for the process is approximated by

$$K_{\text{association}} = \frac{[Et_4N^+ \cdots MnCl_4^{-2}]}{[MnCl_4^{-2}][Et_4N^+]} = \frac{[B]}{[A][C]} \tag{3}$$

If it is assumed that the ion-pairing is a fast process so that the exchange rate between the two paramagnetic components is faster than the hyperfine splitting, the K_a may be determined from a simple rapid-exchange relationship

$$\frac{1}{T_2} = \frac{1}{T_{2A}} + \frac{[C]\,K_a}{1 + [C]\,K_a} \left\{ \frac{1}{T_{2B}} - \frac{1}{T_{2A}} \right\} \tag{4}$$

where T_2^{-1} is the observed resonance width; T_{2A}^{-1} and T_{2B}^{-1} are the observed resonance widths for constituents [A] and [B] as defined above and [C] is the molar concentration of the counterion, Et_4N^+. The quantity $(T_{2B}^{-1} - T_{2A}^{-1})$ may be estimated from the plots of ΔH vs. $\eta M/\rho T$ given in Fig. 6 and the stoichiometric $[MnCl_4]^{-2}$ dilution study illustrated in Fig. 4. Fig. 6 provides the resonance width difference between the completely ion-paired component, B, and a "partially" ion-paired component existing at 0.05 m (0.039 M) $MnCl_4^{-2}$ in the absence of excess Et_4NCl as being approximately 2.0 gauss. Fig. 4 then gives the resonance width difference between the "partially" ion-paired state at 0.039 M Mn^{+2} concentration and the "free" state, A, as the Mn^{+2} concentration goes to zero as being 1.6 gauss. As a result, we estimate $(T_{2B}^{-1} - T_{2A}^{-1}) \approx 3.6$ gauss and the best match between calculation and observation provides us with $K_a \approx 20$.

In summary, the $[MnCl_4]^{-2}$ complex with Et_4N^+ as gegen ion in acetonitrile may best be interpreted in terms of two rapidly exchanging paramagnetic components whose equilibrium distribution is determined by both manganese concentration and Et_4N^+/Mn^{+2} ratio. Due to the absence of frequency effects on the resonance widths and the known dynamical behavior of ionic association in solution, a rapid exchange picture is probably a good approximation for this system. The two components have been designated as an isolated $[MnCl_4]^{-2}$ anion existing at low manganese concentration and $Et_4N^+/Mn(II)$ ratios and a solvent separated or loosely bound complex $[Et_4N^+ \cdots MnCl_4^{-2}]$ existing at higher manganese concentration and $Et_4N^+/Mn(II)$ ratios. Aside from the natural resonance widths of the two paramagnetic components, another relaxation mechanism appears to arise from the short range solvent fluctuation about the paramagnetic ion as described by Garrett and Morgan.[4] Under all circumstances investigated in this system, the relaxation mechanisms and spin Hamiltonian constants are independent of frequency or field. Among other things, this suggests that the correlation time of events leading to relaxation are short and that the observations, to a very good approximation, are in the limit of extreme narrowing, i.e., $\omega\tau \ll 1$. Finally, from a sizeable number of experiments, the average values for the spin Hamiltonian constants are: (1) $[MnCl_4]^{-2}$, $\langle A \rangle = -79.7 \pm 0.2$ gauss, $\langle g \rangle = 2.0027 \pm 0.0005$; (2) $[Et_4N^+ \cdots MnCl_4^{-2}]$, $\langle A \rangle = -78.9 \pm 0.2$ gauss, $\langle g \rangle = 2.0027 \pm 0.0005$.

As the $[MnCl_4]^{-2}$ concentration is increased beyond 0.1 M (Fig. 4) the resonance width increases rapidly and becomes much larger than the ΔH in comparable counterion studies (Fig. 5) in which ion-association should be favored by virtue of mass equilibria. Consequently, it would be difficult to rationalize the sizeable ΔH increase at about 0.10 m $MnCl_4^{-2}$ in terms of an ion-pairing model, but the increased width is certainly dependent on the manganese concentration. A possible candidate for spin relaxation is a dipolar mechanism and this, in fact, has been reported to be operable in other manganese (II) complexes at relatively low concentrations,[4] i.e., 0.01 m. Examination of the spectra at 0.2 m $[MnCl_4]^{-2}$ indicated a definite asymmetry of the hyperfine components, particularly in the extremes. The high field side of the hyperfine components are clearly spread out farther than the low field side. From the moment ratios of the dipolar interaction given by Hinckley and Morgan,[5] it is seen that the individual M_S transition linewidths are not equal and, thus, are not symmetrically disposed about the $| -1/2, M_I > \rightarrow | 1/2, M_I >$ transition as anticipated for an intramolecular process. A dipolar process will indeed cause a spreading out of the high field side transitions ($| -5/2, 1/2 > \rightarrow | -3/2, 1/2 >$ and $| -3/2, 1/2 > \rightarrow | -1/2, 1/2 >$) and this is consistent with our observation.

3.3 $[MnBr_4]^{-2}$

We now turn to the $[MnBr_4]^{-2}$ system. In the previous report,[2] electron spin resonance evidence for bromide ion exchange with $[MnBr_4]^{-2}$ was reported. The interpretation of the results was, however, complicated by the presence of several cooperative phenomena and equilibria which determine the component distribution and consequently also influence the dynamical properties of the system. It is the linear dependence of the resonance widths upon the bromide ion concentration which is interpreted as indicating the presence of bromide ligand exchange. Presumably, the electronic distortion during exchange of ligands is strong so that the lifetimes of the spin states, and hence both the longitudinal and transverse relaxation times, are limited to the chemical lifetime of the complex. The results suggest that ligand exchange is bimolecular involving one Br^- and one $[MnBr_4]^{-2}$ in which the reactants and products are identical.

$$Br^- + [MnBr_4]^{-2} \rightleftharpoons [MnBr_4]^{-2} + Br^- .$$

The data were analyzed according to the expression [6, 7]

$$\left(\frac{1}{T_2}\right)_{\text{exchange}} = k_2 \, [Br^-] .$$

Two sets of bimolecular rate constants were derived assuming partial dissociation ($K_d = 0.5$ [8]) and complete dissociation of the Bu_4NBr; these results are shown in Table II. Recalculation of the rate constant using the extended Debye-Hückel limiting law to determine the mean activity coefficient of Bu_4NBr in CH_3CN has essentially no effect on the results.

Preparation of the $[MnBr_4]^{-2}$ complex in acetonitrile was described in the Experimental section. Bromide ion concentrations above the stoichiometric 4:1 ratio were taken to be the excess concentration. It was found that vacuum preparation of the $[MnBr_4]^{-2}$ was not critical as long as the reactants and solvent were anhydrous. Even

TABLE II. Bimolecular Rate Constants for Ligand Exchange at 300°K.

$[MnBr_4]^{-2}$ Molar Conc.	Frequency	$k_2 \times 10^{-9}$ 1 $mole^{-1}$ sec^{-1} A	D
0.0019	X	1.0	0.8
	K	1.2	0.8
0.0037	X	1.8	1.1
	K	1.7	1.1
0.039	X	1.8	1.1
	X*	1.7	1.2
	K	1.6	1.0
0.100	X	2.2	1.2
	K	2.0	1.1

A. Br^- concentration calculated assuming $K_d = 0.5$ for Bu_4NBr.

B. Bu_4NBr assumed completely dissociated.

* Values reported earlier in reference 2.

in this case, however, sample capillaries were sealed off immediately to prevent any interaction with moisture.

Electron spin resonance spectra observed for $[MnBr_4]^{-2}$ in acetonitrile were treated adequately by the effective spin Hamiltonian (Eq. 1) and its eigenvalues to second-order. In the case of the broad $[MnBr_4]^{-2}$ lines, the individual hyperfine components are highly overlapped and their resonance widths may be considered to be equal. Consequently, the central $| -1/2, M_I > \rightarrow | +1/2, M_I >$ transition of each hyperfine component gives an adequate approximation of the line positions and the Lorentzian derivative curve gives a good approximation of the line shape. By comparing computer synthesized and experimental spectra, it was possible to extract the resonance width, ΔH, hyperfine coupling constant, $<A>$, and the spectroscopic splitting factor, $<g>$. The spin Hamiltonian constants for the $[MnBr_4]^{-2}$ complex are: $<A> = -76 \pm 1$ gauss; $<g> = 2.007 \pm 0.001$. Within the range of 50-95 gauss the spectral characteristics were quite sensitive to the resonance width of the hyperfine components and the estimated error is ± 1 gauss. Outside this range, the resonance width is somewhat more uncertain. Typical spectra of $[MnBr_4]^{-2}$ taken at X and K-band are illustrated in Fig. 7. Agreement between experimental and computer simulated spectra was excellent throughout the wide range of conditions investigated in this study and clearly justified our basic assumptions. Comparison of the X and K-band spectra in Fig. 7 illustrates the presence of a second-order effect reflected in the asymmetry of the X-band envelope. In contrast, the K-band spectra is quite symmetrical due to the smaller second-order effect.

FIGURE 7

Electron paramagnetic resonance spectra of 0.039 M $[MnBr_4]^{-2}$ at X-band frequency (top) and of 0.0019 M $[MnBr_4]^{-2}$ at K-band frequency (bottom). H_0 increases to the right.

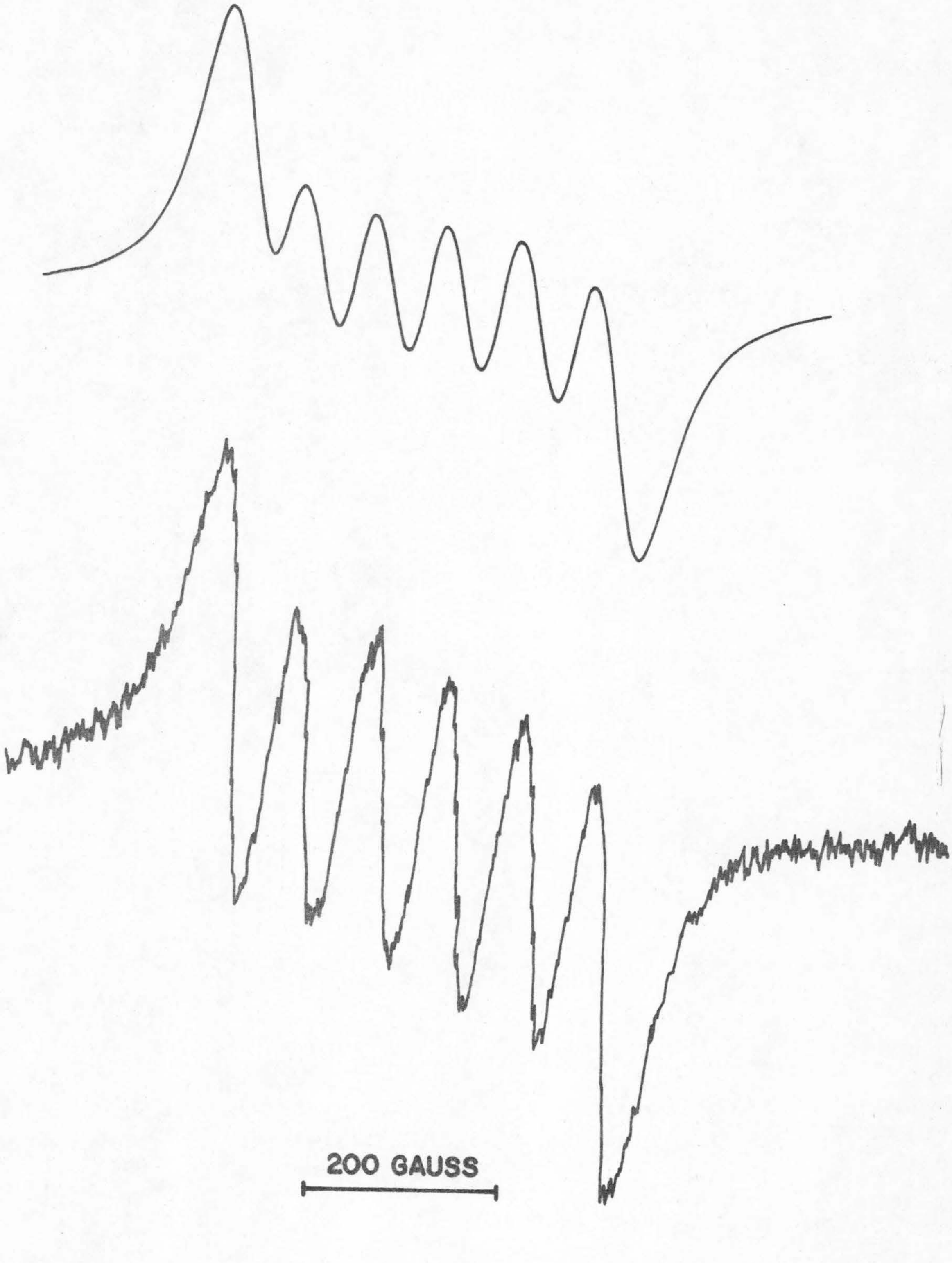
200 GAUSS

In the absence of excess bromide ion and, hence, in the absence of chemical exchange broadening, the stoichiometric complex (Br/Mn = 4.0) still has a large resonance width. For example, a 0.05 m (0.039 M) solution of $[MnBr_4]^{-2}$ has a resonance width of 57 gauss compared to about 9 gauss for the chloride complex. The effect of the stoichiometric $[MnBr_4]^{-2}$ concentration on the overall resonance width is shown in Fig. 8 at K-band frequency. It is evident that the resonance width remains relatively constant between 0.1 and 0.01 M Mn^{+2}. Below this concentration the width drops sharply to 42 ± 2 gauss at 0.001 M Mn^{+2} which is the lower limit of observation. The most important feature of this series of experiments is the constancy of the resonance width above 0.01 M Mn^{+2}. This lack of change indicates that the Bu_4N^+ counterion is not involved in the dominant electron spin relaxation mechanism in solutions containing more than 0.02 M Mn^{+2}. Between 0.02 M and 0.1 M Mn^{+2} the counterion concentration correspondingly increases from 0.04 to 0.2 M, but the resonance width changes only 5 gauss and part of this change can be attributed to the increase of Mn^{+2} concentration and viscosity.

The results shown in Fig. 8 are interpreted as indicating the presence of two paramagnetic components having quite different relaxation times. It is difficult to accurately assess the exchange rate limit under these circumstances but the fact that the spectra maintain a Lorentzian character and the spin Hamiltonian constants do not change suggests that we are observing a rapid exchange limit for two paramagnetic species. A plausible model for the two exchanging species would involve a free or isolated $[MnBr_4]^{-2}$ anion at low manganese

FIGURE 8

Response of K-band resonance width, ΔH, to the stoichiometric $[MnBr_4]^{-2}$ concentration.

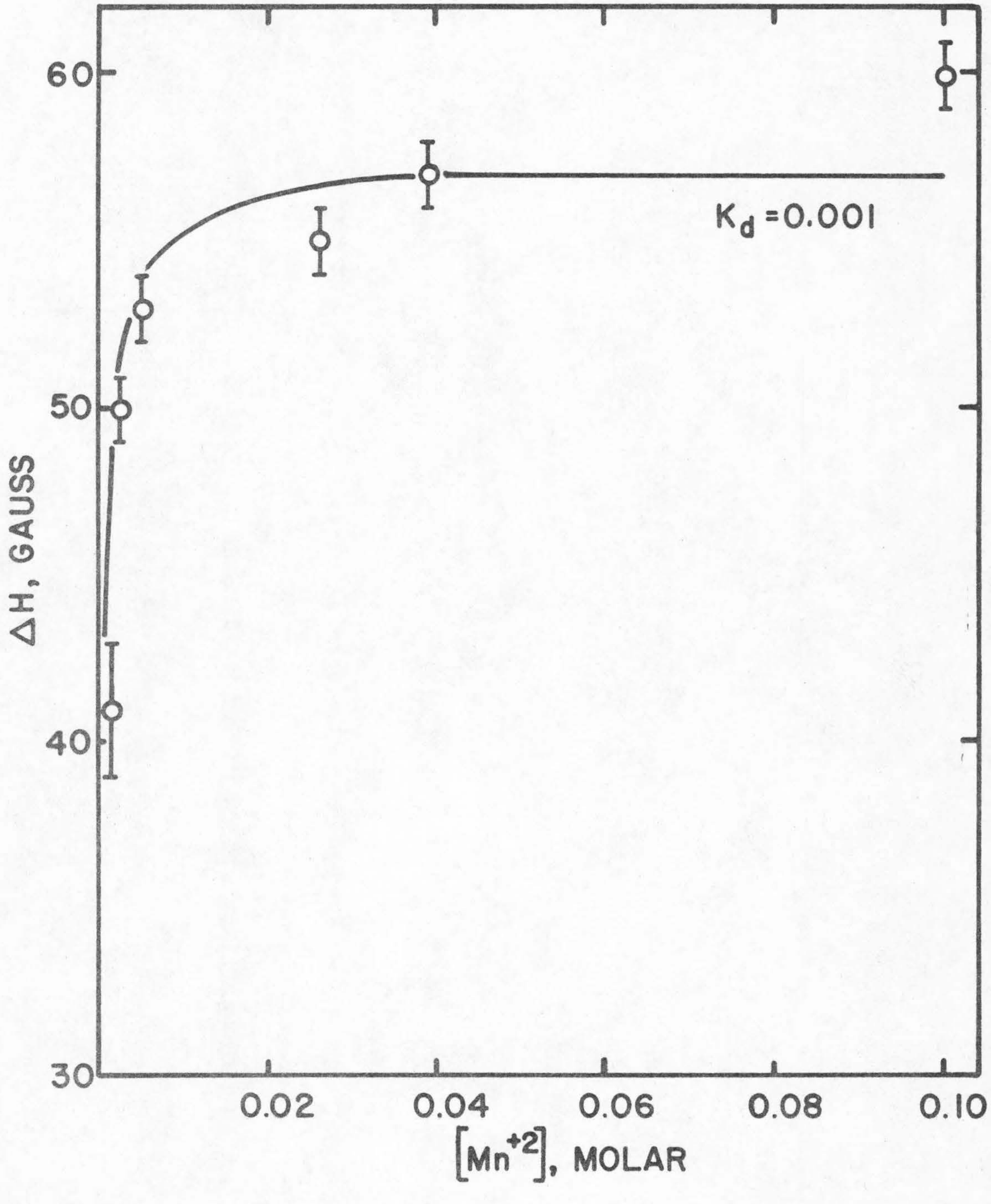
60
50
40
30
ΔH, GAUSS
0.02
0.04
0.06
0.08
0.10
[Mn+2], MOLAR
Kd =0.001

($\leq$ 0.002 M) and counterion concentrations and a solvent separated or loosely bound ion pair designated by $Bu_4N^+ \cdots MnBr_4^{-2}$ at higher manganese ($>$ 0.01 M) concentrations or at higher counterion/manganese ratios. Equilibrium between the two components may be written as

$$\overset{B}{Bu_4N^+ \cdots [MnBr_4]^{-2}} \rightleftharpoons \overset{A}{Bu_4N^+ + [MnBr_4]^{-2}} \qquad (5)$$

and, consequently, the mass action equilibrium constant defining the dissociation of the ion pair may be approximated by

$$K_d = \frac{[Bu_4N^+][MnBr_4^{-2}]}{[Bu_4N^+ \cdots MnBr_4^{-2}]} \quad . \qquad (6)$$

Assuming the rapid exchange picture for A and B and taking $T_{2B} < T_{2A}$, the dissociation constant may be estimated from the relation

$$\frac{1}{T_2} = \frac{1}{T_{2A}} + \frac{[C]}{[C] + K_d}\left(\frac{1}{T_{2B}} - \frac{1}{T_{2A}}\right) + \sum_i T_{2i}^{-1} \qquad (7)$$

where T_2^{-1} is proportional to the overall resonance width; T_{2A}^{-1} and T_{2B}^{-1} are proportional to the resonance widths estimated from the data shown in Fig. 8 based on the two-state model represented by the ion-pair equilibrium in Eq. (5); [C] is the molar concentration of the counterion, Bu_4N^+, and the summation is taken over all other, as yet undetermined, relaxation processes contributing to the overall resonance width. Assuming that ion-pair equilibria dominate the relaxation picture at low Mn^{+2} concentrations and taking reasonable values for T_{2A}^{-1}, T_{2B}^{-1} and $\sum_i T_{2i}^{-1}$, the distribution of components was calculated for a wide range of dissociation constants. The best match between theory and observation was obtained by taking $K_d = 10^{-3}$; this value was used to generate the solid line included in Fig. 8. Since the formation of chemical intermediates undoubtedly reduces the apparent $[MnBr_4]^{-2}$ concentration, the dissociation constant for the ion-pair equilibrium must only be considered as an upper-limit, order-of-magnitude value.

It seems clear that dynamical association of the counterion, Bu_4N^+, to form an ion-pair plays a significant role in determining the overall resonance width for stoichiometric solutions containing less than 0.02 M $[MnBr_4]^{-2}$. Of course, Bu_4N^+ from other sources also favors the ion-paired state. These effects will become apparent during the interpretation of subsequent data in support of our hypothetical ion-pair model.

As mentioned earlier in the section on the $[MnCl_4]^{-2}$ complex, Garrett and Morgan[4] have established that electron spin relaxation in solvated manganese (II) complex arises from solvent fluctuations in the immediate surroundings of the paramagnetic ion. This relaxation mechanism was also apparent[2] in the $[MnBr_4]^{-2}$ system when one examined the dependence of the resonance widths on the viscosity of the solution. However, it is rather insignificant compared to other relaxation effects.

3.4. Frequency Dependence of Resonance Widths

Spin resonance line widths arising through dipolar interactions are dependent on the frequency of the H_1 field. If the correlation times,

τ_a, for the dynamical events leading to these interactions are in a range so that $\omega\tau_a \geq 1$ then this dependence will be strong. Since dipolar interactions affecting line shapes are anticipated in solutions containing more than 0.01 M Mn^{+2}, a series of experiments was aimed at unraveling this mechanism by studying resonance widths vs. excess bromide ion concentration at two different frequencies (X and K-band). The manganese concentration was varied from 0.0019 M to 0.10 M in order to encompass a correspondingly wide range of dipolar interaction. The results are illustrated in Figs. 9 through 12, and, as before, the bromide ion concentration in acetonitrile has been corrected for association at 25°C. Furthermore, our experience in the first exchange study [2] demonstrated that solvent viscosity contributes relatively little to the overall resonance width and, hereafter, shall be ignored.

Several cooperative phenomena can now be clearly distinguished from these results: (1) An abrupt increase of X-band resonance width occurs on addition of a slight Bu_4NBr excess. A less noticeable increase in K-band widths is observed. (2) Beyond the initial non-linear region, the data are essentially linear with similar slopes. The X-band resonance widths are larger than the corresponding K-band results. (3) The difference between X and K-band resonance widths increases markedly with $[MnBr_4]^{-2}$ concentration. (4) For a given excess bromide ion concentration, X-band resonance widths increase more rapidly with $[MnBr_4]^{-2}$ concentration than K-band widths.

The non-linear behavior in both the X and K-band plots at low $[MnBr_4]^{-2}$ and bromide ion concentrations is in agreement with our

FIGURE 9

Resonance width, ΔH, variation of 0.0019 M $[MnBr_4]^{-2}$ as a function of excess molar Bu_4NBr at X and K-band frequencies.

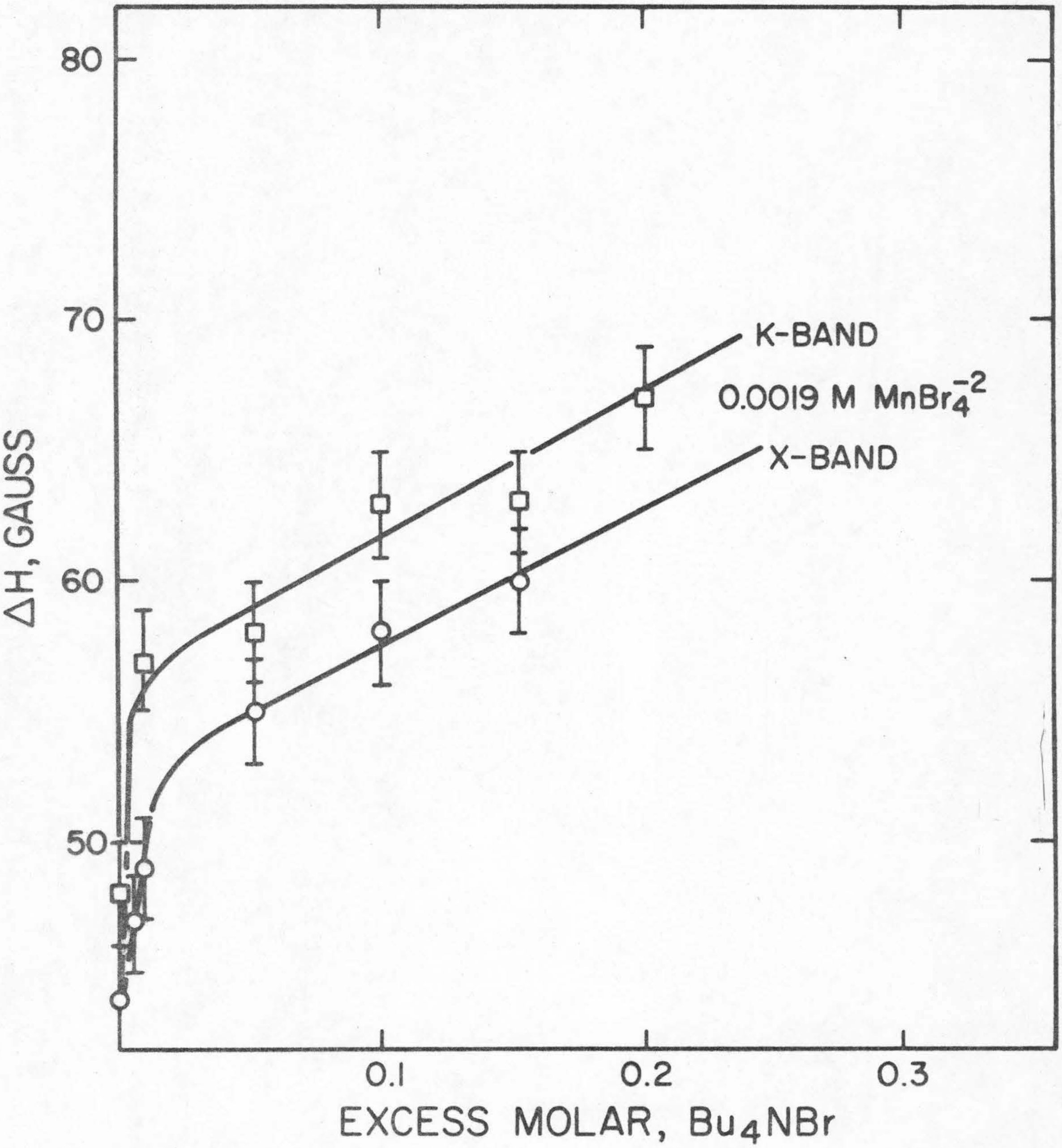
80
70
60
50
ΔH, GAUSS
0.1
0.2
0.3
EXCESS MOLAR, Bu4NBr
K-BAND
0.0019 M MnBr4-2
X-BAND

FIGURE 10

Variation of resonance width of 0.0037 M $[MnBr_4]^{-2}$ as a function of excess molar Bu_4NBr at X and K-band frequencies.

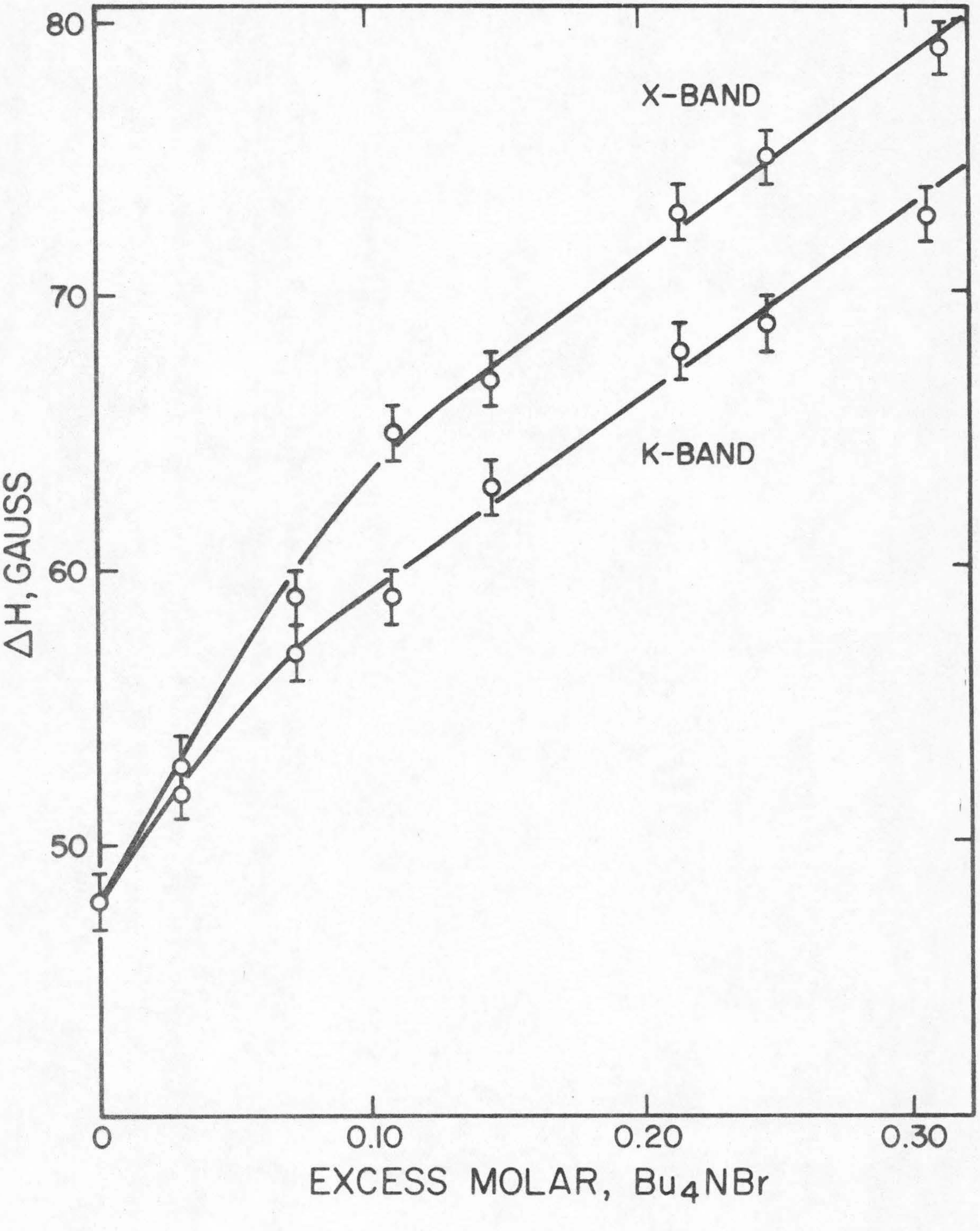
X-BAND
K-BAND
80
70
60
50
ΔH, GAUSS
0
0.10
0.20
0.30
EXCESS MOLAR, Bu4NBr

FIGURE 11

Variation of resonance width of 0.039 M $[MnBr_4]^{-2}$ as a function of excess molar Bu_4NBr at X and K-band frequencies.

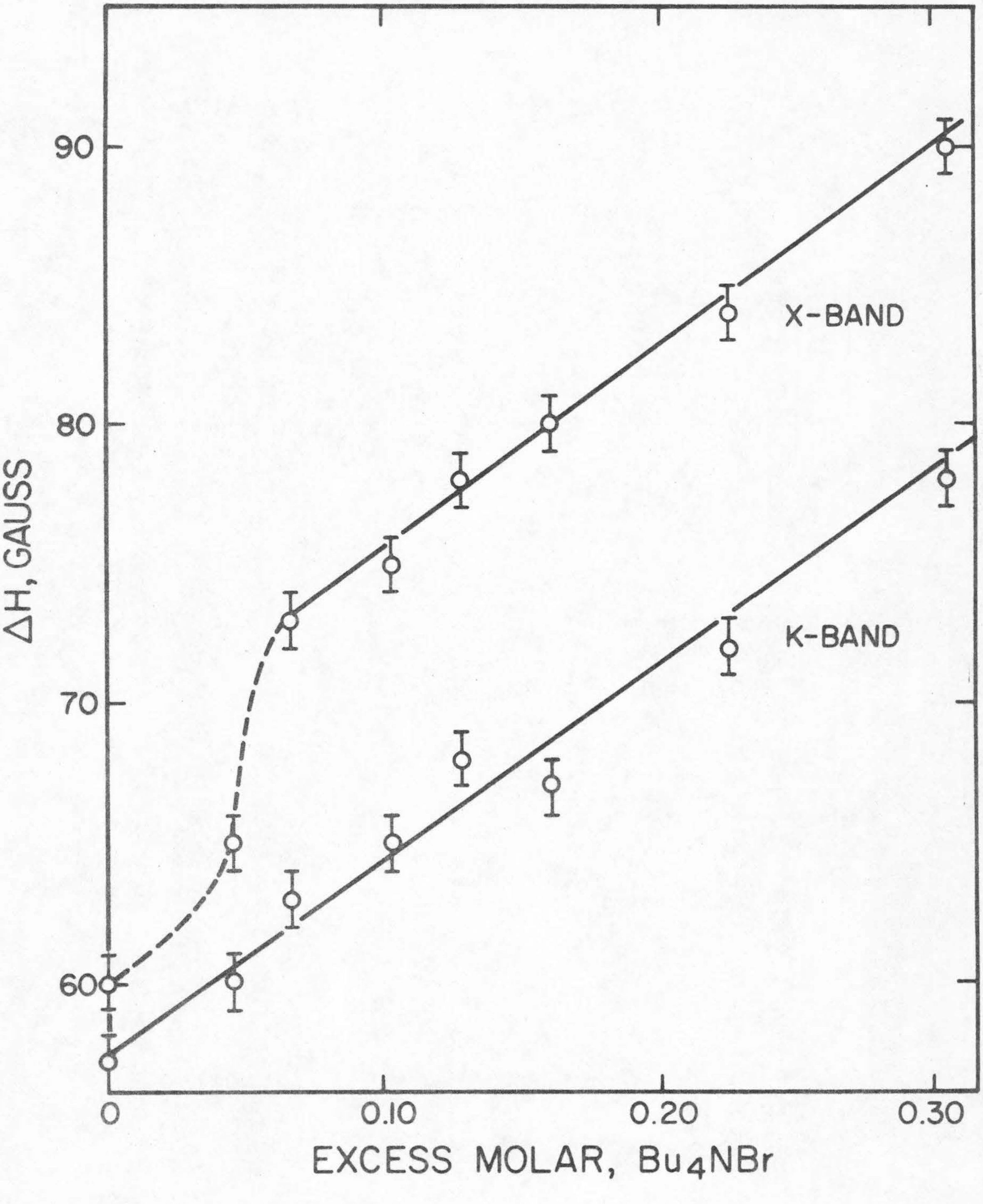
ΔH, GAUSS
90
80
70
60
0
0.10
0.20
0.30
EXCESS MOLAR, Bu4NBr
X-BAND
K-BAND

FIGURE 12

Variation of resonance width of 0.10 M $[MnBr_4]^{-2}$ as a function of excess molar Bu_4NBr at X and K-band frequencies.

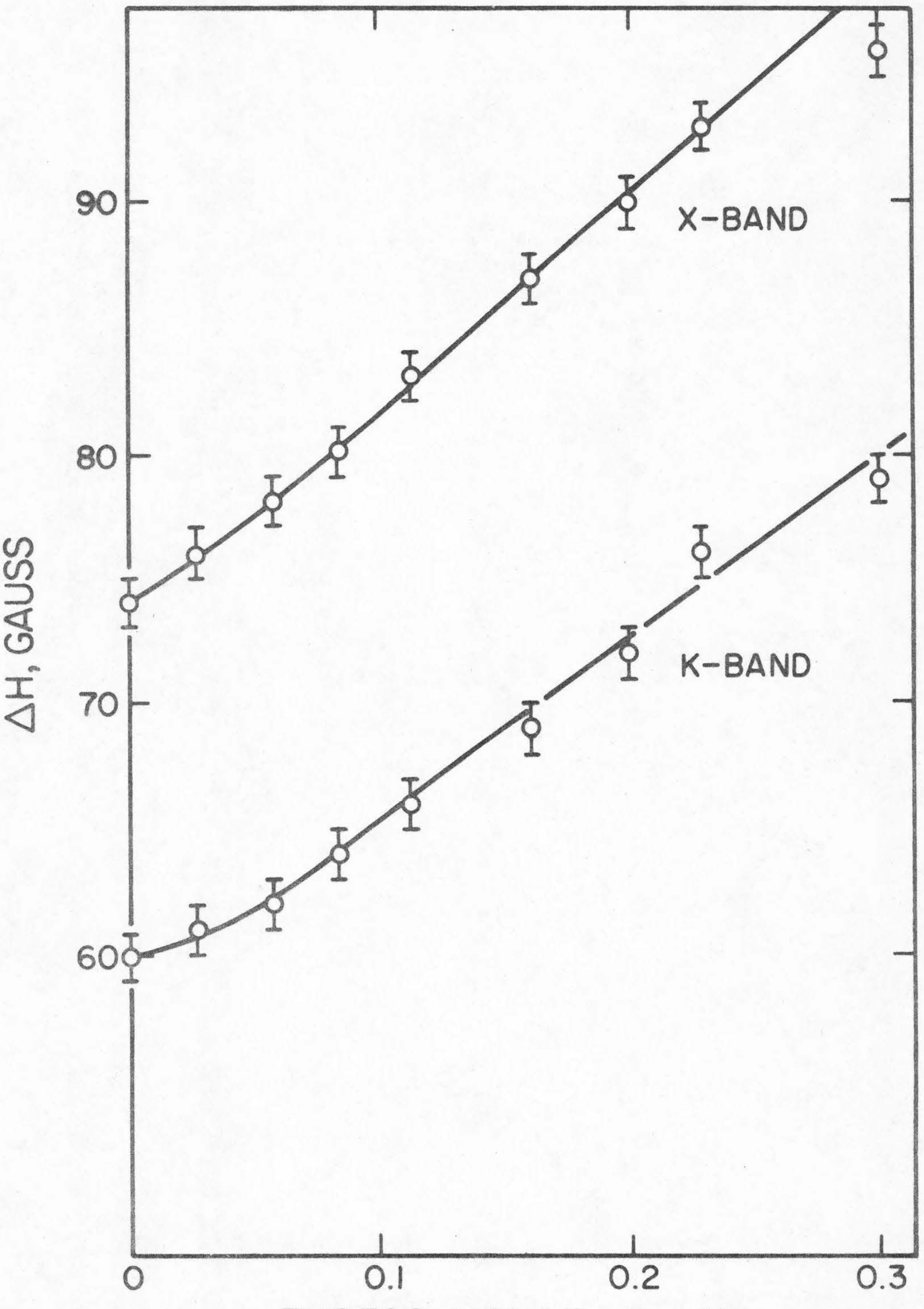
ΔH, GAUSS
90
80
70
60
X-BAND
K-BAND
0
0.1
0.2
0.3
EXCESS MOLAR, Bu$_4$NBr

ion-pair arguments (Fig. 9) but persistence of curvature at higher concentrations probably arises from intermediate equilibria with the solvent. Based on previous intensity measurements,[1] the actual $[MnBr_4]^{-2}$ concentration near stoichiometry ($[Br^-]/[Mn^{+2}] = 4$) must surely be modified by the presence of chemical intermediates. Unfortunately, it is not possible to identify the paramagnetic intermediates since they must possess less than cubic symmetry leading to very short relaxation times and very broad resonance widths. A reasonable conjecture on such a dissociative reaction is

$$MnBr_4^{-2} \ + \ CH_3CN \ \overset{K_d}{\rightleftharpoons} \ Mn(CH_3CN)\,Br_3^- \ + \ Br^- \qquad (8)$$

and the corresponding mass action equilibrium constant estimated from the intensity data is $K_d = 5 \times 10^{-3}$. As can be seen, dissociation of stoichiometric $[MnBr_4]^{-2}$ is significant throughout the entire concentration range included in this work. Since resonance widths, in particular those at X-band, are strongly $[MnBr_4]^{-2}$ concentration dependent, dissociation undoubtedly plays an important role in determining the behavior of the data at low excess bromide ion concentrations. At high manganese concentrations (Fig. 12) and zero excess bromide ion, the complex is in the ion-paired state and sufficiently concentrated to observe a frequency effect on the resonance widths even in the presence of some dissociation.

The data obtained from the linear portion of the plots illustrated in Figs. 9 through 12 were analyzed according to $(1/T_2)_{\text{exchange}} = k\,[Br^-] = \sqrt{3}\,\beta\,\pi\,(g/h)\,\Delta H_{\text{exchange}}$ used in reference 2 to determine the bimolecular rate constant, k_2, characterizing the rate of bromide ligand exchange. The results are summarized in Table II and are based on two cases: (1) complete dissociation of Bu_4NBr in acetonitrile, and (2) partial dissociation taking $K_d = 0.5$.[8] Rate constants calculated from X and K-band data are essentially the same within experimental error. A slight increase for k_2 with increasing manganese concentration probably reflects viscosity changes which have been neglected in the calculations.

Trends in these exchange studies have developed in a consistent manner and frequency dependent line broadening is clearly associated with $[MnBr_4]^{-2}$ concentration.

The experimental situation was then inverted to study line broadening imposed by $[MnBr_4]^{-2}$ in a system containing constant 0.15 excess molar bromide ion concentration. On the basis of our results, the bromide concentration was adjusted to a region where the state of the complex was well defined and where the contribution from bromide ion ligand exchange to resonance width was known. Furthermore, this compromise permits an extension of the line broadening studies to higher manganese concentrations. In Fig. 13, we show the variation of electron spin resonance width vs. the complex, $[MnBr_4]^{-2}$, concentration containing 0.15 excess molar Bu_4NBr at both X and K-band frequencies. Line broadening occurs with increasing $[MnBr_4]^{-2}$ concentration as anticipated from the previous exchange studies. Both plots are approximately linear but have different positive slopes with the X-band possessing the larger of the two: (1) X-band, $\Delta H_{ex}/[MnBr_4]^{-2} = 211$ gauss/mole; (2) K-band, $\Delta H_{ex}/[MnBr_4]^{-2} = 105$

FIGURE 13

Variation of resonance width as a function of $[MnBr_4]^{-2}$ concentration at constant 0.15 M excess Bu_4NBr for X and K-band frequencies.

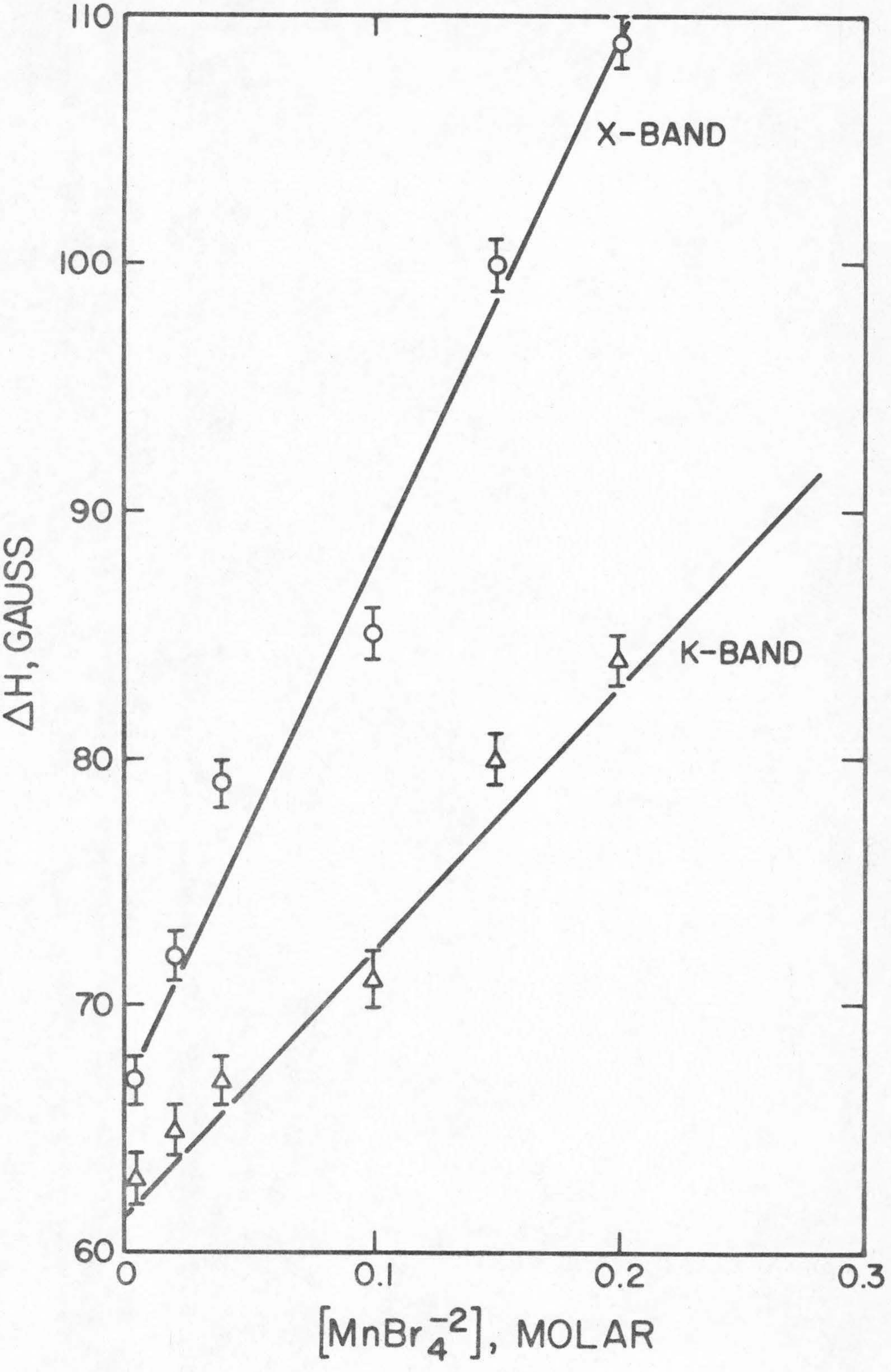
110
100
90
80
70
60
0
0.1
0.2
0.3
ΔH, GAUSS
$[MnBr_4^{-2}]$, MOLAR
X-BAND
K-BAND

gauss/mole. The difference between them is 4 gauss at 0.0037 M $[MnBr_4]^{-2}$ and 25 gauss at 0.2 M $[MnBr_4]^{-2}$. Resonance widths beyond 110 gauss cannot be analyzed with much accuracy. It should be noted by comparison to the exchange studies presented in Figs. 9-12 that manganese dependent broadening at X-band frequencies is considerably greater than bromide ion-ligand exchange broadening.

In view of these experimental results, a possible mechanism for line broadening is superexchange induced by transmission of paramagnetism through diamagnetic carriers, in this case, bromide ions. The superexchange Hamiltonian sometimes referred to as the Heisenberg exchange Hamiltonian has the form

$$H_{ex} = \sum_{j,k} \vec{J}(r_{jk})\, \vec{S}_j \cdot S_k \tag{9}$$

and the extent of interaction can depend on concentration of both the paramagnetic and diamagnetic components. $J(\vec{r}_{jk})$ is the coupling constant characterizing the interaction between the exchanging spins $\vec{S}_j$ and $\vec{S}_k$ over a distance $\vec{r}_{jk}$. Superexchange phenomena are typified by collapse of hyperfine structure, that is, reduction of $< A >$, coupled with a general broadening of the entire spectrum up to a certain point followed by exchange narrowing upon further increase of concentration. These effects have been reported for $MnCl_2$ in molten LiCl [9] and molten LiCl-KCl eutectics [10] where manganese concentrations (0.15-0.30 M) are similar to those reported in the present work although the halide ion concentration was more than an order of magnitude higher. Nevertheless, a careful determination of the effective spin Hamiltonian constants for two $[MnBr_4]^{-2}$ solutions spanning a significant manganese concentration range (0.0047 M $[MnBr_4]^{-2}$ and 0.149$_{ex}$ $[Br^-]$ to 0.200 M ($[MnBr_4]^{-2}$ and 0.150$_{ex}$ $[Br^-]$) was performed and the values remained the same. Within experimental tolerances, no decrease in the hyperfine coupling constant was observed; however, the magnitude of collapse could be small enough to be obscured by the accuracy of our measurements. In addition, the quantitative effect imposed by superexchange mechanisms on the collapse of hyperfine structure, line narrowing, and intricate details of line shape, particularly in liquid media, is still open to question. We suspect that superexchange does not provide a significant relaxation mechanism for $[MnBr_4]^{-2}$ within the concentration range investigated in the present work.

Returning to Fig. 13, depicting the manganese dependent broadening, it is seen that the X and K-band plots converge and almost coincide on approaching zero manganese concentration. Extrapolation of these lines through the ordinate axis gives nearly coincident intercepts within experimental error and defines an "average" overall resonance width in the absence of manganese dependent broadening. Since the average overall resonance width is now accountable to previously discussed mechanisms including intrinsic contributions, we can assign broadening above the point of convergence to interactions involving only manganese. Comparison of Fig. 13 to Figs. 9-12 depicting bromide ligand exchange effects, clearly demonstrates that manganese dependent interactions provide the dominant relaxation mechanism in this system.

Looking back on the results we can empirically represent the overall resonance width as a sum of three major components

$$\frac{1}{T_2} = \sum_i \frac{1}{T_{2i}} + k_2 [Br^-] + D(\omega) [MnBr_4]^{-2} \qquad (10)$$

The first term on the right contains all intrinsic contributions to broadening mentioned earlier. The plots of ΔH (X and K-band) as a function of $[Br^-]$ shown in Figs. 9-12 contained different concentrations of manganese and, yet, they all had essentially the same slope. This observation is clearly consistent with our interpretation that the slope characterizes a dynamical exchange process between free Br^- and $[MnBr_4]^{-2}$ occurring on a time scale amenable to electron spin resonance. The second term represents this source of broadening. At constant Br^- and variable $[MnBr_4]^{-2}$ concentrations the resonance widths also respond in a linear fashion but their slopes denoted by $D(\omega)$ depend markedly on the exciting H_1 frequency, ω. It is interesting to recall that analogous experiments on Et_4NCl-$MnCl_4^{-2}$ showed no such concentration or frequency dependency. We proposed that the frequency dependent resonance widths have their origin in dynamical dipolar interactions between the paramagnetic anions. Since the $[MnBr_4]^{-2}$ complex is larger than its chloride analogue, it is perfectly reasonable on an intuitive level to expect the larger species to rotate more slowly in solution. Consequently, dipolar interactions between Mn^{+2} ions in the larger complex can persist over a longer period of time. Moreover, the tetraalkylammonium counterions probably diffuse in a cooperative fashion along with the complex to further modify dynamical processes.

The frequency dependent resonance widths appear to originate from the dipolar interactions as modulated by the relative motions of the paramagnetic anions. Dipolar linewidths have a general form depicted by

$$\left[\frac{1}{T_2}\right]_{\text{dipolar}} = D\left(\tau_c + \frac{\tau_c}{1+\omega_0^2\,\tau_c^2} + \cdots\cdot\right) \qquad (11)$$

which approximates the nature of the frequency dependency, ω_0, where D is the interaction constant and τ_c is the rotational correlation time for the interaction. A temperature study of resonance widths should then reveal the usual predictable behavior expected of a diffusion controlled process. Moreover, we can test the relative importance of the $\omega_0\,\tau_c$ term since it is also temperature dependent. In other words, we have two ways of changing $\omega_0\,\tau_c$ at our disposal and we shall exploit them both in the following section to gain deeper insight into the dynamical nature of molecular interactions.

3.5. Temperature Dependence of Resonance Widths

If the dominant spin relaxation mechanisms are diffusion controlled processes, the temperature dependence of the resonance widths can be examined on the basis of the liquid theory model[11] proposed by Frenkel. In his analysis of liquids, Frenkel assumes that the equilibrium position of atoms in a liquid are not absolutely permanent and that each atom can jump to a new equilibrium position at a distance δ after a certain time. The expression derived for the temperature dependence of the viscosity is

$$\eta = \frac{k\,T\,\tau_0}{\pi\,a\,\delta^2}\,e^{W/kT} \qquad (12)$$

where a is the radius of the molecule, τ_0 is a constant representing the free vibrational period of the diffusing component about an equilibrium position and W is the activation energy required for transport to an adjacent site; the other parameters have their usual meanings.

The rotational correlation time, τ_c , is given by

$$\tau_c = \frac{4\pi\eta a^3}{3\,kT} \qquad (13)$$

Thus, by substitution for η

$$\tau_c = \frac{4}{3}\,\frac{a^2\tau_0}{\delta^2}\,e^{W/kT}$$

$$\tau_c = (\text{constant})\;e^{W/kT} \qquad (14)$$

In the limit of extreme narrowing ($\omega^2\tau_c^2 \ll 1$) which should be more applicable to the X-band results, the resonance width is proportional to the diffusional correlation time and we may rewrite Eq. (14) to give the very familiar relation

$$\ln(\Delta H) = \text{constant} + W/kT\ . \qquad (15)$$

In Fig. 14, we have plotted ln (ΔH) vs. $10^3/T$ for two solutions containing the same concentration of excess bromide ion but different concentrations of $[MnBr_4]^{-2}$. Excess bromide ion not only guarantees the state of the manganese but also provides an exchanging system exhibiting considerable line broadening. A linear relationship is

FIGURE 14

ln (ΔH) vs. $10^3/T$°K for solutions containing 0.1 M (O) and 0.2 M (Δ) $[MnBr_4]^{-2}$ and 0.15 M excess Bu_4NBr.

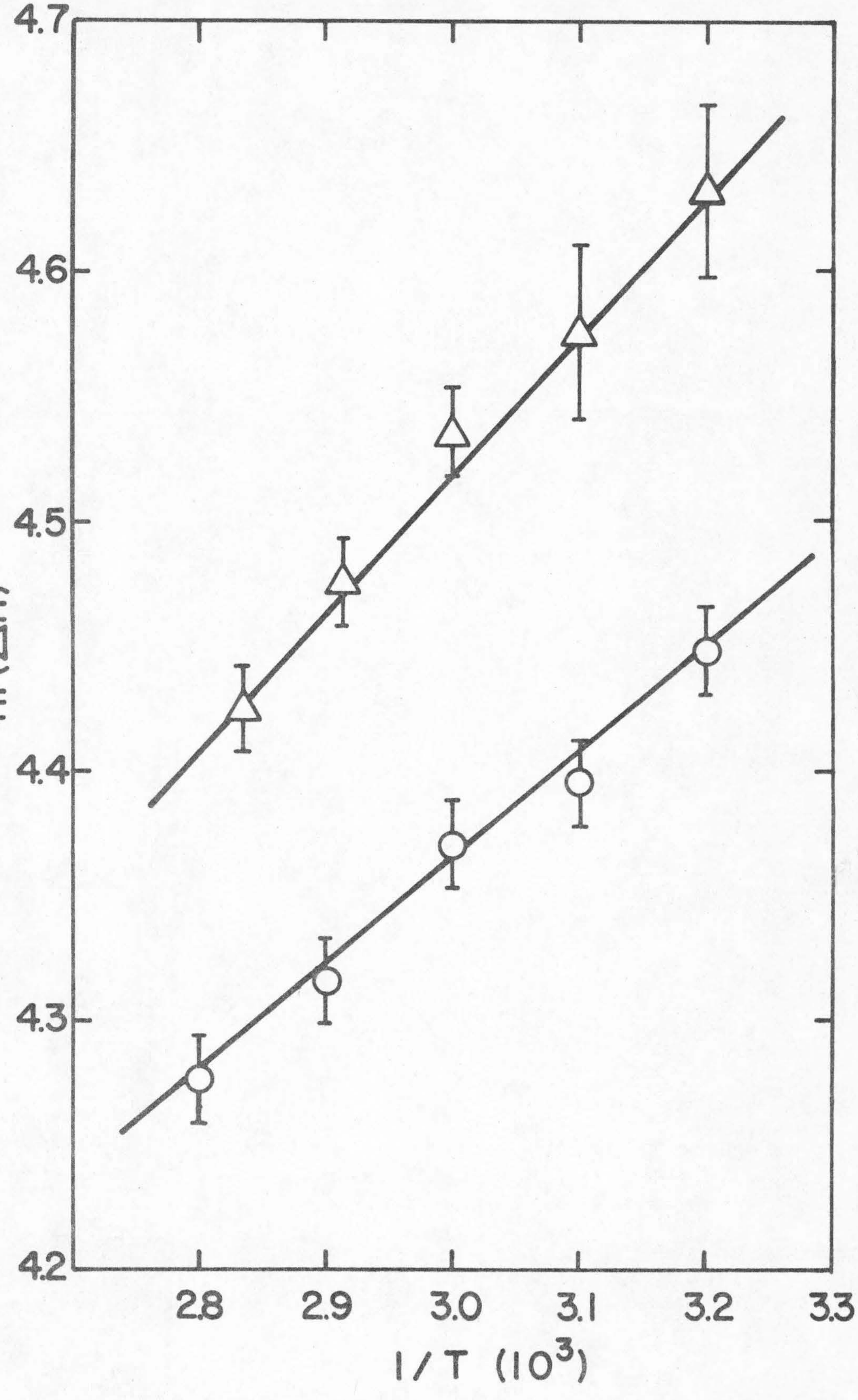
4.7
4.6
4.5
4.4
4.3
4.2
ln (ΔH)
2.8
2.9
3.0
3.1
3.2
3.3
1/T (10^3)

observed in each case and the diffusional activation energies for 0.1 and 0.2 molar concentrations of $[MnBr_4]^{-2}$ are 5.0 and 6.4 kcal/mole, respectively, compared with 3 kcal/mole observed for water.[12] As expected, the decrease in activation energy, W, probably reflects a decrease in viscosity, although it is conceivable that a mixture of dipolar and exchange relaxation could lead to the same effect.

To further illustrate the dynamical nature of the dipolar interactions we have plotted in Fig. 15 the X and K-band resonance widths as a function of temperature for a solution containing 0.039 M (0.05 m) $[MnBr_4]^{-2}$ and 0.150 excess M Bu_4NBr. As expected, resonance widths respond inversely to changes in temperature. The most significant feature of this experiment, however, is that the difference in X and K-band resonance widths diminishes with increasing temperature and practically vanishes at the highest temperature (73°C). From previous data[2] we know that η/T typically decreases by a factor of three over this temperature interval. Accordingly, we expect the $\omega_0^2 \tau_c^2$ term in Eq. (11) to reflect this change as a factor of nine. Hence, for K-band observations at the high temperature end (73°C), we expect this change to partially neutralize the ω_K^2 so that once more the extreme narrowing case is realized, i.e., $\omega_K \tau_c < 1$. Referring, again, to Eq. (11) we note that the change in τ_c ($\tau_c \propto \eta/T$) imposed by adjusting the temperature elicits a particularly important effect at K-band frequencies due to the magnitude of $\omega_K^2 \tau_c^2$. We predict that X and K-band resonance widths converge at higher temperatures and this convergence was observed experimentally as shown in Fig. 15.

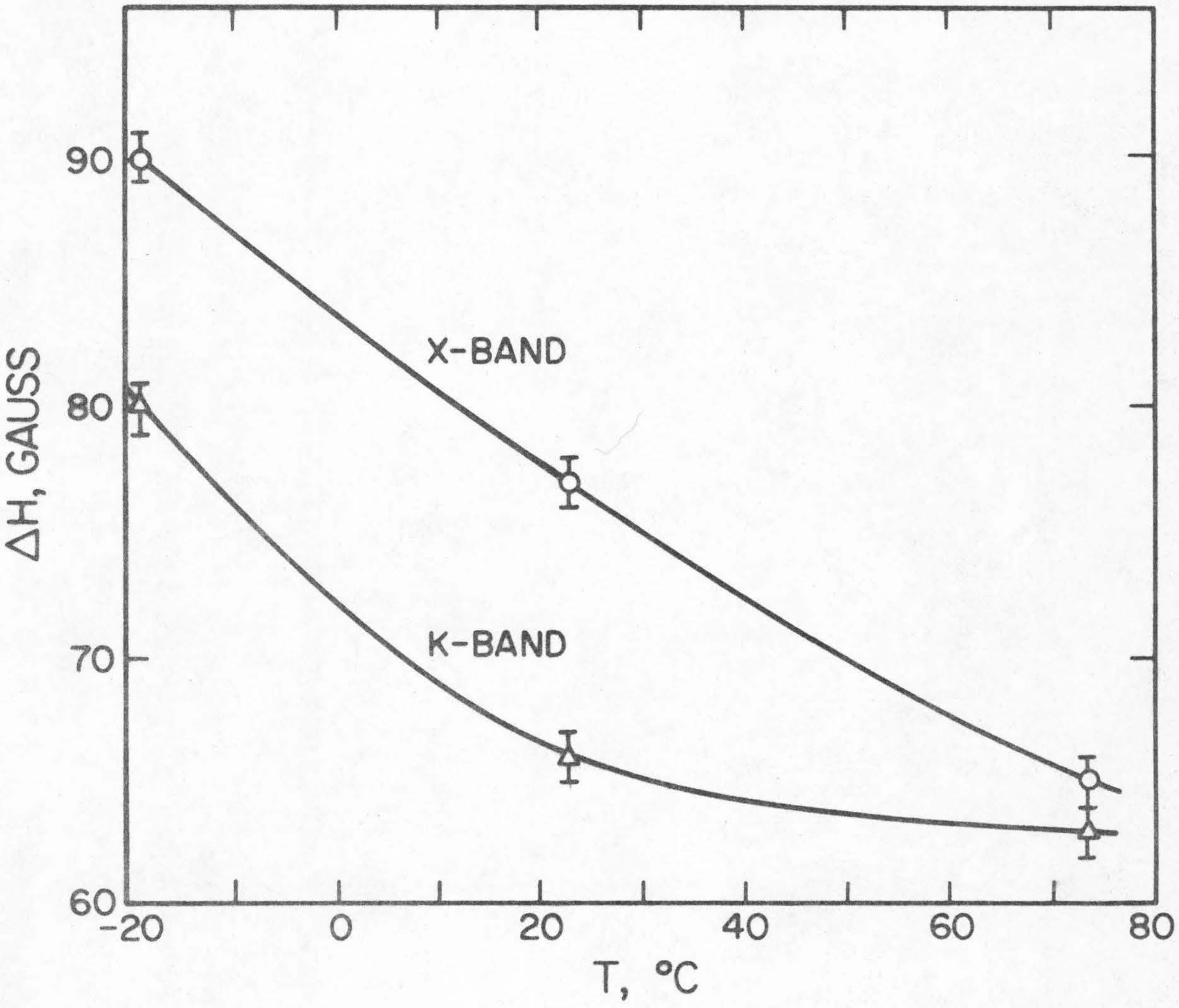

FIGURE 15

X and K-band resonance widths, ΔH, as a function of temperature. Solution contained 0.039 M $[MnBr_4]^{-2}$ and 0.150 M excess Bu_4NBr.

In order to interpret these results more fully within a quantitative framework, we have developed a theory to treat the problem of interacting sextet states.

3.6. Calculations of Resonance Widths

Experimentally there are three contributions to the observed resonance width, an intrinsic part, a part due to ligand exchange and a part due to coupling between spins. Theoretically the line shape of the spectrum of $[MnBr_4]^{-2}$ is very complex as the electron spin of $S = 5/2$ is coupled to a nuclear spin of $I = 5/2$. For example, the $M_I = 1/2$ line (from which all the experimental line widths were taken) consists of five nearly degenerate transitions ($M_S = -5/2 \rightarrow -3/2$, $-3/2 \rightarrow -1/2$, $-1/2 \rightarrow 1/2$, $1/2 \rightarrow 3/2$, $3/2 \rightarrow 5/2$) which are split by the second-order effects of the electron-nuclear coupling. These components have different widths [3] since the diagonal elements of the relaxation matrix differ and they are also strongly mixed by the off-diagonal elements of the relaxation matrix [13] if the widths are comparable to or greater than the separation of the different M_S components. The exact line shapes could be found by solving the matrix equation

$$(\underset{\wedge}{r} - \omega \underset{\wedge}{I} - i\underset{\wedge}{R})\, \underline{\rho} = DM_0\, \underline{\mu} \tag{16}$$

where $\underline{\rho}$ is a vector of the density matrix elements corresponding to the five M_I ($M_S \rightarrow M_S + 1$) transitions, R is the 5×5 relaxation matrix in this space, $\underset{\wedge}{r}$ is a diagonal matrix whose elements are the resonance frequencies of the five transitions, $\underline{\mu}$ is a vector with elements $< M_S + 1 \mid S_+ \mid M_S >$ and ω is the applied frequency.

However, in all the observations made, the width of the $M_I = 1/2$ line was considerably greater than the separation of the different components of the line, so the components were assumed to be degenerate. In this approximation the line shape consists of five superimposed Lorentzian lines with widths given by the eigenvalues of the relaxation matrix and weights that can be derived from the eigenvectors.

The theoretical problem is to set up the relaxation matrix and find its eigenvectors and eigenvalues as a function of concentration, temperature, field, etc. The total relaxation matrix R is the sum of three parts:

$$R = R_{\text{intrinsic}} + R_{\text{ligand exchange}} + R_{\text{spin-coupling}} \tag{17}$$

(a) $\underline{R_{\text{intrinsic}}}$

The intrinsic contribution to the line width may be due to a variety of causes. Garrett and Morgan[4] proposed that fluctuations in the solvent sheath around the ion perturb the electronic wave function, producing an orientation dependent term in the spin Hamiltonian. Another process which is probably more important in these systems is ion pair formation. The terms induced in the spin Hamiltonian are similar to those induced by solvent fluctuations, the only difference being the life time of the perturbed state.

It is probable that the principal contribution to the intrinsic line width is due to an induced zero field splitting which transforms as the second order rotation group. Changes in the g tensor or the nuclear spin coupling tensor would give field dependent or M_I dependent line widths which are not observed. The form of the relaxation matrix for a $D^{(2)}$ interaction is given by Hudson and Luckhurst.[13] In the extreme narrowing situation a single Lorentzian line is obtained as the other four eigenvalues correspond to transitions with no intensity. If the finite life time of the ion pair is taken into account this line width is modified from width $\tau_D R p_D$ to

$$\frac{p_D R \tau_c}{\tau_D \tau_c R + 1}$$

where τ_D is the life time of the spin pair; τ_c is its rotational correlation time; p_D is the proportion of spin pairs. The expression is further modified as p_D increases. However the intrinsic part of the line width was small in the observed systems and it did not prove possible to investigate it in detail.

(b) $R_{\text{ligand exchange}}$

The form of the relaxation matrix for ligand exchange is particularly simple. Ligand exchange occurs through some kind of intermediate presumably of C_3 symmetry. The crystal field in this intermediate is different from that in the tetrahedral state, changing the orbital energy level pattern. Almost certainly there will be sufficient spin-orbit coupling to change the total electron spin quantum number so that

$$\underset{\sim}{R}_{\text{ligand exchange}} = \tau \underset{\sim}{I}$$

where τ is the time between successive ligand exchanges.

(c) $R_{\text{spin-coupling}}$

The form of the relaxation matrix due to coupling between electron spins on different ions was calculated using a model in which individual ions exchange between "monomer" sites and "dimer" sites. "Dimers" consist of two ions whose spin dipoles are directly coupled and which are rotating relative to each other. The monomers are free ions. Although we use the terms monomer and dimer we do not intend to imply a long lived association. The "dimer" situation could equally well be a collision during which the spins interacted as a long lived ion triplet or similar association. In fact we shall deduce from the results of the calculations that the "dimer" is more likely to be a short lived close association, such as a collision, rather than a long lived weak association.

The calculation of $\underset{\sim}{R}_{\text{spin-coupling}}$, the relaxation matrix in the 5 × 5 space of the five sextet transitions is not completely straightforward. The dimers are described by a 36 × 36 density matrix and have 25 rather than five transitions. The dipolar coupling relaxation matrix R_d of the dimers is defined in the dimer space rather than the monomer space. The effect of exchange between monomer and dimer sites couples the monomer and dimer density matrix elements together so that the complete problem involves a 145 × 145 matrix. The line shapes cannot be completely described by a single 5 × 5 relaxation matrix $R_{\text{spin-coupling}}$ unless the proportion of dimers is very small. In the experimental situation this is true and $R_{\text{spin-coupling}}$ can be set up from the 145×145 matrix using perturbation theory.

Experimentally the Mn^{+2} - Mn^{+2} interaction contribution to the line width is field (frequency) dependent showing that extreme narrowing does not apply. Under such conditions one must use an explicit form of the rotational correlation function to calculate the spectral densities used in Redfield's equations.[14] We used the form

$$G(\tau) = G(o) \exp(-|\tau|/\tau_c)$$

Other parameters which were needed for the calculation are ω_0 (the applied frequency), $< r^{-6} >$ the mean inverse sixth power of the separation of the spins in the dimer, the proportion of dimer n_D and the rate of break-up of dimers, k.

The dimers are described by a 36×36 density matrix ρ and the monomers by a 6×6 matrix σ. The equations of motion for ρ and σ are coupled by the exchange. In a high temperature, low r.f. field approximation, they can be written

$$[(\omega_0 - \omega_1)\underset{\wedge}{I} - i\underset{\wedge}{K}]\, \underline{\nu} = \gamma B_1 M_0 \underline{S} \tag{18}$$

where $\underline{\nu}$ is a vector whose first five elements are the elements of σ between monomer states with $\Delta M = +1$. ($\sigma_{5/2,\, 3/2}$; $\sigma_{3/2,\, 1/2}$; $\sigma_{1/2,\, -1/2}$; $\sigma_{-1/2,\, -3/2}$; $\sigma_{-3/2,\, -5/2}$) and the rest of the elements are proportional to the elements of ρ between dimer states with $\Delta M = +1$.

$$\begin{aligned} \nu_\alpha &= \sigma_{\alpha_1 \alpha_2} && (\alpha = 1, 5) \\ \nu_\alpha &= \sqrt{3}\, n_D \rho_{\alpha_1 \alpha_2} && (\alpha = 6, 145) \end{aligned} \tag{19}$$

and S is a vector with elements

$$\begin{aligned} S_x &= \langle \alpha_1 \mid S_+ \mid \alpha_2 \rangle && (\alpha = 1, 5) \\ S_x &= \sqrt{3}\, n_D \langle \alpha_1 \mid S_+ \mid \alpha_2 \rangle && (\alpha = 6, 145) \end{aligned} \tag{20}$$

The matrix $\underset{\wedge}{K}$ is symmetrical and has the form

$$\underset{\wedge}{K} = \left[\begin{array}{c|c} n_D\, k\, \underset{\wedge}{I}_1 & \dfrac{-k}{2} \dfrac{\sqrt{n}_D\, \underset{\wedge}{C}^+}{\sqrt{3}} \\ \hline \dfrac{-k}{2} \dfrac{\sqrt{n}_D\, \underset{\wedge}{C}}{\sqrt{3}} & k\, \underset{\wedge}{I}_2 + \underset{\wedge}{R}_d \end{array} \right] \tag{21}$$

where I_1 is the unit matrix spanning the monomer subspace, $\underset{\wedge}{R}$ is the dipolar relaxation matrix in dimer subspace and $\underset{\wedge}{C}$ is the matrix of coefficients of monomer elements in the trace over one spin of the dimer. n_D is the ratio of dimers to monomers.

The matrix K can be split into two submatrices by using the symmetry of the dipolar relaxation Hamiltonian under spin inversion. If we take symmetrical and antisymmetrical combinations of elements of ρ and σ which are related by spin inversion, K has no cross terms between these. As antisymmetrical combinations do not contribute to the spectrum, they can be discarded. In the limit of small n_D

with which we are concerned the problem is further simplified. To first order in n_D the spectrum is due to the monomers, and consists of three Lorentzian lines with widths and intensities given by the eigenvalues and eigenfunctions of an effective relaxation matrix defined in the space spanned by the three symmetric combinations of the elements of σ, that is, $\{1/\sqrt{2}\,(\sigma_{5/2,\,3/2} + \sigma_{-3/2,\,-5/2}),\ 1/\sqrt{2}\,(\sigma_{3/2,\,1/2} + \sigma_{-1/2,\,-3/2}),\ \sigma_{1/2,\,-1/2}\}$.

The form of the effective relaxation matrix $\underline{R}^{\mathrm{eff}}$ in monomer space is obtained by applying perturbation theory to the complete matrix $\underline{K}$, and taking terms to second order in $\sqrt{n_D}$. It is

$$R_{ij}^{\mathrm{eff}} = k\, n_D \left[\delta_{ij} - \frac{1}{12} \sum_{\alpha} C_{i\alpha}^{+} \left(\frac{R_{\alpha\alpha}}{k} + 1\right)^{-1} C_{\alpha j}\right] \tag{22}$$

where the summation is taken over eigenvalues of the dipolar relaxation matrix $\underset{\wedge}{R}_d$ in dimer space. A program was written to set up and diagonalize the dipolar relaxation matrix and to use the results to set up the effective monomer relaxation matrix and find the intensities and widths of the three monomer lines. By using the symmetries of the dipolar Hamiltonian with respect to exchange of the spins in the dimer the problem reduces to diagonalization of a 13 × 13 and a 22 × 22 matrix, followed by diagonalization of the 3 × 3 matrix R^{eff}.

The final line widths are proportional to $n_D k$ and in addition are functions of two other parameters, $\omega_0 \tau_{\mathrm{rot}}$ for the dipolar relaxation and a parameter P which is a measure of the relative effects of the rotational and exchange broadening in the dimer,

$$P = 0.075\ \tau_{\mathrm{rot}}\ \tau_D\ \gamma^4\ \hbar^2 < r^{-6} > \tag{23}$$

where τ_D is the lifetime of the dimer and τ_{rot} is the rotational correlation time for the dimer. Fig. 16 shows the calculated line widths / $n_D k$ as a function of P and $\omega\tau$.

In every case the calculated line shape is mainly due to one Lorentzian; the other two having small intensities.

3.7. Applications of Calculations to the $[MnBr_4]^{-2}$ System.

The observed resonance widths of epr spectra of $[MnBr_4]^{-2}$ have the empirical form

$$\Delta\nu = a + b\ [Br^-] + c\ [MnBr_4{}^{-2}]\ . \tag{24}$$

as shown in Eq. (10). This equation is interpreted as being the sum of terms due to the intrinsic line width, the effects of ligand exchange and spin dipolar broadening of dimers.

The constant c which describes the manganese-manganese interaction is a function of temperature and frequency (field). At room temperature c has the values 211 gauss mole^{-1} at X-band ($\nu_0 \approx 9.5 \times 10^9$ Hz) and 105 gauss mole^{-1} at K-band ($\nu_0 \approx 35 \times 10^9$ Hz). This large increase of a factor of 2 in c with a change of 9.5 to 35 GHz in ν_0 can only be fitted with the calculated line widths (Fig. 16) if $\overline{\omega_0\ \tau_c} \sim 1$ and $P \sim 10^{-4} - 10^{-6}$, as the ratio $\Delta \log\ \Delta\nu / \Delta \log\ \omega\tau$ is too small for values of P above or below this limit. Exact comparisons enable us to make the following deductions:

(1) The correlation time for the rotation of the dimer is

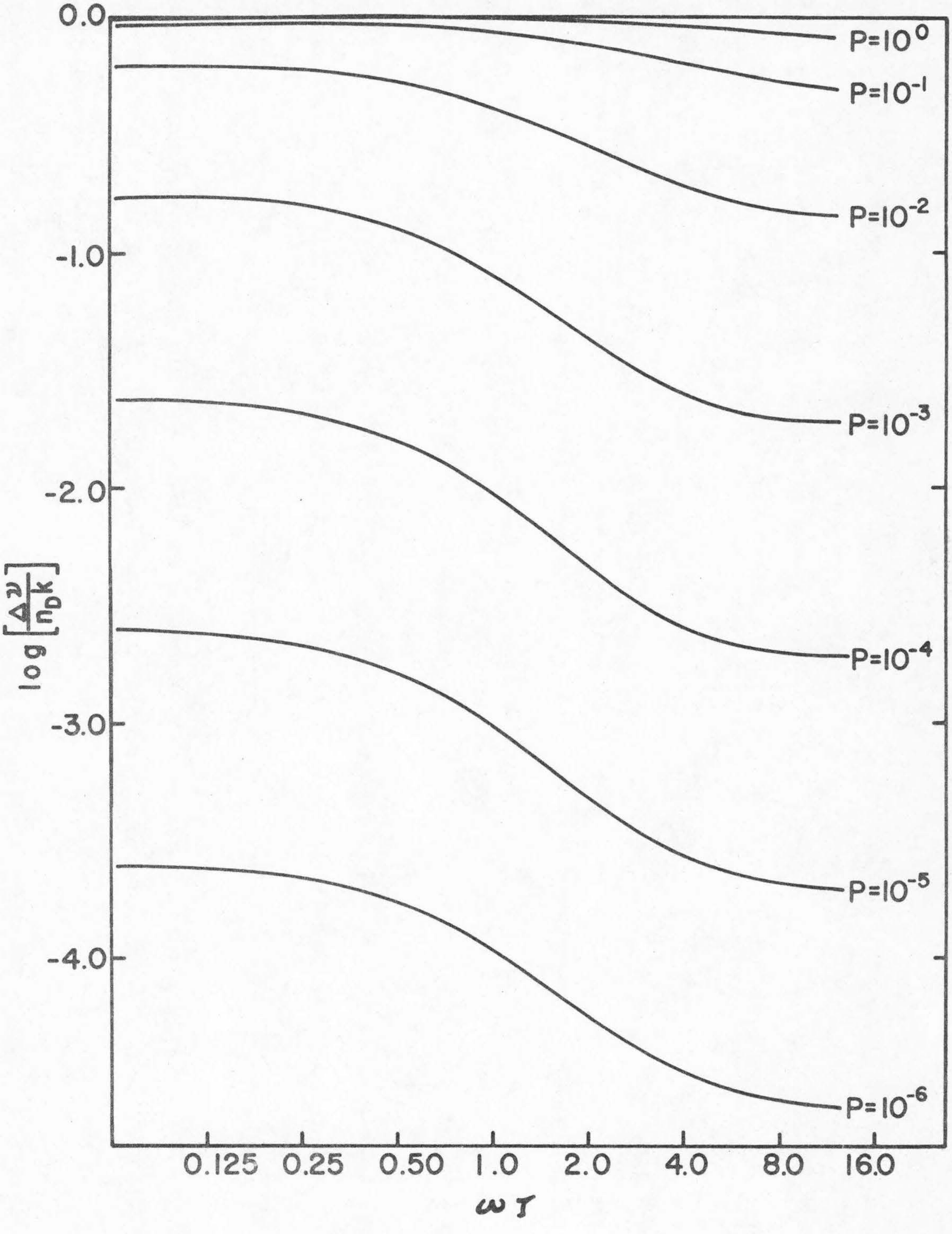

FIGURE 16 Plot of log $\frac{\Delta\nu}{n_D k}$ versus $\omega\tau$.

$$\tau_{rot} = 1.25 \times 10^{-11} \ (\pm 5\%) \text{ sec.}$$

(2) The value of the product of the life time of the dimer and $< r^{-6} >$ is,

$$\underline{\tau_D} \ < r^{-6} > \ = P \times 10^{-11} \qquad \mathring{A}^6 \, S^{-1}$$

$$= 10^{-15} - 10^{-17} \qquad \mathring{A}^6 \, S^{-1}$$

Consequently, if the dimer is large it must have a longer life time to explain the spectrum. However the ratio τ_D / n_D can be obtained by comparing the absolute values of the observed and calculated line widths, within the range of possible P values.

$$\tau_D \approx \frac{n_D \, 10^{-5}}{[\mathrm{MnBr_4}^{-2}]} \ P \qquad \text{moles sec.}$$

$$n_D < r^{-6} > \ \approx 10^{-6} \ [\mathrm{MnBr_4}^{-2}] \ \mathring{A}^{+6} \ \text{moles}^{-1} .$$

If the dimer consists of two $[\mathrm{MnBr_4}]^{-2}$ ions in contact

$$r^{+6} \sim 4 \times 10^5 \text{ and } n_D \sim 4 \times 10^{-1} \ [\mathrm{MnBr_4}]^{-2}$$

while for an ion triplet $r^6 \sim 10^7$ giving up $n_D \sim 10 \ [\mathrm{MnBr_4}]^{-2}$. The latter value is much too large so the possibility of the relaxation being caused by an ion triplet is very unlikely.

The temperature dependence of the constant c (Fig. 17) can be qualitatively understood. As the temperature is raised all three parameters which determine the line widths are altered; τ_{rot} is reduced, P decreases and $n_D k$ increases. The difference between the X and K-band widths depends on τ_{rot} only. When $\tau_{rot}^{-1} \gg \omega_K$

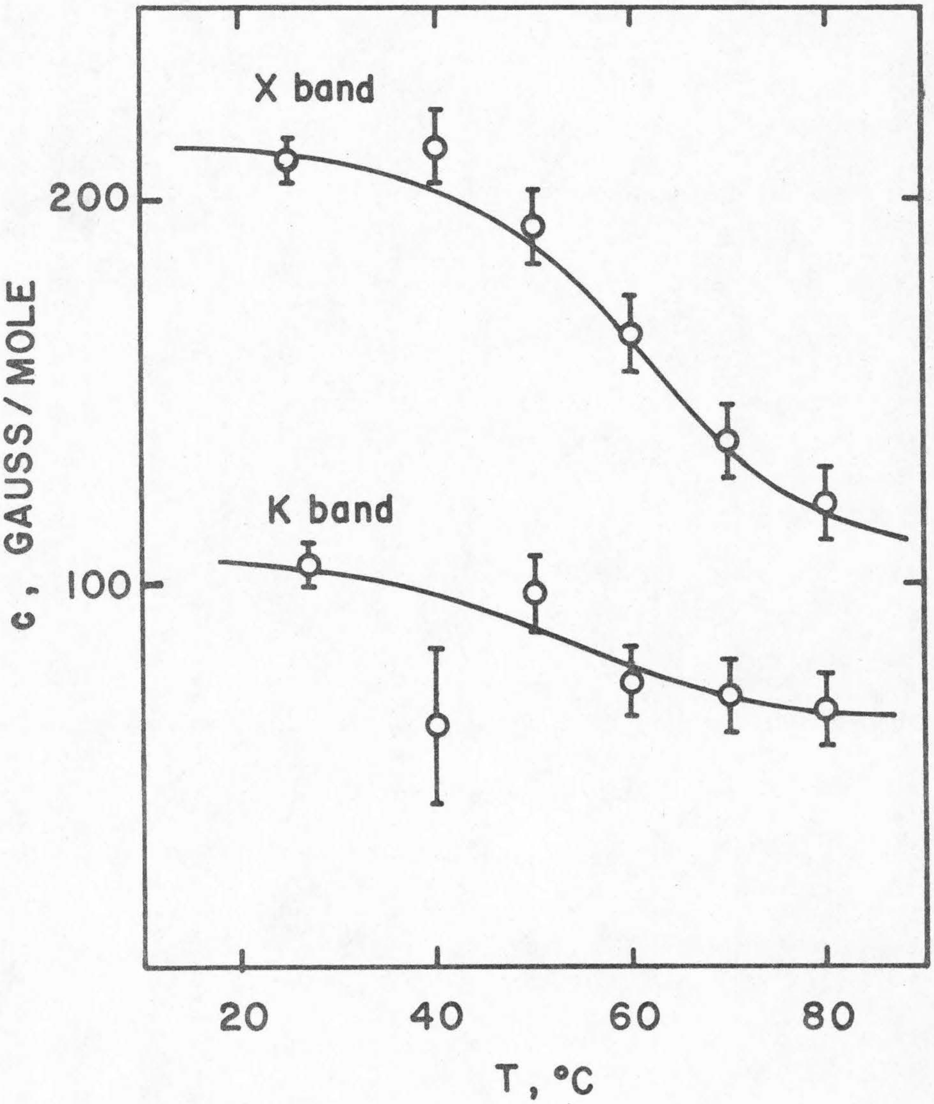

FIGURE 17

Temperature dependence of c.

extreme narrowing applies at both frequencies and the line widths are equal. In Fig. 17 it can be seen that the difference between the X and K widths decreases rapidly at about 55°C; at this temperature

$$\omega_K \, \tau_{rot} \approx \sqrt{2}$$

τ_{rot} has decreased by a factor of 2 between 20° and 55°C. The corresponding low temperature effect was not seen. The overall decrease in line width with temperature is due to the decreased value of P.

Limitations of the Model

It is legitimate to use this model in which the resonance frequency of the dimer has been placed equal to that of the monomer if

$$\left| \omega_{\text{dimer}} - \omega_{\text{monomer}} \right| \ll k + R_{\alpha\alpha}$$

The line widths of the real monomer should be calculated by diagonalizing the complete relaxation matrix in monomer space.

Although these conclusions are based on the diagonalization of $R_{\text{spin-interaction}}$ alone, $R_{\text{ligand exchange}}$ is a multiple of the unit matrix and $R_{\text{intrinsic}}$ is sufficiently small that it is unlikely to affect the spin-interaction contribution to the line width.

4. CONCLUSIONS

A study of electron spin relaxation of three manganese (II) complexes in acetonitrile has provided insight into the structure and dynamical behavior of ionic complexes in liquids. Emphasis is placed on the unusual resonance broadening observed in the tetrahedral bromide complex, $[\mathrm{MnBr_4}]^{-2}$. Parallel studies were conducted on the analogous tetrahedral chloride complex, $[\mathrm{MnCl_4}]^{-2}$, and also on the octahedral solvent complex, $[\mathrm{Mn(CH_3CN)_6}]^{+2}$. In all three cases, the ionic nature of the complex requires the presence of counterions which are naturally interwoven into the interpretation of the results. For the system $\mathrm{Et_4NCl\text{-}MNCl_4}^{-2}$ we found several relaxation mechanisms leading to line broadening. One source appears to arise through spin-orbit interaction caused by modulation of the ligand field resulting from transient distortions of the complex imparted by solvent fluctuations in the immediate surroundings of the paramagnetic ion. An additional spin relaxation mechanism was assigned to the formation of ion-pairs. Although exact structural parameters for the loosely associated pairs are unavailable from spin relaxation measurements because of the stochastic nature of the system, we were, at least, able to tell qualitatively that the paramagnetic anion and its counterion are interacting at short range to produce electron spin relaxation. Moreover, we can define the experimental parameters leading to the apparent dynamical association and assign an equilibrium constant for the process.

The $\mathrm{Bu_4NBr\text{-}MnBr_4}^{-2}$ study was considerably more interesting. As in the former case, solvent fluctuations and ion-pairing of the paramagnetic complex provide significant relaxation for the electronic spin system. Most interesting, however, is the onset of a new relaxation mechanism leading to significant resonance broadening which is best interpreted as chemical exchange. Thus, assuming that resonance widths were simply governed by electron spin state life times, we were able to extract dynamical information from an interaction in which the initial and final states are the same. Previous studies suggested that the exchange is probably diffusion controlled. Furthermore the entropy of activation suggested an associative mechanism for the process in line with current theories proposing the existence of five-coordinate intermediates in reactions involving tetrahedrally coordinated complexes.

An additional important source of spin relaxation in this system stems directly from dipolar interactions between the manganese $3d^5$ electrons. Moreover, the dipolar broadening is strongly frequency dependent. A theory proposing the existence of spin coupled "dimers" was developed to explain the observations. The relaxation matrix due to dipolar spin coupling was calculated using a collisional model proposing an exchange of Mn^{+2} between two well defined states: (1) a free or isolated anion, $[MnBr_4]^{-2}$, and (2) a transient "dimer" in which the spins are coupled through an association permitting independent rotational motion. The observed interactions were consistent with the calculated resonance widths when $\omega_0 \tau_c \sim 1$ and $P \sim 10^{-4} \rightarrow 10^{-6}$ where P represents a measurement of the relative effects of the rotational and exchange broadening in our model. Consequently a correlation time characterizing the dynamical rotation of the "dimer" could be established within a rather narrow limit, $\tau_{rot} = 1.25 \times 10^{-11}$ (± 5) sec. It was possible to make further deductions on the relation between "dimer" size and its life time. For instance, the spectrum can be explained only if "dimer" life time increases with size. This presents a reasonable physical picture as well and, indeed, we did not observe frequency dependent effects for the smaller, less-associated $[MnCl_4]^{-2}$ complex.

The agreement between experimental and theoretical results is quite satisfactory in explaining some of the dynamical behavior displayed by three Mn^{+2} complexes in acetonitrile. We have demonstrated that electron spin resonance line widths can provide unique dynamical information when the time scale of interaction occurs in the right range. For an electron spin resonance experiment the time scale is in the nanosecond range and includes many important phenomena which are not easily accessible by other experimental techniques.

REFERENCES

1. S. I. Chan, B. M. Fung, and H. Lütje, J. Chem. Phys., **47**, 2121 (1967).
2. J. E. Crawford, L. Lynds, and S. I. Chan, J. Am. Chem. Soc., **90**, 7165 (1968).
3. C. W. Davies, "Ion Association," Butterworths, Washington, D.C., 1962, p. 96.
4. B. B. Garrett and L. O. Morgan, J. Chem. Phys., **44**, 890 (1966).
5. C. C. Hinckley and L. O. Morgan, J. Chem. Phys., **44**, 898 (1966).
6. H. M. McConnell, J. Chem. Phys., **28**, 430 (1958).
7. R. G. Pearson and T. Buch, J. Chem. Phys., **36**, 1277 (1962).
8. D. F. Evans, C. Zawoyski, and R. L. Kay, J. Phys. Chem., **69**, 3878 (1965).
9. L. S. Singer and M. C. Haun, Bull. Am. Phys. Soc., **7**, 200 (1962).
10. L. Yarmus, M. Kukk, and B. R. Sundheim, J. Chem. Phys., **40**, 33 (1964); T. B. Swanson, J. Chem. Phys., **45**, 179 (1966).
11. J. Frenkel, "Kinetic Theory of Liquids," Oxford University Press, London, 1946; reprinted by Dover 1955.
12. H. S. Jarrett, J. Chem. Phys., **25**, 1289 (1956).
13. A. Hudson and G. R. Luckhurst, Mol. Phys., **16**, 395 (1969).
14. A. G. Redfield, IBM J. Res. Develop., **1**, 19 (1957).